MECHANICS OF DUMP TRUCK VIBRATIONS IN HIGH-IMPACT SHOVEL LOADING OPERATIONS

by

NASSIB AOUAD

A DISSERTATION

Presented to the Faculty of the Graduate School of the

MISSOURI UNIVERSITY OF SCIENCE AND TECHNOLOGY

In Partial Fulfillment of the Requirements for the Degree

DOCTOR OF PHILOSOPHY

in

MINING ENGINEERING

2008

Dr. Samuel Frimpong, Advisor

Dr. Kwame Awuah-Offei

Dr. Jason Baird

Dr. Jeffrey D. Cawlfield

Dr. Daniel S. Stutts

Dr. Jerry C. Tien

ABSTRACT

The deployment of large machinery for low cost, bulk surface mine production operations has resulted in high-impact shovel loading operations (HISLO). In extreme cases, shovels load large dump trucks with 100-ton (or more) passes generating high-impact forces under gravity. HISLO generates high-frequency shockwaves that cause severe truck vibrations exposing operators to whole body vibrations (WBV). This WBV levels may exceed the recommended International Standards Organization (ISO) limits resulting in long-term lower-back disorders and other health problems. There is a need for fundamental and applied research to determine HISLO vibration levels for heavy mining machinery, their comparisons to ISO 2631 limits and the safety of operators under these conditions.

Previous studies have dealt with vibration problems by designing ergonomic seats with no emphasis on the source of machine vibrations. In this study, the mechanics of truck vibrations under HISLO conditions is developed using Lagrangian formulation for a 9-DOF system. The Fehlberg fourth-fifth order Runge-Kutta numerical method is used to solve the corresponding equations of motion. Furthermore, a 3D virtual truck prototype model with 38-DOF is built and simulated in MSC.ADAMS. Simulation experiments are carried out to determine the dynamic characteristics of the truck under the HISLO conditions and to investigate the potential sources of vibration and their propagation. The simulation results show that the vertical RMS accelerations are equal to 3.56 m/s^2, 1.12 m/s^2 and 0.90 m/s^2 for the operator's seat, lower-back and cervical regions, respectively. These values agree with the experimental results by Kumar (1999) in the oil sands operations. The vibration levels also fall within the extremely uncomfortable zone compared to the ISO 2631 limits, which pose severe health threats to truck operators over long-term exposure.

This pioneering research initiative has developed comprehensive truck vibration theory, dynamic models and virtual prototype simulation for determining accelerations on critical body parts of a dump truck operator. It advances the heavy mining machinery vibrations frontier and contributes immensely to its body of knowledge. It also provides a foundation and a platform for comparing operator WBV exposures to ISO Limits toward creating a safe working environment that guarantees long-term operator health.

ACKNOWLEDGMENTS

I am thankful to my advisor, Dr. Samuel Frimpong, for his help, guidance and encouragement throughout the course of this work.

I also appreciate the guidance and encouragement of my advisory committee members – Dr. Jerry C. Tien, Dr. Jason Baird, Dr. Daniel S. Stutts, Dr. Jeffrey D. Cawlfield and Dr. Kwame Awuah-Offei.

My gratitude also goes to Ms. Barbara Robertson for being there for me throughout my stay in Rolla. Also I am grateful for the assistance of Ms. Judy Russell and Ms. Shirley Hall. I will also like to mention Dr. Ying Li for her encouragement and assistance.

I am grateful to my loving wife Carla, for her endless support and encouragement throughout this endeavor, and for being always there for me and making our stay in Rolla enjoyable.

I am thankful to my parents and sisters for their endless support during my academic pursuit.

TABLE OF CONTENTS

LIST OF FIGURES

Page

LIST OF TABLES

Page

NOMENCLATURE

Symbol	Description
L	Lagrangian L = T – V
V	Potential energy $1/2\,kr^2$
T	Kinetic energy $1/2\,m\dot{r}^2$
R	Dissipation energy $1/2\,C\dot{r}^2$
g	Gravity m/s^2
∇	Gradient function
m	Single particle mass
r	Position vector
$\dot{r}$	Velocity vector
$q_i(t)$	Time dependent generalized coordinates
$\dot{q}_i(t)$	Time dependent generalized velocities
$\ddot{q}_i(t)$	Time dependent generalized accelerations
$Q_j(t)$	External force applied to the system
δ	Dirac Delta
W	Work done on a particle
K_i	Stiffness coefficients of various springs
C_i	Damping coefficients of various springs
$z_i(t)$	Vertical displacements of the various masses
$\dot{z}_i(t)$	Vertical velocities of the various masses

$\ddot{z}_i(t)$	Vertical accelerations of the various masses
$F_i(t)$	Applied forces
$\theta(t)$	Chassis pitch angle
t	Time in seconds
t_0	Initial time in seconds
$[M]$	Mass matrix
$[K]$	Stiffness matrix
$[C]$	Damping matrix
ω	Frequency of oscillation
ω_n	Natural frequency (rad/sec)
f_n	Natural frequency (Hz)
ω_d	Damped frequency $\omega_{di} = \omega_{ni}\sqrt{1-\zeta_i^2}$
ϕ_i	Phase angle $\phi_i = \tan^{-1}\left(\frac{\zeta_i}{\sqrt{1-\zeta_i^2}}\right)$
ζ_i	Zeta, damping ratio $\zeta = \frac{c}{c_c}$
Z_i	Amplitude
λ	Lambda operator $\lambda = \omega^2$
$[M]^{-1}$	Mass inverse matrix
$[I]$	Identity matrix
$[A]$	Dynamic matrix $[A] = [M]^{-1}[K]$
$DET( )$	Determinant of the matrix ( )
β	Rayleigh damping coefficient

α	Rayleigh damping coefficient
$\hat{u}_i(t)$	Eigenvectors, Normal modes
$[P]$	Modal matrix $[P]=\left[\left\{\hat{u}\right\}_i\right]$
$[P]^T$	Transpose of the modal matrix
$[\Omega]$	Diagonal matrix of ω_i^2, $[\Omega]=\lfloor diagonal \quad of \quad \omega_i^2 \rfloor$
$N_i(t)$	$N_i(t)=\sum_{j-1}^{n} u_{ji} F_j(t)$
$q_i(0)$	Initial displacement
$\dot{q}_i(0)$	Initial velocity
τ	Random time in seconds
RHS	Right-hand-side of an equation
LBP	Low back problems
CG	Center of Gravity of the sprung mass
m_0	Unit mass of the soil
m_1	Mass of the body of the truck
m_2	Mass of the chassis of the truck (sprung mass)
m_3	Mass of the suspension system of the truck
m_4	Mass of the cabin of the truck
m_5	Mass of the seat of the truck
m_6	Mass of the seat
a	Distance between the body connection and the CG of m_2

d	Distance between the rear wheel/tire assembly and the CG of m_2
e	Distance between the front wheel/tire assembly and the CG of m_2
f	Distance between the cabin connection and the CG of m_2
K_{2r}, C_{2r}	Rear tire–sprung mass connectivity Stiffness constant and damping coefficient
K_{2f}, C_{2f}	Front tire–sprung mass connectivity stiffness constant and damping coefficient
K_{3r}, C_{3r}	Rear tires stiffness constant and damping coefficient respectively
K_{3f}, C_{3f}	Front tires stiffness constant and damping coefficient respectively
K_4, C_4	Sprung mass–cabin connectivity stiffness constant and damping coefficient
K_5, C_5	Cabin–seat connectivity stiffness constant and damping coefficient

1. INTRODUCTION

1.1. BACKGROUND OF THE RESEARCH PROBLEM

Heavy mining machinery has exposed the human body to extreme conditions that may limit operators' performance and further impact the overall system performance. Large capacity shovels and trucks have been deployed for low-cost, bulk production operations in surface mines around the world. In extreme cases, shovel excavators load large dump trucks with 100-ton passes, as illustrated in Figure 1.1. This high-impact shovel loading operation (HISLO) causes severe truck vibrations that expose operators to whole body vibrations (WBV).

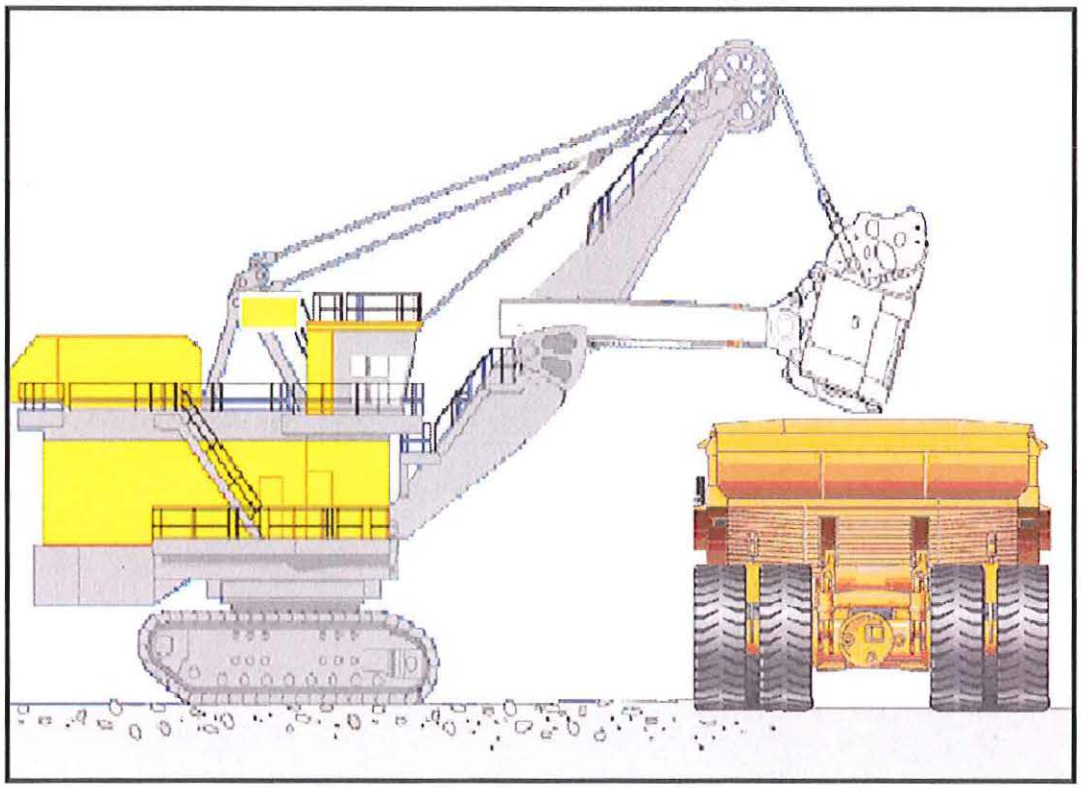

Figure 1.1. High Impact Shovel Loading Operation (HISLO)

The WBV levels may exceed the recommended ISO limits resulting in long-term lower-back disorders and other health problems. This problem has been recognized for a long time in other industries, including agriculture, military, commercial transport and automotive industries. Previous research studies have investigated and developed solutions to the problems associated with machine vibrations, WBV exposure and their effects on operators. These research efforts have concentrated on smaller equipment in these industries, and thus, are limited in their applications to heavy mining machinery. Large-scale surface mining operations feature some of the largest equipment in intense vibration-prone activities, with long-term impact on operators' health and safety.

1.2. STATEMENT OF THE RESEARCH PROBLEM

Haul trucks constitute a significant component of surface mine production costs. The cost data from Syncrude's Aurora mine shows that truck haulage constitutes 26% of the total production cost, as shown in Figure 1.2 (Awuah-Offei, 2005). Hustrulid and Kuchta (1995) have shown that the percentage of loading costs ranges between 3% and 35% based on statistical data from surface mining operations.

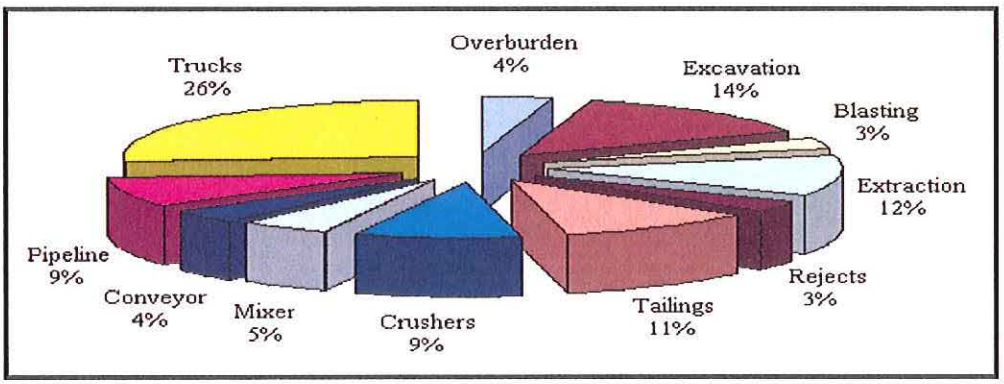

Figure 1.2. Total Production Cost for Syncrude's Aurora Mine

The production costs depend on the capacity of the deployed equipment, with the economies of scale driving large scale surface mining operations towards larger shovels and trucks. Frimpong (2006) also showed that the use of larger trucks significantly reduces the operation costs as compared to a smaller capacity truck, as illustrated in Figure 1.3. For example, the 380-ton reduces production costs by 88% compared to 120-ton truck (see Figure 1.3).

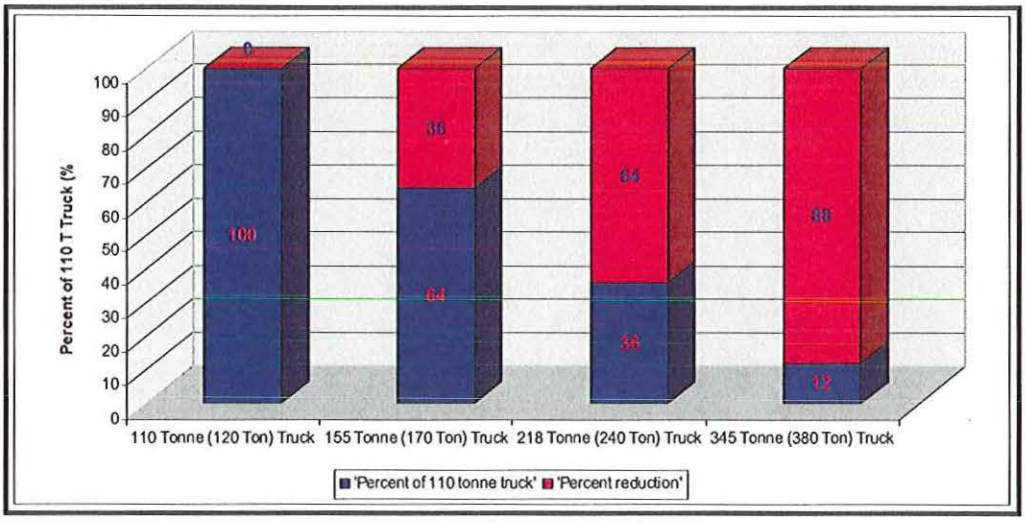

Figure 1.3. Percent Reduction in Operation Cost for Various Trucks

Technological advancements have made the shovel-truck system a more flexible, economic and productive method for surface mining operations. Figure 1.4 shows productivity comparisons for various dump truck capacities. The figure shows that the truck productivity (in BCM per hour), for a 380-ton truck, increases by exactly 4 times compared with that of a 120-ton truck (Frimpong, 2006). Thus, it can be concluded that larger trucks, matched with larger shovels, are by far more economic than smaller trucks and smaller shovels, even though larger equipment is more capital- intensive.

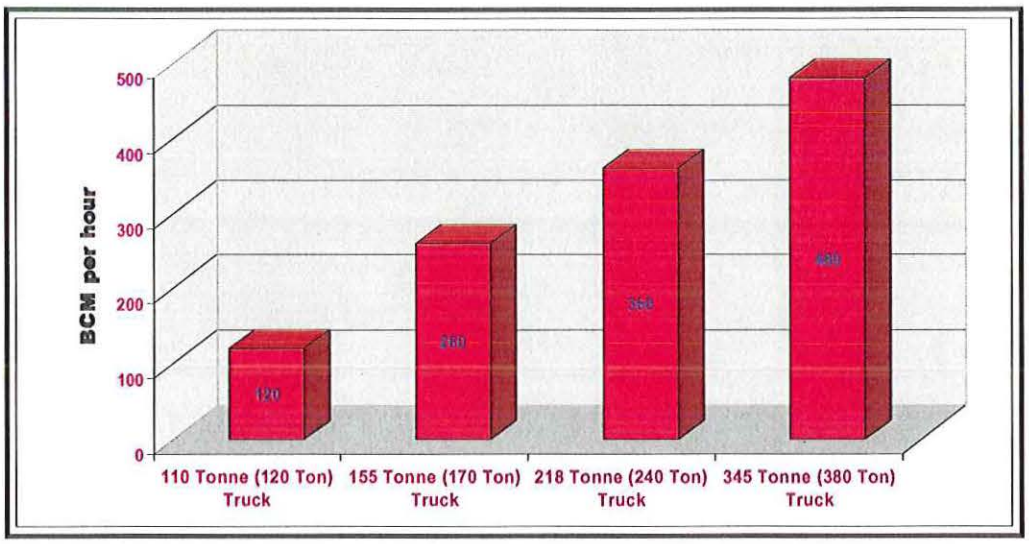

Figure 1.4. Comparisons in Truck Productivity for Various Trucks

Large-capacity shovels load large-capacity dump trucks with over 100-ton passes under gravity dumping conditions. The gravity dumping of large tonnage passes creates large impact forces on the truck machinery, and thus, generates high frequency shockwaves. These shockwaves are propagated through the dump truck body, chassis, and cabin and to the operator's seat. In most cases, the operator's lower torso, lower back, legs, feet and hands are exposed to these high-frequency shockwaves. This experience is termed *whole body vibration (WBV)* in machinery vibration and control mechanics.

The International Standards Organization (ISO) provides recommendations on safe limits beyond which long-term exposure could cause lower back problems and other long-term disabilities. The applicable ISO standards in vehicular vibrations include Sections 1, 2, 4 and 5 of ISO 2631 (1997, 2003, 2001 and 2004). Section 1 constitutes the general requirements for evaluating human exposure to WBV. Section 2 constitutes

human exposure to WBV and shock in buildings with respect to comfort and annoyance. Section 4 constitutes the guidelines for evaluating the effects of vibration and rotational motion experienced by humans in fixed guideway transport systems. Section 5 constitutes the methods for evaluating multiple-shock mechanical vibrations. These sections provide specific standards for meeting critical thresholds for the safe operations of vibrating equipment. Whenever the upper critical thresholds of the uncomfortable and extremely uncomfortable regions are exceeded, operators are exposed to severe vibrations, which may affect their health in the long term. These severe conditions may require fundamental and applied research to determine HISLO vibration levels, their comparisons to the ISO limits and the safety of operators.

The introduction of large capacity off-highway dump trucks, such as the CAT 793 and 797 series with corresponding large shovel excavators, such as, P&H 4100TS, 4100BOSS and 4100XPB has brought to the forefront the problems associated with machine vibrations, WBV exposure and their effects on operators in large scale surface mining operations. These HISLO problems are well known in the mining industry, and companies, such as Phelps Dodge/Freeport-McMoRan, Rio Tinto, Syncrude and BHP Billiton, have initiated applied research programs to mitigate their effects. Previous studies have dealt with the vibration problem by designing ergonomic seats with no emphasis on the source of machine vibrations. As a result, HISLO problems persist, and require advanced fundamental and applied research programs for their solutions, with input from academia, manufacturers and the mining industry. This research initiative is a pioneering effort towards developing practical solutions of HISLO problems in surface

mining operations. The research findings will further extend the HISLO research frontier and create the basis for developing potential technologies for improving workplace safety, operators' performance and total system efficiency.

1.3. RESEARCH OBJECTIVES AND SCOPE

The primary objective of this research study is to provide understanding into HISLO problems, and to formulate a theoretical basis for potential technologies that could reduce vibrations and/or attenuate their impact on operators and improve production efficiency. The elements of this primary objective include: (i) modeling and analyzing of the mechanics of HISLO vibrations; (ii) developing virtual prototype simulator of a 3D multi-body dump truck vibrations model; (iii) developing a dynamic model that will serve as a guidance to modify the truck design to absorb the shockwaves beyond the ISO standards; and (iv) minimizing truck fatalities and long-term operator injuries in the workplace.

This research study is limited to the high impact shovel loading operation (HISLO) in surface mining operations. The study focuses on the CAT 793 series and their corresponding shovel excavators. However, the theoretical underpinnings of this study can be applied to other mining trucks and equipment. The corresponding shovel excavator is matched with a haul truck such that three to four shovel passes would fill the haul truck in a given application. The number of passes is only constrained by the rated truck capacity and the loose density of the loaded material (Frimpong et al., 2007). The HISLO research study is further divided into several dimensions that provide

comprehensive solution strategies to the underlying problems. These dimensions include the dumping process, the generation and propagation of high-frequency vibrations through the truck machinery, the truck tire-ground interactions at the oil sands operations where the ground is affected by the weather conditions, operator cabin and seat vibrations, and comparisons with applicable ISO standards.

1.4. PROPOSED RESEARCH METHODOLOGY

This research will combine the use of analytical survey of the required literature, mathematical, numerical and dynamic modeling techniques to build virtual prototype simulators for studying the HISLO problem. Verification and validation processes, as well as, experimental design and experimentation of the virtual prototype simulators, will be used to obtain relevant results for studying the HISLO problem. Critical review and analysis of the relevant literature will provide the current body of knowledge and the research frontiers in heavy mining machinery vibrations and WBV exposures vis-à-vis the recommended ISO limits. This process ultimately places the research study at the frontiers of this research paradigm and provides a rationale for the PhD research. Mathematical models will be developed to capture the dumping process, the generation and propagation of high-frequency vibrations through the truck machinery, dump truck tire-ground interactions and the operator cabin and seat vibrations.

The main cause of truck vibrations is the large impact force in the HISLO process. The impact force is modeled as a function of the increment in mass and the initial velocity of the material. It mainly depends on the physical and mechanical

properties of the dumping material, shovel operating conditions and the prevailing environmental conditions. The material properties include density, water content, cohesion and fragmentation. The shovel operating conditions include the shovel dipper/bucket size, dumping height and time, dumping process, loading method and shovel-truck interactions. The environmental conditions include the terrain conditions, space limitation and operator visibility. A time-dependent dynamic impact force function will be generated as a function of material, shovel operating and environmental conditions. The Lagrangian formulation is employed to generate the equations of motions governing the vibrations of the haul truck components. The dynamic modeling will capture the 3D components of the forces, moments, displacement and accelerations on the haul truck during the HISLO.

The resulting coupled second order ordinary differential equations, with appropriate boundary conditions, governing the multi-degrees of freedom HISLO system will be solved using numerical methods in the MAPLE® software (Maplesoft, 2006). The results of the numerical modeling techniques will provide a basis for designing comprehensive virtual prototype simulators for the HISLO problem. The virtual haul truck prototype simulators will be verified, validated and simulated for various HISLO experiments within the MSC.ADAMS® software (MSC Software, 2007). Detailed WBV measurements of an operator, as well as, seat, cabin, chassis and body vibrations will be carried out for extended simulation run times under different HISLO conditions. The models will be validated with the existing field data collected at Syncrude's oil sands operations in Canada (Kumar, 1999). The WBV and seat vibrations measurements will

then be compared with the ISO recommended standards for heavy mining machinery use over the normal shifts in surface mining operations. Detailed analysis of the simulation results will provide knowledge on: (i) WBV exposure within the allowable ISO standards; and (ii) the optimized set of HISLO parameters that minimize WBV exposures.

1.5. INDUSTRIAL AND ACADEMIC CONTRIBUTIONS

This research advances the heavy mining machinery vibrations frontier and contributes immensely to the body of knowledge on machinery vibrations under HISLO conditions. The overall truck vibration under HISLO conditions, the 3D multi-body dump truck dynamic models, and the 3D vibrations propagation have previously never been carried out to provide solutions to HISLO problems. The research study is a pioneering effort toward developing the dynamic models for the HISLO problem. It also pioneers the development of 3D virtual prototype simulators for simulating the HISLO problem under different operating paradigms and conditions. The use of the MSC.ADAMS software environment provides appropriate industry standardization that allows easy modification, transformation and advancement because of the wide use of this software by several industries. The results of the research study will provide a basis for developing technologies to improve workplace safety and operators' health and safety in surface mining operations. The derived technologies could save the surface mining industry significant energy and human safety liability costs resulting in competitive and growing companies. The results could maximize machine availability, minimize maintenance costs, and maximize production economics.

1.6. THE PHD PHILOSOPHY

The dump truck must be fully understood in terms of its elements, dimensions and how the vibration shockwaves propagate in order to solve the vibrations problem under HISLO conditions. This section illustrates the vibration dimensions and propagation, as well as, the system suspensions that support the truck weight and reduce the vibration propagation. The analytical philosophy and procedures associated with the dump truck vibration model have also been described to provide understanding in to the fundamental basis of this research study.

1.6.1. Vibration Dimensions and Propagation. The truck vibration mechanics constitute a 3D problem in the x-, y- and z- directions. The shockwaves are predominantly in the z-direction, because the input force has amplitude in the z-direction due to the free-falling material under gravity. Thus, the z-components of the displacement, velocity and acceleration vectors are computed in the theoretical analysis. The x- and y- components are retained in the virtual prototype truck model even though they are small compared to the z-components. This is done in order to guarantee the completeness and accuracy of the simulation results.

The shockwaves are generated by a non-periodic force. This source of vibration is impulsive and shock loading in nature. The terrain conditions are included to recreate simulated environments similar to actual mining environments. The Syncrude's Athabasca oil sands operations in Canada are used in this study (Kumar, 1999). This terrain absorbs part of the shockwaves and its properties are dependent on the weather

conditions. The winter conditions are selected where the roads and loading areas are totally frozen. This condition creates the worst case scenario because the very hard surface reflects most of the upcoming shockwaves back to the truck structure. This worst case scenario will automatically satisfy all the other terrain conditions, such as mushy conditions, where the terrain has a positive effect on the overall vibration absorption.

1.6.2. System Suspension. The truck suspension systems consist of a set of spring-damper systems, as well as, rubber contacts between other components of the truck. This suspension system is a hybrid hydraulic-pneumatic system. It uses oil-over-nitrogen struts to dissipate haul road and loading impacts for longer frame life and a more comfortable ride. The suspension consists of four independent self-contained cylinders with variable rebound. The front cylinders are mounted to the frame and serve as steering kingpins for a tight turning radius with excellent maneuverability and low maintenance. The rear cylinders allow axle oscillation and absorb bending and twisting stresses caused by uneven and rough haul roads rather than transmitting them to the main frame. The rear axle is connected to the frame via four-bar linkage. The linkage directs the load onto the frame allowing it to be spread through the structure (Caterpillar, 2007).

The spring-damper model introduces limitations in the analysis and simulation due to the lack of exact dimensions, stiffness and damping coefficients. Therefore, the virtual simulation will be validated using available data for commercial trucks (Trangsrud et al., 2004) and data from Caterpillar (2007). Alternatively, the analytical study is totally

symbolic. The symbolic formulation is a generic model for capturing vibration propagation under HISLO conditions for any truck type and model.

1.6.3. Analytical Philosophy and Procedures. This research provides an analytical tool to determine the intensity of vibrations reaching the operator under HISLO conditions. The analytical model, as well as, computer simulation model is built using the multi-body system concept that captures the truck vibrations in the vertical direction and 3D space, respectively. The solutions are generated to isolate the high frequencies without the need to conduct a physical experiment on the field that can be very costly. The simulation models capture the 3D dump truck vibrations under HISLO conditions and create the basis for understanding truck vibration generation and propagation.

The truck is treated as a sum of the different masses within its exterior envelope. Each mass has its own center of gravity (CG) and represents a component of the truck structure. The mathematical model is derived from the physical truck model based on a free body diagram of the truck and its corresponding applied forces. This mathematical framework is essential because it provides the analyst with a systematic approach for deriving the equations of motion (EOM) and for classifying the active and reactive forces. These forces are responsible for the translational and rotational motion of the truck components. The assumptions underlying this study include: (i) small displacements and rotations during vibrations relative to the truck dimensions; (ii) linear spring vibrations; and (iii) viscous damping system.

Newton's second law of motion is widely used to derive EOMs, but it becomes cumbersome for a system having multi-degrees of freedom, as in the case of the HISLO problem. Quite often, energy methods are used because they are simpler, and they reduce vector field problems to scalar problems. The benefit of using Euler-Lagrange equations is that, by choosing the appropriate generalized coordinates q_i to exploit symmetries in the system, one can reduce the number of unknown variables. The Lagrange's energy approach is used for the general derivation of the governing equations in this study. Once the EOMs are established, the differential equations are solved using homogeneous and particular solution methods. First, the undamped free vibration problem is solved by setting the RHS side of the EOMs equal to zero, and thus, eliminating damping from the system. This results in a homogeneous solution with the natural frequencies of vibration. The particular solution is obtained for the damped forced vibration problem. The complete solution of the problem consists of adding the homogeneous and particular solutions together and finding the arbitrary constants based on the initial conditions available for the HISLO problem. These initial conditions consist of the displacement, velocity and acceleration being equal to zero, which means that the truck is at complete rest prior to loading.

1.6.4. Dump Truck Vibration Model. The generalized Lagrange's formulation is used as the basis for the generation of the EOMs for truck vibrations under HISLO conditions. This dump truck vibration model consists of five major parts, as well as, ground conditions. The major truck parts are the body of the truck where the material is

dumped, the chassis that includes the frame and part of the suspension system, the tires/wheels assemblies, the cabin, the operators' seat and the ground. The applied forces on this structure are function of space and time. The results allow the designers to isolate the different mode shapes of vibrations generated by the HISLO. These results create a basis for truck design and modeling of the fixtures and dampers in order to filter out the unacceptable frequencies and maintain the harmless frequencies that have no effect on the operators' health and truck structure.

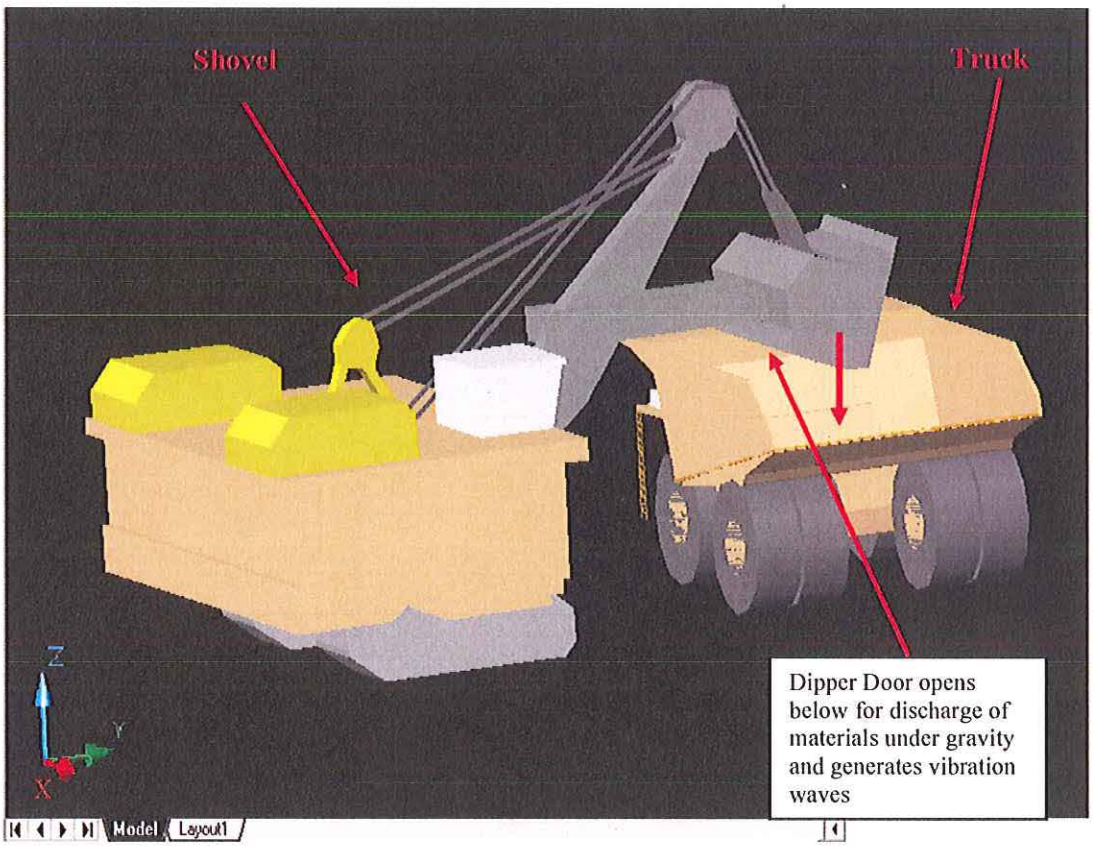

Figure 1.5. High Impact Shovel Loading of a Dump Truck in Surface Mining

Figure 1.5 illustrates the layout of the high impact shovel loading operation (HISLO). The shovel dipper/bucket holds at least 100 tons of materials and the dipper door opens to release the material in a free fall under gravity into the body of the truck. This HISLO generates shockwaves that propagate throughout the chassis causing severe truck vibrations that expose operators to whole body vibrations (WBV). These WBV levels may exceed the recommended ISO limits resulting in long-term lower-back disorders and other health problems.

1.7. STRUCTURE OF THE PHD DISSERTATION

Chapter 1.0 contains an introduction to the PhD dissertation. The introduction lays the groundwork by providing the underlying HISLO problems in large scale surface mining operations, the objectives and scope of the research study, the research methodology and its scientific and industrial contributions. Chapter 2.0 provides a critical review and analysis of the relevant literature and provides a rationale for the PhD dissertation on the current frontiers of the HISLO domain. Chapter 3.0 contains the mathematical models of the HISLO problem using the generalized Lagrangian formulation of a 9-DOF truck vibrations model. Chapter 4.0 illustrates the numerical modeling techniques and the analytical solutions of the 9-DOF truck model. Chapter 5.0 presents the 38-DOF virtual prototype model of the HISLO in the MSC.ADAMS environment and outlines the constraints and limitations of the virtual models. Chapter 6.0 presents the virtual prototype model validation and the parameters determination used for the simulation analysis. It also contains the experimental results that are used for validating the simulation models. Chapter 7.0 presents the virtual prototype simulation

results and comparing them with the experimental results, followed by a discussion of the simulation results. Chapter 8.0 summarizes the findings and presents the conclusions, contributions of this PhD research, as well as, the recommendations for future work. The appendices contain the detailed analysis and formulation of the vibration problem and the solution components. It also contains the complete simulation results, such as the displacement and velocity fields of the truck model components. The references that have been used during the study and the development of the solution of the mechanics of dump truck vibrations under HISLO conditions are listed at the end of this dissertation.

2. LITERATURE REVIEW

This chapter covers a comprehensive review of the literature underlying the research in the mechanics of dump truck vibrations during high impact shovel loading operations (HISLO). This review covers the previous work done in the vibration field and the associated machinery, the whole body vibration (WBV) analysis, and the generalized Lagrangian formulation of vibration. All the symbols, signs and abbreviations used in this Chapter are defined in the Nomenclature Section of this dissertation.

2.1. WHOLE BODY VIBRATION

The whole body vibration (WBV) has significant effect on human health in earthmoving operations. Though these effects are recognized, Griffin (2004) noted that the exact mechanisms underpinning the specific effects require advanced research initiatives to provide appropriate solutions to the associated problems. The WBV problem is experienced by operators of transport machinery and excavators that involve vibration frequencies ranging from 0.5 to 80 Hz. This section will focus on WBV exposures in earthmoving equipment operations, seat design and ergonomics in various applications to provide a basis for understanding the significance of this research study.

Lagrange (1788) carried out a seminal work on vibration. He reformulated Newtonian mechanics by creating Lagrangian mechanics from his results on the application of the calculus of variations to mechanics. The Lagrangian formulation of vibration, widely used to solve various vibration problems, is given in equation (2.1).

$$\frac{\partial L}{\partial q_i} = \frac{d}{dt}\frac{\partial L}{\partial \dot{q}_i} \tag{2.1}$$

Along with Lagrange, Ramazzini (1713) noted that a pervasive form of the stress evoked in humans is WBV, which manifests when vibrating surfaces support the human operator. Hence, the typical vibration mechanism on performance is direct, through mechanical perturbation when it is transmitted to and dissipated within the body. As a result, vibration influences several aspects of performance including sensory and response processes. It also affects an individual's information processing and adaptive process abilities and any attempts to cope with the ambient environment.

In his extensive work on human vibration, Griffin (1990) studied the WBV exposure from a vibrating surface. This mostly occurs when a body comes into contact with a vibrating seat, floor, or body. Furthermore, Kjellberg (1990) concluded that WBV does not have one specific target organ, but rather a variety of health problems. These include backaches, gastrointestinal, reproductive system, visual and vestibular disorders. Aantaa et al. (1977) also analyzed the permanent effects of low frequency vibration on the vestibular system. Seidel (1993), Bovenzi and Hulshof (1999), and Kittusamy and Buchholz (2004) carried out extensive work and provided models, with results that corroborate previous work in these areas.

Kitazaki and Griffin (1998) showed that the body harmlessly attenuates most vibration effects. However, frequencies between 1 and 20 Hz cause the body, specifically, the pelvis and spine to resonate leading eventually to structural damage and

health problems, including lower-back pain, spinal degeneration, gastro-intestinal track, neck and sleep problems, headaches, autonomic nervous system dysfunction, hearing loss, and nausea. Beevis and Foreshaw (1985) and Shwarze et al. (1998) showed the evidence of inter-vertebral disc problems and degeneration of spinal vertebrae in this frequency zone.

Eger et al. (2005) measured the WBV exposure levels at the vehicle and operator seat interfaces, during the operation of both small and large load-haul-dump (LHD) vehicles. The results were compared to the ISO 2631-1 health guidance caution zones to determine safe exposure durations. These results indicated that the tested LHD operators were exposed to high WBV levels that exceeded the recommended ISO 2631-1 exposure guidelines, putting them at risk for long-term injuries. The magnitudes of the vibration signals were high in all axes for large LHDs, with the highest magnitudes between 0.89 - 1.18 m/s^2 in the z-axis. In smaller LHDs, the highest vibration magnitudes were observed in the x-axis, with the maximum vibration magnitudes between 0.55-0.64 m/s^2.

Kittusamy (2002) undertook an ergonomic evaluation of excavating operations to provide an understanding into musculoskeletal epidemiology and workstation design. The main objective was to systematically characterize the ergonomic hazards associated with excavating operations. Using pilot experimental analysis, the study showed that the digging and hauling operations had higher levels of total weighted acceleration than idling. The study also showed that the seats were not designed to protect the operator from long-term effects of vibration levels. Kittusamy et al. (2002 and 2004) extended the

previous study into awkward postural requirements. The study showed that heavy construction equipment operators are afflicted by musculoskeletal injuries of the arms, shoulders, neck and lower back. They concluded that WBV and the postural requirements are important risk factors that contribute to the development of the musculoskeletal disorders.

Kittusamy et al. (2003) compared NIOSH-designed seats to the existing seats on underground haulage vehicles. The NIOSH-designed seats incorporated ergonomic design features ranked most favorable for comfort and vibration reduction. The NIOSH-designed seats were found superior to existing seats based on operators' experience, visual analog scale (from VAS) and measured data. Kittusamy et al. (2005) also evaluated the effectiveness of a continuous passive motion system for reducing low back discomfort among operators of heavy earthmoving equipment. The results showed that this design could effectively reduce this problem significantly.

In military applications, Pope et al. (1985) conducted a study on the Black Hawk helicopter and showed that vehicle vibrations produced significant discomfort in the lower back and buttocks of operators. The general recommendation was to use cushioned materials, which minimize the transmission of the vibration to the operator. VanIngen-Dunn and Richards (1992) also found substantial reports of low back pain and general discomfort after about four hours of flight in both the Army and Air Force Black Hawk helicopter pilots. Smith (1996) used driving point impedance and transmissibility techniques to evaluate the effects of military helicopter seat cushions on human body

vibration response. Small females (5%) and large males (95%) were exposed to vibration frequency range of 3 to 21 Hz at 0.59m/s^2 RMS (0.06g RMS).

Rigid mass tests showed that single resonance frequency and the associated peaks were significantly lower for the prototype cushioned seats versus the current inventory cushioned seats. Moreover, there were significant differences in the stiffness and damping properties between the two tested cushioned seats. Smith (1998) showed that the prototype cushioned seats were less stiff with greater vibration attenuation capability compared to the current inventory cushioned seats. The most dramatic effects in humans were observed between 4 and 6 Hz for peak head and spine transmissibilities, with the use of the prototype cushioned seat. Both the inflated and deflated seats significantly increased the peak head and spine transmissibilities in females, while attenuating that in males compared to the current rigid cushioned seat.

Rosen and Arcan (2003) modeled the human body-seat system in a vibrating environment along the X, Y and Z axes. The study showed that the resonance frequencies and apparent mass modulus, with a backrest, were higher than the corresponding parameters of the first mode without the backrest. Experimental measurements showed that the first mode of vibration appeared to arise from a motion of the whole upper body. The second mode arose from the horizontal response of the musculoskeletal system, in which the buttocks and the hips were out of phase with the shoulders. The model along the Z axis was based on the database from Fairely and Griffin (1989), and it correctly simulated the experimental data, with a resonance frequency of 4.25 Hz and a normalized

apparent mass modulus of 1.5. The operators exposed to 0.25-2m/s^2 vibration magnitudes were using their lower back muscles to control the movement of the upper body according to Fairely and Griffin (1989).

A study conducted by Harrer et al. (2005), at the Naval Medical Center on MH-60S pilots, found that pilot fatigue is a concern due to the increased frequency of extended durations of missions (6 to 8+ hours). Current seats are designed primarily to meet crashworthiness requirements, not for the wide range of pilot anthropometry or to mitigate WBV. Current Hazard Reports (HAZREP) indicate that the pain in both pilots' legs and backs begin 2 to 4 hours into a flight and increases with time. Situational awareness also decreases with increasing flight duration due to the constant distraction of pilots shifting in their seats. Froom (1987) reported a dose-response relationship between the length of military helicopter flights and back discomfort. He also concluded that this pain is typically dull, over the lower back, and its prevalence and intensity are dependent on the total flight hours of exposure.

The study evaluated WBV produced in the pilot seating systems onboard the MH-60S and compared the effectiveness of three different seat cushions, the current seat cushion versus two anti-vibration seat cushions A and B. The results showed that, in the z-axis at 16 Hz, anti-vibration seat cushion A outperformed the MH-60S's current seat cushion and the anti-vibration seat cushion B by exhibiting significantly reduced vibration levels. The results also showed that pilots of the MH-60S could operate the helicopter with the current seat cushion for less than 6 hours and the anti-vibration seat

cushion B for approximately 8 hours without being overexposed to WBV. Since the average flight during a deployment or mission could last up to 8 hours, the current exposure places the pilots at an unacceptable risk of injury, lack of mission readiness, and possible equipment damage.

Dhingra et al. (2003) showed that the human-seat interface pressure on soft seats is more evenly distributed on a larger effective contact area than on a rigid seat. The pressure distribution on a seat is affected by the seat height, posture, type of cushion and the vibration frequency. The increase in vibration excitation causes increased maximum pressure and maximum effective contact area around the resonance frequency of between 4.5 and 5.0 Hz. Yoshimura et al. (2005) studied the human response to vibration as a multi-body dynamics model of a seated human body under WBV exposure for assessing vibration risk. The vibration transmissibilities from the seat surface to the spinal column and to the head were measured during the exposure to the vertical half-sine input excitation. The results showed that the dynamic characteristics of the human body can be approximated to a linear viscously damped system under exposure to a stationary random excitation.

Hopcroft and Skinner (2005) investigated the human vibration in the cargo compartment of the C-130J-30 Hercules aircraft for the Australia air force. The results showed that the high vibration zone (HVZ) is located in the cargo compartment, more particularly in locations near the plane propeller. They concluded that passengers who

will be required to undertake high risk military operations, e.g., air-drop and combat air-land operations should not be seated in the HVZ for prolonged periods.

McDowell et al. (2006) carried out an investigation into WBV exposure of operators using vibration hand tools. The study concluded that these operators have the potential for developing health problems associated with repeated forceful actions and exposures to hand transmitted vibration. The results showed that vibration exposure significantly affected grip and push force-recall accuracy. The vibration effect was particularly pronounced with vibration exposures between 31.5 Hz and 63 Hz. This frequency range coincides with that of hand-arm system resonance.

2.2. VEHICLE VIBRATION AND PROPAGATION

Occupational exposure to whole body vibration has long been associated with increased incidence of low back pain and low back injuries. Machinery vibration affects the human operator with damaging effects. Hence, this section will cover the work done in the field of vehicles vibration and their propagation. The vibration magnitude and frequency along the z-axis vehicle seat are time-variant, which are influenced by not only vehicle vibration characteristics themselves but also road surfaces, speeds and the human operator.

Yaguchi et al. (1994) have proposed a method to evaluate automobile seat vibration that is based on judgments using a subjective mental state for a whole body vibration and operating comfort. Their method focused on the time-variant magnitude of

the peak frequency on a power spectrum density. Suzuki (1997), in his study on the vibration factors determining the riding comfort of railway vehicle, has emphasized that vehicle vibration should be judged by a series of vibration stimuli. This reasoning is due to the fact that vehicle vibration is time-variant and not a matter of the relationship between a single vibration stimulus and a subjective response. It also showed that the relationship between the frequency-weighted RMS acceleration calculated and the vehicle vibration discomfort every five seconds. This study clarified that the human perceptions of vehicle vibration discomfort changes every moment.

Fries et al. (1993) conducted a study on eight freight locomotives. The majority of the vibration levels did not exceed the "fatigue-decreased proficiency boundary" set forth in the ISO 2631-1 standard. The highest vibration occurred in the vertical direction. A more recent study by Johanning et al. (2002) focused on locomotive vibration where they assessed 22 U.S. locomotives. Their results showed that the weighted seat pan acceleration ranged from 0.07 to 0.15 m/s^2 RMS in the x-direction, from 0.15 to 0.30 m/s^2 in the y-direction, and from 0.36 to 0.63 m/s^2 in the z-direction.

Kittusamy (2003) has studied the cab design of construction equipment and generated a checklist for evaluating the existing design. His results showed a relationship between awkward posture and development of fatigue and musculoskeletal disorders, which has been reported in the laboratory. He generated a checklist to help the diagnosis of poorly designed cabs and work procedures that are causing the fatigue problems. Furthermore, Kittusamy (2003) generated a biomedical model of spinal loading due to

jarring and jolting of heavy equipment operators. He assessed the risk of low back disorders due to occupational exposure to jarring and jolting. The proposed model and evaluation methods provided a satisfactory way of evaluating the effectiveness of various interventions.

Winthrop (2004) studied the nonlinear behavior of variable stiffness concepts. He pioneered the solution of the damped single degree of freedom variable stiffness-initial value problem using a general on-off control law. The purpose of his research was to extend semi-active control vibration isolation tools and methods, for applications in space launch and on-orbit systems. The exact solution was used to develop an approximate viscously damped system, which can reasonably reproduce the true system. It was discovered that it is possible to switch the system between under-damped and over-damped states, removing significantly more energy from the system than a viscously damped system could by itself. His results can be used to measure efficiency of real devices.

Krüger et al. (2004) stated that military and civil off-road vehicles are subject to large vibrations that have severe affects on drivers, crew and load. The operating quality is influenced by vehicle vibrations, which may be induced by a variety of sources including roadway roughness or off-road terrain. The vibrations may also be internally generated forces produced by vehicle subsystems, such as engine, or suspension mechanisms of weapons. Both short but high vibration peaks, as well as long-duration, high frequency vibrations can pose either disorientation and safety problems or a health

threat to passengers of a vehicle. In their study, they evaluated the active damping for reduction of noise, vibration and motion of ground vehicles by multi-body simulation. The results of this study showed that the active damping suspensions are able to reduce vertical vibrations of a vehicle. The technology has reached maturity and finds its widest application in luxury cars. Furthermore, prototypes exist for use in military land vehicles, railway vehicles and aircraft landing gears, and the solutions have shown the potential of semi-active suspensions in these fields.

Bohn et al. (2004) studied the effect of the usage of active vibration control in engine mountings to improve the vehicle ride comfort and achieve reduction in noise and vibration levels. The results of the experiment showed that the engine firing orders 2, 4 and 6 are predominant at idling speed without active control. However, a significant reduction of up to 37 dB in these engines can be achieved by using the active vibration control. Moreover, the measured steering wheel acceleration for a constant drive at 4400 RPM showed a significant improvement of the vibration and noise levels with and without active vibration control mountings.

Hoy et al. (2005) studied the risks from WBV and posture for low back pain among forklift truck drivers. The measured vibration exposures suggested the presence of severe shock loading. The results indicated that WBV acts associatively with other factors, not independently to precipitate the low back pain. The results compared to ISO 2631 showed that acceptable levels of vibration exposure (i.e., below 0.5 m/s^2) are generated by forklift trucks in the x- and y-directions, but not in the z-direction (0.73

m/s^2) with a peak ranging between 1.24 and 24.46 m/s^2. The results also showed that the axial vibrations tended to occur with frequencies between 5 and 7 Hz.

Nakashima et al. (2006) have proposed a method of evaluating vehicle seat vibration with consideration of subjective judgment. They applied the method for the vehicle seat z-axis vibration considering the time-variant, on the hypothesis that the final subjective evaluation must be conducted from the judgment summarizing a series of vibration stimuli. The results showed the discomfort by four subjects matched up to the frequency-weighted RMS acceleration calculated every five seconds. The experiment was carried out on the right side of a vibrating bench using the floor vibration with acceleration of 0.822 m/s^2 over the range 0.5-20 Hz with four male subjects and four suspension seats.

Mayton et al. (2006) focused on the seat designs for the mid-coal seam shuttle car and compared subjective comfort data collected from five operators. This study was based on the ISO 2631 reduced comfort boundary (RCB) analysis of recorded vibration levels. The results showed that operators sensed from 45 to 87% less discomfort with NIOSH seat designs compared to the existing seat design. The RCB analysis during no-load operation showed that NIOSH seat designs, compared to the existing seat design, generally provided an increase in allowable exposure time for the vehicle operator, in the 4 to 8 Hz range. During full-load operation, the RCB analysis showed little difference in allowable exposure time for either the NIOSH or the existing seat designs. Their study also showed that foam or air-filled tires provide primary damping or attenuation of jars

and jolts when the vehicle mass is increased with the full load of coal. Seat performance in attenuating of jars and jolts is thus secondary.

Smith et al. (2006) conducted a study to evaluate the transmissibility characteristics of occupied suspension seats in multi-axis vibration environments using locomotive seats due to several reports of back pain from locomotive engineers. Exposures included a flat acceleration spectrum and two signals extracted from locomotive floor data. The results showed that transmissibilities have minimal off-axis contributions to the seat responses, but were evidenced at the chest and head for the flat spectrum exposure. The locomotive floor showed a concentration of vibration in the frequency range below 10 Hz with notable peaks occurring around 1.5 to 2.0 Hz, particularly in the fore-and-aft X direction of the seated occupant. The most notable peak transmissibilities occurred in the X and Z directions with values between 2 to 3 Hz and 3 to 3.5 Hz respectively. For the exposure in the Y direction, the peak seat responses occurred in the vicinity of the peak Y locomotive vibration that ranges between 5.5 Hz to 9.0 Hz.

Gibson et al. (2006) conducted WBV analysis aboard seven commercially available passenger and/or recreational vehicles. The vehicles included sedan; sport-utility vehicle (SUV); pickup truck; moving truck; motorcycle; all-terrain vehicle (ATV); and boat. The purpose of the test was to measure and assess WBV exposure in a range of typical vehicle environments in order to gain understanding of typical exposure levels characteristic of normal day to day activities. All vehicles were tested with their standard

factory-installed seats and were operated under a range of normal operating conditions and speeds typical of intended vehicle use. The results showed that the acceleration felt by the sedan, SUV and pickup truck ranged between 0.30 m/s^2 to 0.38 m/s^2 in the Z direction. The acceleration of the moving truck, motorcycle, ATV and boat ranged between 0.53 m/s^2 to 1.02 m/s^2 in the Z direction.

2.3. VIBRATIONS MONITORING AND CONTROLS

The presence of vibration in earthmoving machinery or any piece of equipment requires the search for approaches and techniques to monitor and control the harmful levels of vibration. This section will focus on the effort that has been done in this area in terms of research and experimentation in order to lower the risk of injuries and exposure to vibrations and maintain a level of comfort while operating these machines.

Aldinger et al. (1995) found in their study on surface coal mining that equipment operation was the most common category of accident for haulage trucks (46.3%). The most common type of equipment operation accidents was jarring (37.7%), which results in back injuries of haulage truck drivers. Therefore, with the presence of vibration and its effect to human body, ideas and techniques were developed to control and minimize the amount of vibration reaching the operators of earthmoving machineries. There are different ways to control the vibration in machinery; the most common are the passive and active controls. Singh and Ram (2000) studied the dynamic absorption by passive and active control methods. The results of their analysis showed that the steady state motion of a viscously damped vibrating system cannot be totally eliminated by adding a

spring and a damper, i.e., a passive control. On the other hand, this motion may be eliminated by attaching an appropriate damped dynamic absorber, i.e., an active control system, implementing a single sensor and an actuator.

Accelerometers are a practical electromechanical tool to monitor vibrations by measuring acceleration forces. These forces may be static, or they could be dynamic. There are different types of accelerometers. Some of them use the piezoelectric effect. They contain microscopic crystal structures that get stressed by accelerative forces, which cause an electric charge signal proportional to vibration acceleration. Other methods are also available, including the use of the piezoresistive effect, hot air bubbles, and light.

Miller et al. (2000) carried out an investigation on how to control and reduce the jolting and jarring to trucks in surface mining operations. The study suggested that combining acceleration data with information obtained from a GPS could generate results with a variety of uses. The potential results from this research would be useful in providing feedback about equipment operations and identifying unusual causes of jolting. Hence, a data collection system that ties acceleration and GPS location data has been successfully demonstrated at a mine site. Personnel reviewing the data produced can see the acceleration history of the truck and monitors very low-level accelerations and increases functionality.

Later, Miller et al. (2004) developed a device and software called Shox Boxes to be installed onboard equipment that already have a GPS system onboard. The Shox Box

system reviews data in real time, onboard the vehicles, 24 hours a day, and sends pertinent information via radio to a central database. The Shox Box system was prototyped in a surface mining environment and showed to be durable and reliable. The equipment interaction and miles per jolt applications are two of the system's features, which can be readily duplicated in any heavy equipment environment.

Arn (2004) introduced a different type of control method. She designed, built and tested a non-contact vibration measurement and analysis system for electronic board test system. Her system provides a quick, low cost method for capturing multiple points on the test object during vibration testing. The results showed that the system captured the natural frequency and peak displacement of the board's first mode within 1.5% accuracy and 0.7% accuracy respectively when compared with accelerometer testing. This device provides a highly versatile, accurate, and low cost optical alternative to accelerometers. The use of this system eliminates questions of whether the mass loading effects affected the vibration test data by introducing errors, particularly for small specimens.

Law et al. (2004) have developed a system to control the excessive vibration of modern flexible footbridge structures. Analysis on the London Millennium Footbridge showed that the maximum lateral acceleration experienced on the bridge was between 200 and 250 mg. The loading effect has been found to be due to the synchronization of lateral footfall forces within a large crowd of pedestrians on the bridge with a frequency of 2 Hz. Their study resulted in the development of the hybrid slotted bolted connection element that constitutes a frictional damper and two truss elements. The stiffness of the

connection element changes when the load changes in a cyclic manner resulting in energy dissipation through the hysteretic loop. Similarly, damping was reached by energy dissipation in the structure through the hysteretic loops of the dampers.

Friedmann (1997) conducted a research to control the vibration in the Agusta-Westland EH-101 helicopter fuselages, known as the Active Control of Structural Response (ACSR) approach. The results of his study showed that vibrations in the helicopter fuselage were reduced by 0.04g throughout the flight envelope with relatively modest control effort and low control power requirements. He also developed a coupled rotor/fuselage model capable of simulating the vibrations in the fuselage and their control using the ACSR system.

McManus et al. (2002) integrated in their study the magnetorheological (MR) fluid based active damping system into vertical suspension seats widely used in vehicles to isolate passengers from WBV and shock. This active system consists of a controllable MR fluid damper, a control computer integrated with a sensor and three-position ride mode switch offering light, medium or firm damping. The test results showed that the MR fluid damper was able to provide three to four times the amount of damping force compared to conventional units. Moreover, without an application of an electric current, the MR fluid unit acts as a passive vibration absorber.

Choi et al. (2003) have proposed a vibration control method for a landing gear system featuring electrorheological (ER) or magnetorheological (MR) fluids. These fluids

contain non-conducting oils with varying percentage of particles dispersed randomly throughout the oil substrate that exhibit reversible changes in rheological behavior in the presence of a magnetic or electrical field, respectively. During touchdown, an aircraft is exposed to short duration impulsive impact that may lead to structural damage and high dynamic stresses in the airframe, as well as crew and passenger discomfort. The results of their study led to the implementation of an active shock absorber system based on the ER/MR fluid for off-road vehicles, such as the US Army's high-mobility multi-purpose wheeled vehicle or heavy vehicles such as trucks. The simulation results showed that acceleration and displacements were significantly attenuated by MR/ER fluid based landing gear systems regardless of parameter variations such as vehicle mass, viscous damping, impact speed.

Wickramasinghe et al. (2004) investigated techniques to reduce vibration and noise in the cabin of helicopters and propeller aircrafts to improve habitability, effectiveness, and safety for passengers. The main sources of vibration in these aircrafts include harmonic vibrations induced by propeller or rotor, engine and gearbox operation, and structural excitations caused by unsteady aerodynamics. They introduced a novel approach called the smart spring that controls combinations of impedance properties of a structure, such as stiffness, damping, and effective mass. It uses stacked piezoceramic actuators to adaptively vary structural impedance at strategic locations to suppress mechanical vibration. This approach can be used in an effective manner to suppress low frequency vibration and structure-borne noise significantly over a broadband of frequencies. Extensive experimentation using mechanical shaker tests demonstrated the

ability of the smart spring to control impedance properties in an adaptive manner to suppress vibration. The wind tunnel tests demonstrated that the smart spring is capable of suppressing both the vibratory displacement, as well as the reaction force transmitted under unsteady excitation conditions.

Moses (1997) used a 1/16th scale model of an F/A -18 to compare two types of actuators for active damping of buffet vibrations; an active rudder and piezoelectric actuators. When controlling vibrations at the first bending mode using simple gain in a single-input-single-output control scheme, the piezoelectric actuators reduced vibrations up to 60 percent at 37^{o} angle of attack. Hanagud et al. (2005) conducted a study to control buffet-induced vibrations in the vertical tails of F/A -18 aircraft during high angle of attack (AOA) maneuvers. The unsteady vortices, emanating from the wing leading edge where it connects to the fuselage, impinge on the fins and induce oscillatory aerodynamic loads according to Hanagud (2005). The results showed that it is possible to obtain the required control authority for tail buffet alleviation by using piezoceramic stack-based actuators.

Wang (2006) studied the vibration control of mistuned periodic structures utilizing the electromechanical coupling and damping characteristics of piezoelectric networking. He developed an active coupling enhancement approach through negative capacitance to increase the piezoelectric electromechanical coupling. The results of this study showed that the vibration localization level in a mistuned periodic structure can be reduced by using the piezoelectric networking. The vibration level can be further

improved by the negative capacitance and used as an effective means for vibration suppression of mistuned bladed disk systems under multiple spatial harmonic excitations, and are effective for mistuned systems.

2.4. DYNAMIC SIMULATION OF VEHICLE STRUCTURES

Virtual prototype models have shown impressive results and abilities to simulate behavior of complex engineering systems. They make it possible to study the effects of any type of dynamic input for a wide range of systems. Moreover, system variables can be varied in a controlled manner, to optimize the design. The goal is to achieve a higher level product quality at an earlier stage in the development process while using fewer physical prototypes. This is facilitated by the increased computing power and simulation software with increasing predictive capabilities in the last five years.

The increased product quality should be achieved during the early stages of development when physical prototype models are not yet available. This is referred to as frontloading of development activities with analytical predictions at early stages. Computer Aided Engineering (CAE) models present the best approach for upfront prediction of vehicle behavior. Meaningful results can be derived, and projections made, only if the CAE results are correlated against real-world tests.

Barber (1999) has identified the factors that affect the practical application of the Empirical Dynamics Modeling method. He showed how it can be used to generate high accuracy black box models for vehicle suspension components, when both amplitude and

frequency dependencies are present. He listed in his paper the limitations for a successful empirical dynamics modeling, which included repeatable lab test, the choice of input, the black box boundaries, the inertial force measurement and the choice of the coordinate systems.

Wenzhang et al. (2000) have studied the non-linear dynamic characteristic of rubber component in a vehicle dynamics simulation model based on the MSC.ADAMS software and a user written subroutine. The exciting frequency used was 11Hz, the damping ratio was 0.2 and the mass of the component was 245 kg and the dynamic stiffness of the rubber component was found to be 14 kN/mm. The results showed that the effect of linear and non-linear dynamic characteristics of rubber component in a vehicle can be considered in the process of vehicle dynamic analysis. These results indicate that the system will vibrate with a natural frequency of 11 Hz, representing a typical linear one degree of freedom vibration system. For the non-linear stiffness characteristic of rubber component, the results showed that the response frequency is abundance, and peaks at 12 Hz with a displacement of 0.1 mm.

Subramanyam et al. (2000) have developed a methodology for correlating between experimental analysis and analytical dynamic simulation of an all-wheel drive minivan using MSC.ADAMS/Pre. First, they presented a detailed component and system level, static and dynamic tests, including tire tests that were performed for inputs to the model. Second, they presented the static correlation of the model, in particular, the front and rear suspension kinematics and compliance correlation. Finally, they discussed the

dynamic correlation of the model, for the constant radius test and the swept steer test. The results showed that the coil spring front suspension response for the analytical dynamic simulation correlates exactly the experimental model. As for the leaf spring rear suspension, results show a good correlation between the simulated and the experimental models. The leaf spring model has fewer parameters to experiment with than the coil spring model, and this explains the differences in suspension behavior, and the over-prediction of cornering compliances for the rear suspension. The MSC.ADAMS/Pre vehicle simulation procedure enables the development of well-correlated models. These models help to predict vehicle handling characteristics upfront.

Uehara et al. (2000) introduced a new approach to create a vehicle's natural frequency map as reference data when vehicle vibration problems are studied utilizing the MSC.ADAMS virtual prototype vehicle. A customized version of the MSC.ADAMS system, MSC.ADAMS/Isuzu, has been used to build accurate and complex virtual prototype vehicles. Results showed that the virtual prototyping technology has been successfully used for evaluating vehicles under development in order to shorten development time and to cut cost compared to experimental methods. Typically, MSC.ADAMS models are easily used to simulate vehicle dynamics with frequency below 3 Hz. The results of the modal analysis on the virtual vehicle showed that the main Eigen values and mode shapes were in good correlation with test in the frequency below 50 Hz with greater accuracy.

Riepl et al. (2000) solved the elasto-kinematics/vehicle dynamics using MSC.ADAMS/Car and calculated the cross-sectional forces as input data for subsequent fatigue life estimation. They showed that the multi-body dynamics method that provided theoretical results during vehicle development was a cost effective technique. They pinpointed the main advantages of the virtual prototyping and simulation of the vehicle dynamics. Moreover, this technique improved model clarity. Hence, the limitations of the model can be identified and corrected earlier than with other techniques. Finally, there is considerable potential to reduce costs due to the time-saving technique for generating the model due to the central model maintenance.

Anderson et al. (2001) have developed a virtual prototype model for a heavy duty truck using special customized MSC.ADAMS/Car templates. The results showed a duplication of the level of accuracy and fidelity. The templates allowed the use of the models in a more structured and flexible manner. They also provided the opportunity for substantial increases in model building efficiency. Also, the parametric relationships provide an advantage in accommodating the large number of configuration variants offered by truck original equipment manufacturers. Virtual prototypes were used early in the design process to cascade design targets to the design community during the early conceptual design phase. Also, several of the prototypes in the hardware prototype fleets were simulated with MSC.ADAMS before critical design and tooling release milestones.

Kim et al. (2001) proposed an Active Height Control (AHC) system that consists of an automatic air leveling and semi-active suspension system for sport utility vehicles.

The vehicle was modeled with flexible body frame and AHC system using MSC.ADAMS with 86-DOF. The vehicle control and handling performances for various driving conditions were analyzed by simulating the virtual prototype model. The modal analysis showed 8 mode shapes, ranging from 26.9 Hz for the first mode to 54.4 Hz for the eighth mode. The simulation results showed that the AHC system automatically responded to the addition of an extra 200 kg on the rear side of the SUV. The spring was compressed by 25 mm due to this extra load. The AHC system leveled back the spring to its normal position after 19.62 sec by supplying compressed air for 4.03 sec. The leveling speed was about 1.6 mm/sec, which will not cause passenger discomfort.

Hong and Moshchuk (2001) analytically simulated motion and load behavior of a car on both truck haulage and railcar shipping simulators using MSC.ADAMS. They also discussed details of tie down chain loads, motion envelope of shipping vehicles, and durability assessments of some chassis parts under the shipping conditions. The results showed that the MSC.ADAMS simulation provided an effective way of modeling shipping events. Loads and motion envelope were predicted reasonably well and confirmed by comparison with actual test data.

Dittmann et al. (2002) have validated dynamic models of physical test rigs and correlated between virtual model and physical prototype. The same load histories were applied to the virtual model with a comparison between the physical prototype and the responses. The results for the vertical front wheel showed a good agreement between physical test and virtual prediction. The force transducer was in the direct chassis to body

load path. However, the validation of the damper force showed good agreement with respect to amplitude, but there is a phase shift between the physical and virtual models. The prediction by the virtual model requires, therefore, improvement to reduce the phase error. The transducer is in the load path of chassis to body, but due to the vicinity of the axle a kinematic influence of the axle was noticeable.

Yamakawa et al. (2002) studied a new vehicle modeling with detailed force elements using MSC.ADAMS. They developed a theoretical design, experimental and CAE models of vehicle dynamics, and carried out the prototype testing for millions of miles to improve the characteristics of the new vehicle. The results showed an agreement between the experiment and simulation results. The maneuver angle versus the steering effort force was in agreement between the actual test and the virtual prototype. The results also showed that the lateral acceleration is similar between the experimental and the simulation models for identifying the tire model on real road surface.

Prakash et al. (2006) analyzed automotive components that experience many types of vibration from simple sinusoidal to complex random excitation. By using computer aided engineering, the durability due to vibratory stresses can be simulated for predicting fatigue life. They have modeled an exhaust system assembly subject to dynamic loading. The analysis results showed that the fatigue life predictions using the transient dynamic (time domain) and random vibration (frequency domain) methods were comparable at 7.97E05 cycles. They concluded that the frequency domain random

vibration analysis is simpler and is devoid of the need to address solution convergence issues generally associated with the transient dynamic analysis methodology.

2.5. THE ISO STANDARDS

The International Standard Organization (ISO) was founded on February 23rd, 1947. The organization proclaims world-wide industrial and commercial standards. It is headquartered in Geneva, Switzerland. It has the ability to set standards that often becomes a law, either through treaties or national standards. The ISO has developed over 16,500 International Standards on a variety of subjects and 1,250 new ISO standards are published every year. ISO has 157 national members out of 195 total countries in the world (ISO ©, 2007). ISO has three membership categories: (i) Member bodies; (ii) Correspondent members; and (iii) Subscriber members. The United States falls into category (i) that consists of the national bodies that are considered to be the most representative in each country who have the right to vote. Category (ii) consists of the countries that do not have their own standard organization. As for category (iii), it consists of countries with smaller economies that can follow the development of standards.

The ISO standards that will be used in this PhD research study will be ISO 2631 parts 1, 2, 4 and 5. ISO 2631 – 1 (1997) is titled as "Mechanical vibration and shock -- Evaluation of human exposure to whole-body vibration -- Part 1: General requirements". This part of ISO 2631 defines methods for the measurement of periodic, random and transient whole-body vibration. It indicates the principal factors that combine to

determine the degree to which a vibration exposure will be acceptable. Informative annexes indicate current opinion and provide guidance on the possible effects of vibration on health, comfort and perception and motion sickness. The frequency range considered is - 0.5 Hz to 80 Hz for health, comfort and perception, and - 0.1 Hz to 0.5 Hz for motion sickness. Although the potential effects on human performance are not covered, most of the guidance on whole-body vibration measurement also applies to this area. It also defines the principles of preferred methods of mounting transducers for determining human exposure. It does not apply to the evaluation of extreme magnitude single shocks such as occur in vehicle accidents. This part of ISO 2631 is applicable to motions transmitted to the human body as a whole through the supporting surfaces such as, (i) the feet of a standing person; (ii) the buttocks; and (iii) back and feet of a seated person or the supporting area of a recumbent person. This type of vibration is found in vehicles, in machinery, in buildings and in the vicinity of working machinery.

ISO 2631 – 2 (2003) is titled "Mechanical vibration and shock -- Evaluation of human exposure to whole-body vibration -- Part 2: Vibration in buildings (1 Hz to 80 Hz)". This part of ISO concerns human exposure to whole-body vibration and shock in buildings with respect to the comfort and annoyance of the occupants. It specifies a method for measurement and evaluation, comprising the determination of the measurement direction and measurement location. It defines the frequency weighting Wm which is applicable in the frequency range 1 Hz to 80 Hz where the posture of an occupant does not need to be defined. Acceptable magnitudes of vibration are not stated in ISO 2631 – 2. The mathematical definition of the frequency weighting Wm is given in

Annex A. Guidelines for collecting data concerning complaints about building vibration are given in Annex B.

ISO 2631 – 4 (2001) is titled as "Mechanical vibration and shock -- Evaluation of human exposure to whole-body vibration -- Part 4: Guidelines for the evaluation of the effects of vibration and rotational motion on passenger and crew comfort in fixed-guideway transport systems". This part of ISO 2631 provides guidance on the application of ISO 2631 – 1 to the evaluation of the effects of mechanical vibration on the comfort of passengers and crew in fixed-guideway systems. These guidelines establish methods for the evaluation of relative comfort between systems, as opposed to absolute levels of comfort. This part of ISO 2631 is applicable to people in normal health exposed to rectilinear vibration along their x-, y- and z-axes, as well as rotational vibration about these (body-centered) axes. It is intended to provide guidance on the assessment of comfort as a function of motions along and about vehicle axes that produce the body motions. This part of ISO 2631 is not applicable to high-amplitude single transients that may cause trauma, such as those resulting from vehicle accidents or "run-ins" produced by "longitudinal slack action," nor is it applicable to high-amplitude vibration which may affect health. It provides guidance on the effects of very low-frequency accelerations (0.1 Hz to 0.5 Hz) experienced as vertical forces.

ISO 2631 – 5 (2004) is titled as "Mechanical vibration and shock -- Evaluation of human exposure to whole-body vibration -- Part 5: Method for evaluation of vibration containing multiple shocks". This part of ISO 2631 addresses human exposure to

mechanical multiple shocks measured at the seat pad when a person is seated. The adverse health effects of prolonged exposure to vibration that includes multiple shocks are related to dose measures. The method described in ISO 2631 – 5 is generally applicable in cases where adverse health effects in the lumbar spine are concerned. The calculation of the lumbar spine response described in ISO 2631 – 5 assumes that the person subjected to the vibration is seated in an upright position and does not voluntarily rise from the seat during the exposure. Different postures can result in different responses in the spine.

These ISO standards are very important in establishing a limit of vibration and minimizing the WBV injuries in dump truck applications in the surface mining industry. They present guidelines for vibration analysis in HISLO and how to measure the amount of vibration and shock waves generated by this operation. These ISO standards will allow us to compare the results from the dynamic virtual model with the limits established throughout experimental data collected over the years. This research will set criteria for defining limits of vibration exposure to operators through the virtual prototype model constructed and simulated for the HISLO. This requires the measurement of frequency-weighted acceleration at the point of entry into the body. Acceleration measurements must be performed along three mutually perpendicular directions in space. The sensitivity of the body to vibration at different frequencies is accounted for by frequency weightings inserted into the measurement chain.

Rasmussen (2006) showed that the human body is both physically and biologically a system of an extremely complex nature. As a mechanical system, it can be considered to contain a number of linear, as well as, non-linear elements, and the mechanical properties are quite different from person to person. The knowledge about comfort and fatigue-decreased proficiency is based on statistical data collected under practical and experimental conditions. Much of the knowledge about the damaging effects has been obtained from experiments on animals and simulators not on human beings. The experiments with human beings are difficult, time consuming and in extreme cases unethical. He also classified the symptoms for vibration exposure at frequencies of 1 to 20 Hz, which are listed in Table 2.1. The frequency ranges given are those where the symptoms are most predominant.

Table 2.1. Classifications of Symptoms for Vibrations and Frequencies

Symptoms	Frequency (Hz)
General feeling of discomfort	4 - 9
Head symptoms	13 - 20
Lower jaw symptoms	6 - 8
Influence on speech	13 - 20
"Lump in the throat	12 - 16
Chest pains	5 - 7
Abdominal pains	4 - 10
Urge to urinate	10 - 18
Increased muscle tone	13 - 20
Influence on breathing movements	4 - 8
Muscle contractions	4 - 9

Joubert (2002 and 2007) has studied the WBV exposure among forklift drivers. He has used the ISO 2631 – 1 (1997) methodology as a guideline on a small group of forklift trucks. The results showed that the majority of vibration results exceeded the ISO 2631 – 1 root mean squared exposure values of 0.5 m/s^2 for 8 hours of operation. The ISO 2361 – 1 does not give specific limits of vibration magnitude as related to comfort due to the many factors, which vary with each type of environment and application. The standard, however, does give values with an approximate indication of likely reactions from exposed drivers to various magnitudes of overall vibration values as a health guidance caution zone. For an 8 hour daily exposure, numerical values of the acceleration defining the comfort zone are listed in Table 2.2.

Table 2.2. Expected Comfort Reactions to Vibration (ISO 2631 – 1)

Acceleration Value (RMS)	Comfort Zone
Less than 0.315 m/s^2	not uncomfortable
0.315 m/s^2 to 0.63 m/s^2	A little uncomfortable
0.5 m/s^2 to 1 m/s^2	fairly uncomfortable
0.8 m/s^2 to 1.6 m/s^2	uncomfortable
1.25 m/s^2 to 2.5 m/s^2	very uncomfortable
Greater than 2 m/s^2	extremely uncomfortable

Moreover, Hedge (2007) performed studies concerning the WBV, and showed that the exposure can be harmful and permanent. The different sources of vibration from his study included: (i) Ride quality for people movers, elevators and escalators; (ii) Swaying buildings; (iii) Building vibrations, highway traffic and (iv) Mobile workplaces

such as cars, buses, trains, planes and boats. Vibration analysis has attracted many researchers to find a solution for the harmful frequencies because of the versatility in encountering vibration with every object that has a dynamic acceleration.

Hedge (2007) also restated the ISO 2361 (parts 1, 2, and 4) exposure limits and their different types as (i) Reduced-comfort boundary; (ii) Fatigue-decreased proficiency boundary; (iii) Exposure limits and (iv) Severe discomfort boundaries. In (i), this implies for the comfort of people traveling in airplanes, boats, and trains. Exceeding these exposure limits makes it difficult for passengers to eat, read or write when traveling. Part (ii) describes the limit for time-dependent effects that impair performance. For example, fatigue impairs performance in flying, driving and operating heavy vehicles. Part (iii) is used to assess the maximum possible exposure allowed for whole body vibration. Also, part (iv) applies to the WBV exposures in the 0.1 Hz to 0.63 Hz range for 8-hour, 2-hour and 30-minute. In the ISO 2361 standard, the exposure limits are given as acceleration for one third octave band frequencies and three directions of exposure: longitudinal (from head to toe) and transverse (from back to chest and from side to side). It shows that the exposure limit is the lowest for frequencies between 4-8 Hz because the human body is most sensitive to WBV at these frequencies.

2.6. RATIONALE FOR PHD RESEARCH

Vibration research has focused on dynamics of light trucks, cars and trains and their responses to various stimuli from road conditions. Other studies, such as military, focused on whole body vibration with operating machinery such as fighter jets and

helicopters. Many of these research studies were performed experimentally and analytically but lack the virtual dynamic analysis. The virtual prototyping has found solid applications in the automotive industry. The literature shows extensive work done on car dynamic virtual models. They provide a full understanding of vehicle behavior in various operating conditions including vibration response. Other research initiatives have focused on vehicle vibrations attenuation by modifying suspension systems for lighter vehicles, but most of them neglect the effects on drivers or passengers.

Eger et al. (2005) measured the WBV exposure levels at the vehicle and operator seat interfaces, during the operation of both small and large LHD vehicles. The results showed that the operators are subjected to high levels of vibration. Their study lacked a complete virtual model that could be needed to understand the vibration propagation. This complete model would allow the designer to categorize the levels of exposure and modify the design to eliminate the harmful wavelengths. Kittusamy et al. (2002 and 2004) showed that heavy construction equipment operators are afflicted by musculoskeletal injuries of the arms, shoulders, neck and lower back. They concluded that WBV and the postural requirements are important risk factors that contribute to the development of the musculoskeletal disorders. Their work on construction equipment lacked the development of solutions to the vibration problems arising in mining equipments and did not introduce a solution to minimize this vibration by locating the source. Furthermore, it must be noted that construction equipments do not fall into the large mining trucks category.

Moreover, no comprehensive work has yet been done on large scale mining trucks that are subjected to high impact shovel loading. The forces applied to the truck are time dependent forces, i.e., impulse type forces introduced by the amount of material in the shovel bucket. The environmental conditions in the mining applications make these types of forces inevitable. These forces are nothing but the weight of the material in the bucket acting vertically under gravity and generate large amount of shockwaves and vibrations that travels throughout the truck. Hence, the shockwaves generated from HISLO that affect the operator's health, as well as, the machine structure are not fully understood. The attempt to build a fully virtual dynamic model and test it for severe operating conditions has not yet been done for mining equipment. The work carried out in the automotive industry using virtual dynamic modeling has saved time and cost in the development stages of building a new car model. The virtual dynamic model provides a complete understanding of the dynamic behavior of the new car model. There must be an environment (virtual prototyping) where the mining trucks are fully modeled, tested and designed according to the machine behavior due to the dynamics of the work conditions and forces applied to the trucks. All the existing research studies and vibration models in the literature lack in one or more of these qualities. These qualities include virtual prototype models that generate full understanding of the behavior of the truck in the extreme environmental conditions in surface mining applications, as well as vibration analysis at the operator's seat. This is the first attempt to develop comprehensive dynamic virtual models of large mining trucks during high-impact shovel loading operations, with detailed vibration analysis on the operator's seat, cervical and lumbar regions.

Research efforts on vibrations monitoring and controls have been in the military fields, where Friedmann (1997) conducted a research to control the vibrations in the Agusta-Westland EH-101 helicopter fuselages. Wickramasinghe et al. (2004) also investigated techniques to reduce vibration and noise in the cabin of helicopters and propeller aircrafts to improve habitability, effectiveness, and safety for passengers. These studies were not adapted commercially and were mainly focused on military applications. Therefore, the lack of expertise and understanding of how to monitor, control and even define the type of vibration generated in mining trucks is encountered in the surface mining industry. The military applications well established the different types of vibrations and shockwaves propagation according to the studies done. The two types of vibrations involved are the free and forced vibrations. As for the mining industry, the type of vibrations experienced in the HISLO is the forced vibrations induced by the material impact. This application is different from the military applications and findings due to the fact that the machine is stationary and the excitation force introduced by the shovel dumping the load in the truck body is dynamic. This is the first attempt to study this type of vibrations on dump trucks in surface mining operations and will create a frontier in this area by modeling the vibration and creating a dynamic virtual truck model. This research will further create understanding into the long-term effects of HISLO on operators' health conditions, as well as, the machine health.

This PhD research study will provide appropriate insights, through fundamental vibration theory for minimizing and possibly eliminating the effects of shockwave vibration during HISLO. This study will reduce the associated whole body vibrations of

dump truck operators to within acceptable limits of ISO whole body vibrations standards. This study will provide a complete understanding of vibrations during the HISLO and allow the researcher to build a catalogue of vibration control strategies. Also, it will provide a basis for developing an operations manual for achieving ISO standards by operators and equipment manufacturers. The results could also be used to develop virtual prototype simulators and data for developing a new generation of truck suspension mechanisms. The simulator will be used to test various operating conditions to understand the human body responses to truck vibrations. The effective control and elimination of HISLO problems will create a safe working environment, healthy workforce, production efficiency and economic operations. This study will alternatively expand knowledge and frontiers in dump truck vibrations in HISLO operations.

Modeling and analyses of the HISLO system dynamics and shockwave propagation are required in the development and design of the new generation of mining trucks with control measures that attenuate shockwaves prior or during propagation to insure the operator's health as well as minimize machine damage. Therefore, appropriate vibration analysis will be done to provide a basis for developing controls to significantly reduce or eliminate the resultant vibrations that affect the seated operator. This vibration analysis will result in the most cost effective design of dump trucks.

Furthermore, limitations in the literature of the presence of a full dynamic model for dump trucks in the mining industry demand an extensive study to be carried out to be able to develop general vibration models from actual truck suspension system using

Newton-Euler-Lagrange theory. The analysis is carried out in order to develop a comprehensive truck vibration model to capture the 3D multi-body dump truck vibrations under HISLO conditions. Thus, virtual simulators are used to simulate the behavior of the integrated 3D truck-operator vibration model with MSC.ADAMS.

2.7. SUMMARY

Extensive literature survey has been carried out by reviewing the relevant literature to evaluate the contributions and limitations of the previous and current body of knowledge on the WBV, machinery vibration and dynamic modeling. It is obvious that truck operators' health and their efficiency are very crucial to the overall mine performance. The U.S. mining companies have employed bigger trucks in their operations to minimize cost and increase productivity, which introduced higher impact forces acting on these trucks and hence higher exposure to shockwaves propagation for operators as well as trucks. However, 3D dynamic modeling and virtual simulation models of the haul truck has not yet been studied as much like cable shovels, hydraulic shovels, backhoes and frontend loaders.

Many researchers have focused on the WBV as one aspect of machinery vibration. Griffin (1990) studied the WBV exposure from a vibrating surface. While, Kjellberg (1990) concluded that WBV does not affect one specific target organ, but rather a variety of health problems that include backaches, gastrointestinal, reproductive system, visual and vestibular disorders. Frequencies between 1 and 20 Hz cause the pelvis and spine to resonate leading eventually to structural damage and health problems including

lower-back pain, spinal degeneration, among other problems. Eger et al. (2005) measured the WBV exposure levels at the vehicle and operator seat interfaces, during the operation of both small and large LHD vehicles. Hoy et al. (2005) also studied the risks from WBV and posture for low back pain among forklift truck drivers. Another attempt was the research done by Gibson et al. (2006), who conducted WBV analysis aboard seven commercially available passenger and/or recreational vehicles.

No studies have yet been carried out on vibrations and WBV exposures for large mine trucks. This is the first attempt to study vibrations on dump trucks in surface mining operations and will create a frontier in this area by modeling the vibration under the HISLO conditions through the dynamic virtual truck model. Therefore, the work presented by the above research studies in this area has many limitations such as it was not applied to heavy dump trucks, the CAT 793 series. Therefore, the contribution from this research into the body of knowledge of haul truck vibrations and the effects on operators' health due to WBV will be a significant asset to the truck manufacturers as well as the mining companies.

Other vibration studies focused on seat ergonomics and seat design that eliminates or minimizes the operator's exposure to vibrations. Pope et al. (1985) conducted a study on the Black Hawk helicopter and showed that vehicle vibrations produced significant discomfort in the lower back and buttocks of operators. VanIngen-Dunn and Richards (1991) found substantial reports of low back pain and general discomfort after about four hours of flight in both the Army and Air Force Black Hawk helicopter pilots. These

studies were based on experimental results and lacked the dynamic modeling and virtual prototyping of the machines in study. Kittusamy et al. (2003) did extensive research on seat ergonomics. Smith et al. (2006) showed that the transmissibility characteristics of occupied suspension seats in multi-axis vibration environments of the locomotives were mostly notable in the x and z-directions, respectively.

Research studies have also focused on the methods to control and monitor the amount of vibrations to keep the frequency levels within the ISO safe range. Aldinger et al. (1995) found, in their study on surface coal mining, that equipment operation was the most common category of accident for haulage trucks resulting in back injuries of haulage truck drivers. Furthermore, Miller et al. (2000) carried out an investigation on how to control and reduce the jolting and jarring of trucks in surface mining operations. There are different methods to control the vibration in machinery. The most common methods are the passive and active controls. Singh and Ram (2000) studied the dynamic absorption by passive and active control methods. Kim et al. (2001) proposed an Active Height Control (AHC) system that consists of an automatic air leveling and semi-active suspension system for sport utility vehicles. Winthrop (2004) studied the nonlinear behavior of variable stiffness concepts. Wang (2006) studied the vibration control of mistuned periodic structures utilizing the electromechanical coupling and damping characteristics of piezoelectric networking. The above analyses were limited in the development of a solution to isolate the vibrations and how to monitor the shockwaves that are generated during various operations without trying to solve the source of vibrations by building a complete model for their studies.

Virtual prototyping and dynamic modeling techniques have found solid applications in the automotive industry, but they are limited in use in large scale surface mining industry. Wenzhang et al. (2000) have studied the non-linear dynamic characteristic of rubber component in a vehicle dynamics simulation model based on the MSC.ADAMS software and a user written subroutine. Subramanyam et al. (2000) have developed a methodology for developing a correlation between experimental analysis and analytical dynamic simulation of an all-wheel drive minivan using MSC.ADAMS/Pre. Uehara et al. (2000) introduced a new approach to create a vehicle's natural frequency map as reference data when vehicle vibration problems are studied utilizing the MSC.ADAMS virtual prototype vehicle. Riepl et al. (2000) have solved the elasto-kinematics/vehicle dynamics using MSC.ADAMS/Car and calculated the cross-sectional forces as input data for subsequent fatigue life estimation. In later studies, Yamakawa et al. (2002) developed a full vehicle virtual model with detailed force elements using MSC.ADAMS. Furthermore, Dittmann et al. (2002) have validated dynamic models of physical test rigs and correlated between virtual model and physical prototype. Additionally, Prakash et al. (2006) analyzed automotive components that experience many types of vibration from simple sinusoidal to complex random excitation.

3. MECHANICS OF DUMP TRUCK VIBRATIONS

The theoretical mechanics of dump truck vibrations provide an analytical tool to determine the frequencies of vibrations that affect operators' health under HISLO conditions. It is based on a multi-body system, with rigid elements, connected together by springs and damping mechanisms. This mathematical model of the truck vibration is developed using the generalized Lagrangian formulation of vibration. The mathematical model provides a framework for carrying out a comprehensive modeling and analysis using a 9-DOF system. The different truck components are modeled as masses connected with each other via a spring-damper system. The 9-DOF system accounts for the vertical displacement of each mass, such as the body, chassis, tire/wheel assemblies, cabin, the operator's seat and ground movement, as well as, the pitch of the truck with respect to the ground.

This 9-DOF truck vibration problem is solved for the displacement, velocity and acceleration vector fields. These components are used to calculate the vibration frequencies for the associated shockwaves that might be harmful to the operator and the machine. The undamped free vibration is solved to provide a basis for the modal analysis of the forced damped vibration problem. A modeling framework is established using the necessary assumptions and limitations in order to generate the major parameters of truck vibrations and the operator's health. The input variables, such as, the weight of the truck components, the spring stiffness and damping coefficients are related to the output variables by second order nine coupled differential equations.

3.1. FORCE VECTORS ON THE DUMP TRUCK SYSTEM

The main cause of truck vibrations is the huge impact force during the HISLO process. These HISLO forces that act on the dump truck are described with the right hand rule convention. Thus, the forces acting in the vertical or upward direction are considered to be in the positive z-direction. The positive y-direction is toward the plane of the paper and the positive x-direction is to the right of the paper[1]. The three vectors orientations are at right angles to each other as illustrated in Figure 3.1. The input force is acting in the negative z-direction. The x-direction is the direction describing the front-back motion, the y-direction describes the right-left motion and the z-direction describes the up-down motion of the truck.

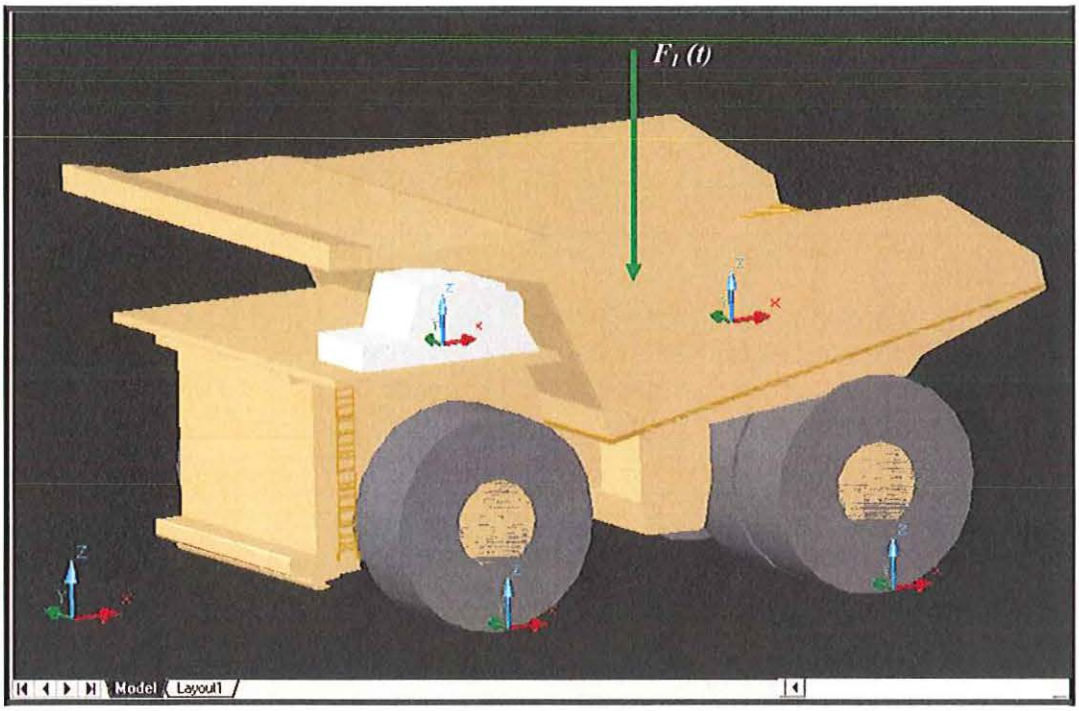

Figure 3.1. Vectors Orientation of the Truck Model

[1] This definition will be used throughout the dynamic and numerical modeling components of the research study.

The impact force is modeled as an impulse force function of the increment in mass and the initial velocity of the material dumped by the shovel. This impulse force mainly depends on the dumped material properties, truck weight and other operating factors. The material properties include density, fragmentation, water content, and cohesion. The other operating properties include the height and time of dumping, the dumping process, as well as, the shovel bucket capacity. Thus, the HISLO forces consist of the input force on the truck acting in the z-direction due to the load dumped by the shovel, as well as, the internal forces. These internal forces are the reaction to this input force and are generated by the spring-damper systems. The input force is generated from the free fall of the material in the shovel bucket under gravity, and is referred to as an impulse force. The impulse force or impulse function creates very large forces over a short period of time. This impulse force is modeled by the integration of the Dirac delta function δ at time, $t_0 = 0.1sec$, for the shovel first pass then repeated after *38 sec*, for the shovel second pass. The *38 sec* accounts for *3 sec*, the time to dump the first load, and then *35 sec*, the time allowing the shovel to swing back, load, then swing towards the truck before dumping. At any other time, this force is zero. F_0 is a constant force that represents the capacity of the shovel bucket. The input force on the truck is defined in equation (3.1).

$$F_1(t) = \begin{cases} F_0 \int_0^{\infty} \delta(t - t_0)\, dt & t = t_0 \\ 0 & t \neq t_0 \end{cases} \tag{3.1}$$

The reactive forces are the dynamic forces of the different components generated in response to the input force. These forces include the suspension system reaction due to the excitation, such as the reactions of the springs and dampers due to an external stimulus. These reactions are assumed to move in the z-direction due to the fact that the physical connections that they represent are pinned in the vertical orientation.

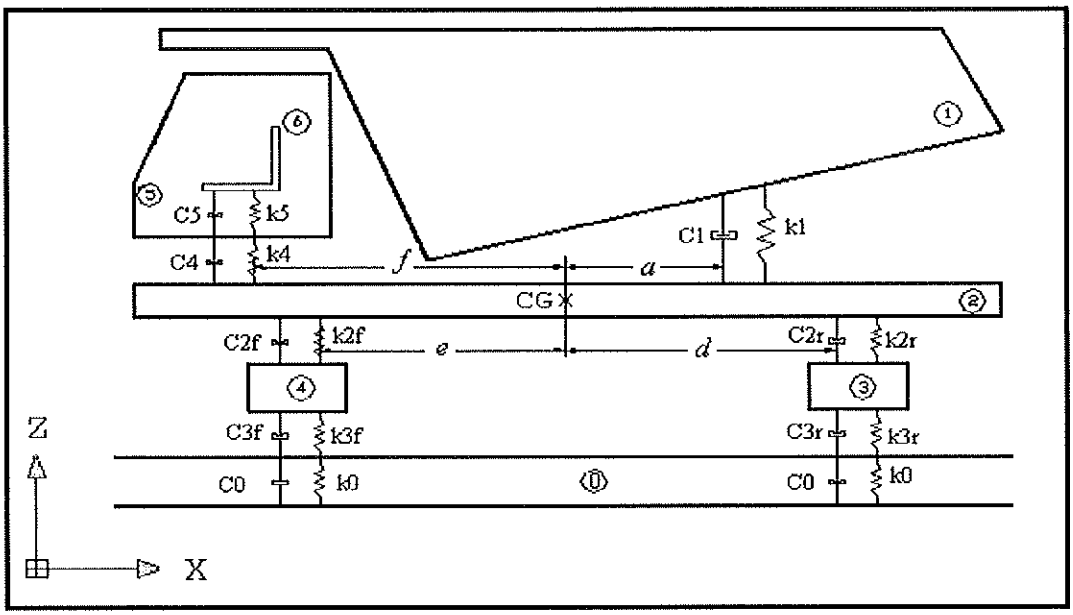

Figure 3.2. Response of the Truck Components to HISLO

0: Frozen Soil having spring-damper characteristics
1: Truck body having a mass m_1
2: Sprung mass ~ frame and suspension components having mass m_2
3: Rear wheel/tire assembly having mass m_3
4: Front wheel/tire assembly having mass m_4
5: Cabin having mass m_5
6: Truck seat having a mass m_6

Figure 3.2 illustrates the response of the truck's structural components under the HISLO conditions. It accounts for the translational and rotational behavior of the truck. The distances of the applied forces from the chassis *(m_2)* are different from the top and

the bottom of the chassis. The body and the cabin are connected at respective distances *(a)* and *(f)* from the center of mass of the chassis. The location of the rear and front suspension system are *(d)* and *(e)* from the chassis center of mass, respectively, as illustrated in Figure 3.2. The alpha-numeric symbols in Figure 3.2 represent the various components of the truck structure. These components include the springs-dampers connections, as well as, the basic truck, such as the body, chassis, tire/wheel assembly, ground conditions, cabin and operator's seat. The chassis and portion of the suspension system are combined together to form the sprung mass, with a center of gravity (CG) shown in Figure 3.2.

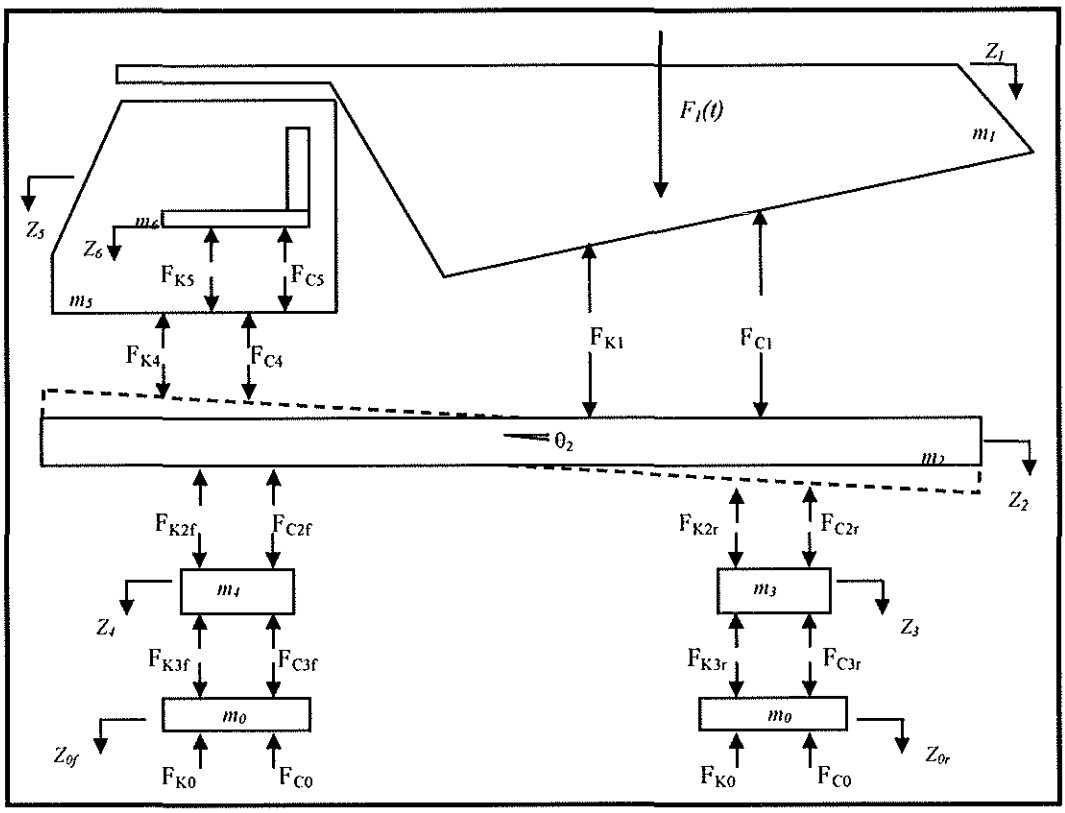

Figure 3.3. Free Body Diagram of Each Mass

Figure 3.3 shows the free body diagram (FBD) of the truck model describing the propagation of the shockwaves throughout the truck under HISLO conditions. The external excitation force, $F_1(t)$ is generated by the free-falling material under gravity from the shovel bucket to the truck body.

The external excitation force $F_1(t)$ acting on the body of the truck is transferred through the connection between the body and the chassis (m_2). It creates action forces, F_{k1} and F_{C1}, acting on the sprung mass, moving it downward (z_2) and pitching it with respect to the ground at an angle θ_2. This causes the spring-dampers systems holding the tires/wheels assemblies and the cabin to react against these disturbances. The body structure rests on the frame with rubber contact areas. The body is connected to the frame via hydraulic pistons, bearings and springs-damper systems. The sprung mass is the combination of the frame that carries the weight and portions of the weight of the suspension members, such as the driveshaft, springs, shock absorbers and suspension links. This combination is used to maintain the suspension characteristics and to create a sprung weight that captures the vehicle's physical behavior. The shockwaves travel through the sprung mass, where a portion of the energy is dissipated through damping and the remainder is transmitted to both the front and rear tires/wheels assemblies. These forces are F_{k2r}, F_{C2r}, F_{k2f} and F_{C2f} for the front and rear tires/wheels assemblies, as well as, F_{k4} and F_{C4} for the cabin, respectively. The tire assemblies are flexible, and thus, they absorb the road imperfections as part of the vibration-isolation system. The tires are an elastic body that can be modeled as a spring and damper system, although the damper is often included to present the small amount of damping inherent in the visco-elastic nature

of the tire (Gillespie, 1992). The reactions of these spring-damper systems are then transmitted to the ground (F_{k3r}, F_{C3r}, F_{k3f} and F_{C3f}) and the operator's seat as well (F_{k5} and F_{C5}). The ground reacts to the excitations coming from F_{k3r}, F_{C3r}, F_{k3f} and F_{C3f}. As a response, the ground reaction forces are hence, F_{k0} and F_{C0}.

The transmitted shockwave energy to the front tires is dissipated via two outlets. These outlets include the tire-ground interaction and the operator's cabin. This is due to the fact that the cabin is directly connected to the frame by rubber mounts. Thus, the connection between the cabin and frame will have equivalent stiffness and damping coefficients. This equivalency results in an action force, which captures the shockwaves propagation throughout the cabin. A component of this shockwave is transmitted to the operators' seat. This seat is fixed to the cabin floor by a spring-damper system. The seat cushioning effect will absorb some unwanted shockwaves. As it travels throughout the truck, a component of the shockwaves is dissipated through the spring-damper system, and the remainder through the operator cabin and the tire-ground interaction. This research will quantify the components of the shockwaves that reach the operator's cabin. Long-term exposure of an operator to vibrations levels that exceed the ISO recommended levels may result in lower back problems (LBP) and musculoskeletal diseases (Kittusamy, 2003).

3.2. GENERALIZED LAGRANGIAN FORMULATION

The Lagrangian formulation allows an efficient resolution of the system dynamics into the appropriate set of equations to capture the system vibrations. The total energy of the vibrating system consists of two major components, the kinetic and the potential energies. The equations of motion, using the energy approach in Lagrangian mechanics, are called Lagrange's equations also known as Euler-Lagrange equations (Rao, 1995). The Lagrange's equations are developed by considering a single particle with mass m and position vector r in a vibrating system. The applied force, F, on this vibrating particle can be expressed as the gradient of a scalar potential energy function V(r, t) as in equation (3.2).

$$F = -\nabla V \tag{3.2}$$

The motion of the particle can be completely described by six independent variables, or *degrees of freedom*. An obvious set of variables are r_j and r_j' (j = 1...3) representing the Cartesian components of r and their time derivatives, at a given instant of time (i.e. position (x, y, z) and velocity (v_x, v_y, v_z)).

The vibration systems can be resolved using a set of generalized coordinates, q_j, and their time derivatives, (i.e., the generalized velocities, q_j'). The position vector, r, is related to the generalized coordinates by the transformation equation in equation (3.3).

$$\mathbf{r} = \mathbf{r}(q_i, q_j, q_k, t) \tag{3.3}$$

The work done by the applied force F on an arbitrary particle with an arbitrary displacement δr is defined as $\delta W = F \cdot \delta r$. This work can be written as equation (3.4) by using Newton's second law.

$$F\,\delta r = m\,\ddot{r}\,\delta r \tag{3.4}$$

The work done on this particle is a physical scalar quantity. Thus, equation (3.4) can be re-written in terms of the generalized coordinates and velocities. The LHS of equation (3.4) can be written as equation (3.5), and the RHS as equation (3.6).

$$\begin{aligned} F\,\delta r &= -\nabla V \sum_i \frac{\partial r}{\partial q_i}\delta q_i \\ &= -\sum_{i,j} \frac{\partial V}{\partial r_j}\frac{\partial r_j}{\partial q_i}\delta q_i \\ &= -\sum_i \frac{\partial V}{\partial q_i}\delta q_i \end{aligned} \tag{3.5}$$

and,

$$m\,\ddot{r}\,\delta r = \sum_i \left[\frac{d}{dt}\frac{\partial T}{\partial \dot{q}_i} - \frac{\partial T}{\partial q_i}\right]\delta q_i \tag{3.6}$$

Where $T = 1/2\, m\dot{r}^2$ is the kinetic energy and $V = 1/2\, kr^2$ is the potential energy of the particle. The equation for the work done on the particle can be written as equation (3.7).

$$\sum_i \left[\frac{d}{dt} \frac{\partial T}{\partial \dot{q}_i} - \frac{\partial (T-V)}{\partial q_i} \right] \delta q_i = 0 \tag{3.7}$$

However, this must be true for any set of generalized displacements δq_i, and thus, equation (3.7) becomes equation (3.8).

$$\left[\frac{d}{dt} \frac{\partial T}{\partial \dot{q}_i} - \frac{\partial (T-V)}{\partial q_i} \right] = 0 \tag{3.8}$$

For each generalized coordinate δq_i, the work done can further be simplified by noting that V is a function solely based on r and t, and r is a function of the generalized coordinates and t. Therefore, V is independent of the generalized velocities, as stated in equation (3.9).

$$\frac{d}{dt} \frac{\partial V}{\partial \dot{q}_i} = 0 \tag{3.9}$$

Substituting equation (3.9) into equation (3.8) and substituting L = T – V (called the Lagrangian) results in the Lagrange's equations in equation (3.10).

$$\frac{\partial L}{\partial q_i} = \frac{d}{dt} \frac{\partial L}{\partial \dot{q}_i} \tag{3.10}$$

There is one Lagrange equation for each generalized coordinate q_i. When $q_i = r_i$ (i.e. the generalized coordinates are simply the Cartesian coordinates), the Lagrange's equations reduce to Newton's second law of motion.

3.3. VIBRATION MECHANICS OF A NON-CONSERVATIVE SYSTEM

The Lagrangian model in equation (3.10) is derived based on the concept of conservative systems. Young et al. (1999) stated that a conservative system is a system in which the work done by a force is (i) independent of its path; (ii) equivalent to the difference between the final and initial values of an energy function (no dissipation of energy); and (iii) completely reversible.

Conservative systems are usually ideal systems. Most real –world systems, such as truck vibrations under HISLO conditions, are not ideal, and thus, are considered as non-conservative systems. A Non-conservative system dissipates its vibration energy into heat energy. The Lagrangian formulation is extended to include the applied forces and the energy dissipation for the dump truck vibration under HISLO conditions. Therefore, equation (3.11) represents the general form of the complete Lagrangian equations for a non-conservative system.

$$\frac{d}{dt}\left(\frac{\partial L}{\partial \dot{q}_i}\right) - \frac{\partial L}{\partial q_i} + \frac{\partial R}{\partial \dot{q}_i} = Q_i(t) \qquad (3.11)$$

R is the dissipation energy of the system through the dampers. $Q_j(t)$ is the non-conservative generalized force corresponding to the generalized coordinate q_j and can represent any type of external force or excitation to the truck structure.

Equation (3.11) can be generalized for a system of N particles. There will be $6N$ generalized coordinates, which corresponds to three translational and three rotational coordinates for each particle respectively.

3.4. VIBRATION ANALYSIS OF THE 9-DOF SYSTEM TRUCK MODEL

Continuous systems consist of infinite degrees of freedom that describe their physical dynamic behavior. The mathematical model of such systems generates an infinite number of coupled differential equations that cannot be solved even with the use of powerful computers. The simulation time is dependent on the complexity and the number of equations for the vibrating body. However, a discrete system can be derived from the continuous system by maintaining the physical behavior of the system while minimizing the number of degrees of freedom. A 9-DOF system is developed and solved numerically. This theoretical model serves as a basis for building the complete truck vibration model using MSC.ADAMS.

The free body diagram of the 9-DOF system and the corresponding forces acting on each component of the truck model are illustrated in Figures 3.4 and 3.5, respectively.

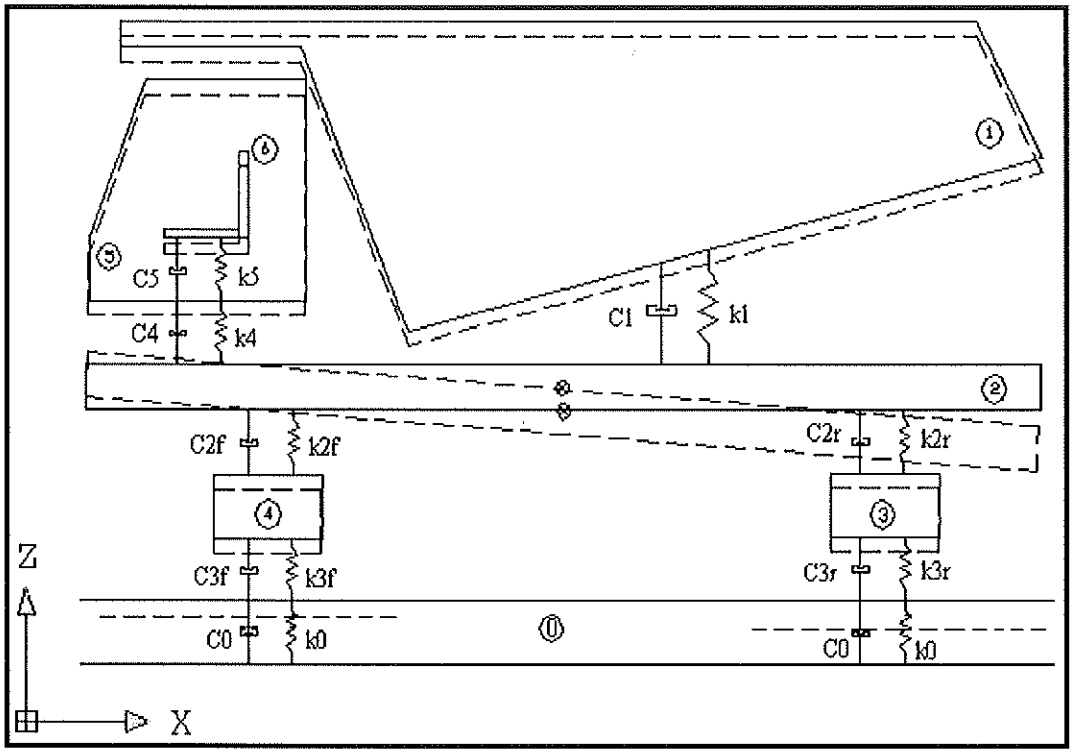

Figure 3.4. Free Body Diagram of the 9-DOF System

The free body diagram of the truck model leads to one EOM for each displacement. This leads to nine equations with nine unknowns (i = 1...9) for the seven major truck component displacements and two ground displacements. The free body diagram shown in Figure 3.4 represents the CAT 793 haul truck. The first two shovel passes are considered in the analysis because these passes are the most critical and primarily responsible for vibrations and shockwaves propagation.

Figure 3.5 shows a detailed free body diagram of the truck with all the internal forces applied to each component including the initial impact force $F_1(t)$ that causes the vibrations throughout the truck. The structural components of the truck include the truck body, the chassis (the sprung mass), the cabin, operators' seat and the tires/wheels

assemblies. The ground is modeled as two unit masses for the front and rear tire-ground interaction, respectively. The applied forces on this structure are functions of space and time.

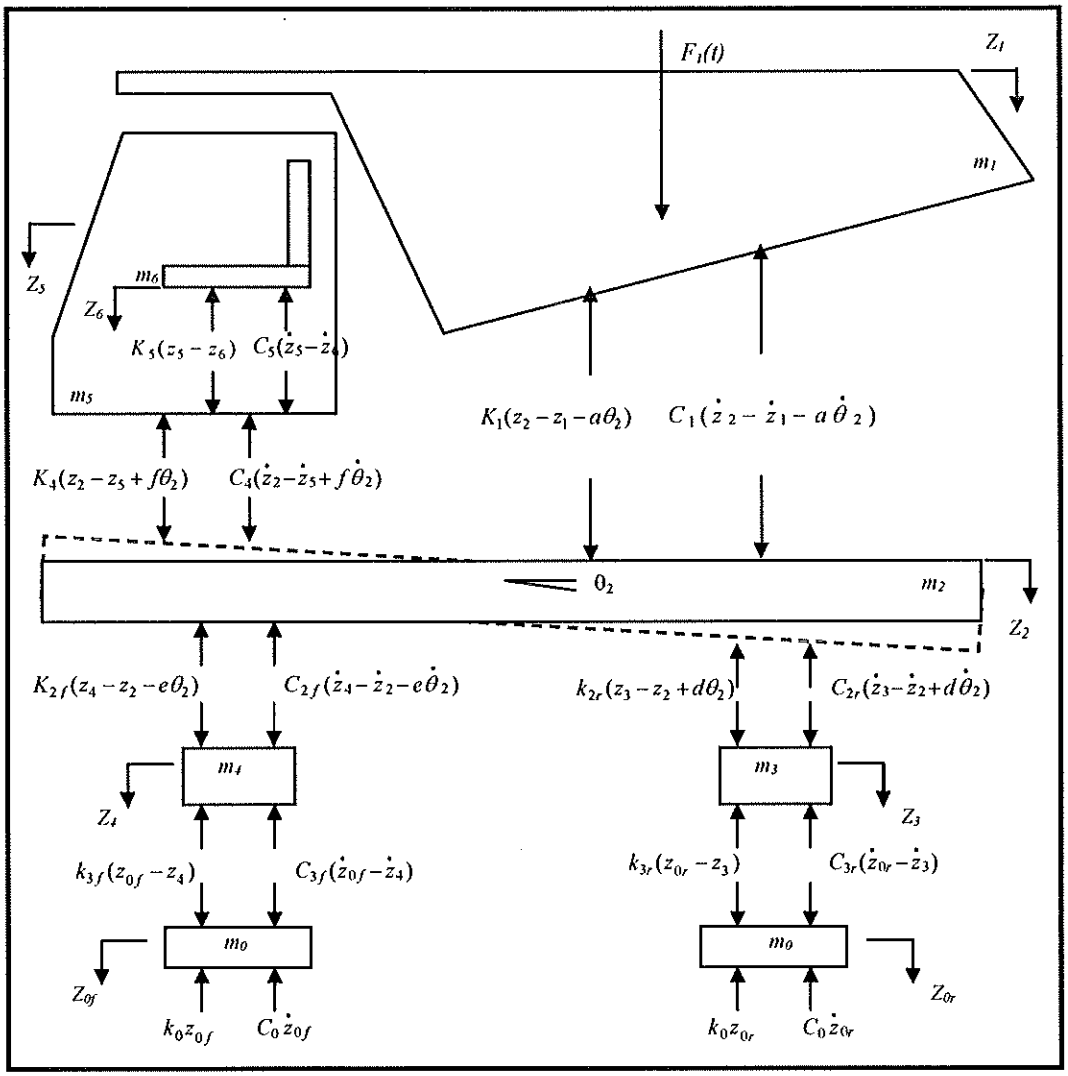

Figure 3.5. Free Body Diagram of Each Mass

3.4.1. Lagrangian Vibration Formulation of the 9-DOF System. The governing equations for the 9-DOF system can be derived using the Lagrangian formulation in equation (3.11). From Figure 3.5, the kinetic energy of the 9-DOF system is written as shown in equation (3.12).

$$T=\frac{1}{2}m_0(\dot{z}_{0f}^2+\dot{z}_{0r}^2)+\frac{1}{2}m_1\dot{z}_1^2+\frac{1}{2}m_2\dot{z}_2^2+\frac{1}{2}I_2\dot{\theta}_2^2 \\ +\frac{1}{2}m_3\dot{z}_3^2+\frac{1}{2}m_4\dot{z}_4^2+\frac{1}{2}m_5\dot{z}_5^2+\frac{1}{2}m_6\dot{z}_6^2 \tag{3.12}$$

The potential or strain energy can also be written as equation (3.13).

$$V=\frac{1}{2}k_1(z_2-z_1-a\theta_2)^2+\frac{1}{2}k_{2r}(z_3-z_2+d\theta_2)^2+\frac{1}{2}k_{2f}(z_4-z_2-e\theta_2)^2 \\ +\frac{1}{2}k_{3r}(z_{0r}-z_3)^2+\frac{1}{2}k_{3f}(z_{0f}-z_4)^2+\frac{1}{2}k_4(z_2-z_5+f\theta_2)^2 \\ +\frac{1}{2}k_5(z_5-z_6)^2+\frac{1}{2}k_0(z_{0f}^2+z_{0r}^2) \tag{3.13}$$

The dissipation energy is given as equation (3.14).

$$R=\frac{1}{2}C_1(\dot{z}_2-\dot{z}_1-a\dot{\theta}_2)^2+\frac{1}{2}C_{2r}(\dot{z}_3-\dot{z}_2+d\dot{\theta}_2)^2+\frac{1}{2}C_{2f}(\dot{z}_4-\dot{z}_2-e\dot{\theta}_2)^2 \\ +\frac{1}{2}C_{3r}(\dot{z}_{0r}-\dot{z}_3)^2+\frac{1}{2}C_{3f}(\dot{z}_{0f}-\dot{z}_4)^2+\frac{1}{2}C_4(\dot{z}_2-\dot{z}_5+f\dot{\theta}_2)^2 \\ +\frac{1}{2}C_5(\dot{z}_5-\dot{z}_6)^2+\frac{1}{2}C_0(\dot{z}_{0r}^2+\dot{z}_{0f}^2) \tag{3.14}$$

The general form of the Lagrange's formulation in equation (3.11) can be expanded to introduce the kinetic and potential energies as in equation (3.15).

$$\frac{d}{dt}\left(\frac{\partial T}{\partial \dot{q}_i}-\frac{\partial V}{\partial \dot{q}_i}\right)-\frac{\partial T}{\partial q_i}+\frac{\partial V}{\partial q_i}+\frac{\partial R}{\partial \dot{q}_i}=F_i(t) \tag{3.15}$$

$\frac{\partial V}{\partial \dot{q}_i}$ and $\frac{\partial T}{\partial q_i}$ vanish because they are independent of $\dot{q}_i$ and q_i respectively. Hence, the final form of the Lagrange's equation for the 9-DOF system is given in equation (3.16).

$$\frac{d}{dt}\left(\frac{\partial T}{\partial \dot{q}_i}\right)+\frac{\partial V}{\partial q_i}+\frac{\partial R}{\partial \dot{q}_i}=F_i(t)\Bigg|_{i=1\ldots9} \tag{3.16}$$

Applying equation (3.16) for the first displacement variable $q_1=z_1$ yields equation (3.17).

$$\frac{d}{dt}\left(\frac{\partial T}{\partial \dot{z}_1}\right)+\frac{\partial V}{\partial z_1}+\frac{\partial R}{\partial \dot{z}_1}=F_1(t) \tag{3.17}$$

By calculating each term in equation (3.17), using equations (3.12), (3.13) and (3.14) yields the first EOM in equation (3.18). $F_1(t)$ is defined in equation (3.1).

$$m_1\ddot{z}_1+C_1(\dot{z}_1-\dot{z}_2+a\dot{\theta}_2)+K_1(z_1-z_2+a\theta_2)=F_1(t) \tag{3.18}$$

Similarly, the Lagrange's equation (3.18) is written in terms of the second displacement variable z_2 as shown in equation (3.19).

$$\frac{d}{dt}\left(\frac{\partial T}{\partial \dot{z}_2}\right)+\frac{\partial V}{\partial z_2}+\frac{\partial R}{\partial \dot{z}_2}=F_2(t) \tag{3.19}$$

$F_2(t) = 0$ because there are no applied forces on the sprung mass. Calculating each term in equation (3.19) yields the second EOM for the system, stated in equation (3.20).

$$\begin{aligned} &m_2\ddot{z}_2+C_1(\dot{z}_2-\dot{z}_1-a\dot{\theta}_2)+C_{2r}(\dot{z}_2-\dot{z}_3-d\dot{\theta}_2)+C_{2f}(\dot{z}_2-\dot{z}_4+e\dot{\theta}_2) \\ &+C_4(\dot{z}_2-\dot{z}_5+f\dot{\theta}_2)+K_1(z_2-z_1-a\theta_2)+K_{2r}(z_2-z_3-d\theta_2) \\ &+K_{2f}(z_2-z_4+e\theta_2)+K_4(z_2-z_5+f\theta_2)=0 \end{aligned} \tag{3.20}$$

Using Lagrange's equation for the third displacement variable z_3 (equation (3.21)) yields the third EOM in equation (3.22).

$$\frac{d}{dt}\left(\frac{\partial T}{\partial \dot{z}_3}\right)+\frac{\partial V}{\partial z_3}+\frac{\partial R}{\partial \dot{z}_3}=F_3(t) \tag{3.21}$$

$F_3(t) = 0$ because there are no applied forces on this mass. Hence, the third EOM is derived as in equation (3.22).

$$m_3\ddot{z}_3+C_{2r}(\dot{z}_3-\dot{z}_2+d\dot{\theta}_2)+C_{3r}(\dot{z}_3-\dot{z}_{0r})+K_{2r}(z_3-z_2+d\theta_2)+K_{3r}(z_3-z_{0r})=0 \quad (3.22)$$

Equation (3.23) shows the fourth Lagrange's equation for the displacement variable z_4 with $F_4(t) = 0$.

$$\frac{d}{dt}\left(\frac{\partial T}{\partial \dot{z}_4}\right)+\frac{\partial V}{\partial z_4}+\frac{\partial R}{\partial \dot{z}_4}=F_4(t) \quad (3.23)$$

Each term in equation (3.23) is calculated to generate the fourth EOM in equation (3.24).

$$m_4\ddot{z}_4+C_{2f}(\dot{z}_4-\dot{z}_2-e\dot{\theta}_2)+C_{3f}(\dot{z}_4-\dot{z}_{0f})+K_{2f}(z_4-z_2-e\theta_2)+K_{3f}(z_4-z_{0f})=0 \quad (3.24)$$

Similarly, equation (3.25) shows the Lagrange's equation for the fifth displacement variable z_5 with no applied forces on mass m_5. This implies that $F_5(t) = 0$.

$$\frac{d}{dt}\left(\frac{\partial T}{\partial \dot{z}_5}\right)+\frac{\partial V}{\partial z_5}+\frac{\partial R}{\partial \dot{z}_5}=F_5(t) \quad (3.25)$$

Each term in equation (3.25) is calculated to generate the EOM for the fifth mass in equation (3.26).

$$m_5\ddot{z}_5+C_4(\dot{z}_5-\dot{z}_2-f\dot{\theta}_2)+C_5(\dot{z}_5-\dot{z}_6)+K_4(z_5-z_2-f\theta_2)+K_5(z_5-z_6)=0 \quad (3.26)$$

Equation (3.27) is the Lagrange's equation for the sixth displacement variable z_6.

$$\frac{d}{dt}\left(\frac{\partial T}{\partial \dot{z}_6}\right)+\frac{\partial V}{\partial z_6}+\frac{\partial R}{\partial \dot{z}_6}=F_6(t) \tag{3.27}$$

Calculating each term in equation (3.27) with no external forces applied on mass m_6 (i.e., $F_6(t)=0$), leads to the EOM in equation (3.28).

$$m_6\ddot{z}_6+C_5(\dot{z}_6-\dot{z}_5)+K_5(z_6-z_5)=0 \tag{3.28}$$

The kinetic, potential and dissipation energies are derived with respect to the pitch angle θ_2, and $F_2(t)=0$. The resulting derivation of equation (3.29) generates the seventh EOM of this system in equation (3.30).

$$\frac{d}{dt}\left(\frac{\partial T}{\partial \dot{\theta}_2}\right)+\frac{\partial V}{\partial \theta_2}+\frac{\partial R}{\partial \dot{\theta}_2}=F_2(t) \tag{3.29}$$

$$\begin{aligned} &I_2\ddot{\theta}_2+C_1a(\dot{z}_1-\dot{z}_2+a\dot{\theta}_2)+C_{2r}d(\dot{z}_3-\dot{z}_2+d\dot{\theta}_2)+C_{2f}e(\dot{z}_2-\dot{z}_4+e\dot{\theta}_2) \\ &+C_4f(\dot{z}_2-\dot{z}_5+f\dot{\theta}_2)+K_1a(z_1-z_2+a\theta_2)+K_{2r}d(z_3-z_2+d\theta_2) \\ &+K_{2f}e(z_2-z_4+e\theta_2)+K_4f(z_2-z_5+f\theta_2)=0 \end{aligned} \tag{3.30}$$

The Lagrange's equation is written in equation (3.31) for the eighth displacement variable z_{0r}.

$$\frac{d}{dt}\left(\frac{\partial T}{\partial \dot{z}_{0r}}\right)+\frac{\partial V}{\partial z_{0r}}+\frac{\partial R}{\partial \dot{z}_{0r}}=F_8(t) \tag{3.31}$$

Calculating each term in equation (3.31), with $F_8(t)=0$, leads to the EOM of mass m_0 in equation (3.32).

$$m_0\ddot{z}_{0r}+C_{3r}(\dot{z}_{0r}-\dot{z}_3)+C_0\dot{z}_{0r}+K_{3r}(z_{0r}-z_3)+K_0z_{0r}=0 \tag{3.32}$$

Finally, the Lagrange's equation is written in equation (3.33) for the ninth displacement variable z_{0f}.

$$\frac{d}{dt}\left(\frac{\partial T}{\partial \dot{z}_{0f}}\right)+\frac{\partial V}{\partial z_{0f}}+\frac{\partial R}{\partial \dot{z}_{0f}}=F_9(t) \tag{3.33}$$

Calculating each term in equation (3.33), with $F_9(t)=0$, leads to the EOM of mass m_0 in equation (3.34).

$$m_0\ddot{z}_{0f}+C_{3f}(\dot{z}_{0f}-\dot{z}_4)+C_0\dot{z}_{0f}+K_{3f}(z_{0f}-z_4)+K_0z_{0f}=0 \tag{3.34}$$

Equations (3.18), (3.20), (3.22), (3.24), (3.26), (3.28), (3.30), (3.32), and (3.34) can be written in an expanded matrix form of 9x9 mass, damping and stiffness matrices,

multiplied by 9x1 acceleration, velocity and displacement vectors and set equal to a 9x1 force vector. This is illustrated in equation (3.35).

$$
\begin{bmatrix}
m_1 & 0 & 0 & 0 & 0 & 0 & 0 & 0 & 0 \\
0 & m_2 & 0 & 0 & 0 & 0 & 0 & 0 & 0 \\
0 & 0 & m_3 & 0 & 0 & 0 & 0 & 0 & 0 \\
0 & 0 & 0 & m_4 & 0 & 0 & 0 & 0 & 0 \\
0 & 0 & 0 & 0 & m_5 & 0 & 0 & 0 & 0 \\
0 & 0 & 0 & 0 & 0 & m_6 & 0 & 0 & 0 \\
0 & 0 & 0 & 0 & 0 & 0 & m_0 & 0 & 0 \\
0 & 0 & 0 & 0 & 0 & 0 & 0 & m_0 & 0 \\
0 & 0 & 0 & 0 & 0 & 0 & 0 & 0 & I_2
\end{bmatrix}
\begin{Bmatrix}
\ddot{z}_1 \\ \ddot{z}_2 \\ \ddot{z}_3 \\ \ddot{z}_4 \\ \ddot{z}_5 \\ \ddot{z}_6 \\ \ddot{z}_{0r} \\ \ddot{z}_{0f} \\ \ddot{\theta}_2
\end{Bmatrix} +
$$

$$
\begin{bmatrix}
C_1 & -C_1 & 0 & 0 & 0 & 0 & 0 & 0 & aC_1 \\
-C_1 & A^* & -C_{2r} & -C_{2f} & -C_4 & 0 & 0 & 0 & B^* \\
0 & -C_{2r} & C_{2r}+C_{3r} & 0 & 0 & 0 & -C_{3r} & 0 & dC_{2r} \\
0 & -C_{2f} & 0 & C_{2f}+C_{3f} & 0 & 0 & 0 & -C_{3f} & -eC_{2f} \\
0 & -C_4 & 0 & 0 & C_4+C_5 & -C_5 & 0 & 0 & -fC_4 \\
0 & 0 & 0 & 0 & -C_5 & C_5 & 0 & 0 & 0 \\
0 & 0 & -C_{3r} & 0 & 0 & 0 & C_0+C_{3r} & 0 & 0 \\
0 & 0 & 0 & -C_{3f} & 0 & 0 & 0 & C_0+C_{3f} & 0 \\
aC_1 & B^* & dC_{2r} & -eC_{2f} & -fC_4 & 0 & 0 & 0 & D^*
\end{bmatrix}
\begin{Bmatrix}
\dot{z}_1 \\ \dot{z}_2 \\ \dot{z}_3 \\ \dot{z}_4 \\ \dot{z}_5 \\ \dot{z}_6 \\ \dot{z}_{0r} \\ \dot{z}_{0f} \\ \dot{\theta}_2
\end{Bmatrix} +
$$

$$
\begin{bmatrix}
k_1 & -k_1 & 0 & 0 & 0 & 0 & 0 & 0 & ak_1 \\
-k_1 & E^* & -k_{2r} & -k_{2f} & -k_4 & 0 & 0 & 0 & F^* \\
0 & -k_{2r} & k_{2r}+k_{3r} & 0 & 0 & 0 & -k_{3r} & 0 & dk_{2r} \\
0 & -k_{2f} & 0 & k_{2f}+k_{3f} & 0 & 0 & 0 & -k_{3f} & -ek_{2f} \\
0 & -k_4 & 0 & 0 & k_4+k_5 & -k_5 & 0 & 0 & -fk_4 \\
0 & 0 & 0 & 0 & -k_5 & k_5 & 0 & 0 & 0 \\
0 & 0 & -k_{3r} & 0 & 0 & 0 & k_0+k_{3r} & 0 & 0 \\
0 & 0 & 0 & -k_{3f} & 0 & 0 & 0 & k_0+k_{3f} & 0 \\
ak_1 & F^* & dk_{2r} & -ek_{2f} & -fk_4 & 0 & 0 & 0 & G^*
\end{bmatrix}
\begin{Bmatrix}
z_1 \\ z_2 \\ z_3 \\ z_4 \\ z_5 \\ z_6 \\ z_{0r} \\ z_{0f} \\ \theta_2
\end{Bmatrix} =
\begin{Bmatrix}
F_1(t) \\ 0 \\ 0 \\ 0 \\ 0 \\ 0 \\ 0 \\ 0 \\ 0
\end{Bmatrix}
\tag{3.35}
$$

The terms A^*, B^*, D^*, E^*, F^* and G^* in the damping and stiffness matrices respectively are defined as follows:

$$\begin{cases} A^* = C_1 + C_{2r} + C_{2f} + C_4 \\ B^* = eC_{2f} + fC_4 - aC_1 - dC_{2r} \\ D^* = a^2C_1 + d^2C_{2r} + e^2C_{2f} + f^2C_4 \\ E^* = k_1 + k_{2r} + k_{2f} + k_4 \\ F^* = ek_{2f} + fk_4 - ak_1 - dk_{2r} \\ G^* = a^2k_1 + d^2k_{2r} + e^2k_{2f} + f^2k_4 \end{cases} \tag{3.35a}$$

Equation (3.35) can be presented in a compact form as in equation (3.36).

$$[M]\{\ddot{z}(t)\} + [C]\{\dot{z}(t)\} + [K]\{z(t)\} = \{F(t)\} \tag{3.36}$$

The EOMs generated by the energy method shown in the matrix form in equation (3.35) are second order coupled differential equations. There are many techniques for decoupling these equations; among them are the direct integral and the modal analysis. The modal analysis is used to generate the final solution of the set of equations in this study.

3.4.2. Modal Analysis for the Forced Damped Vibration. The response of the free vibration model does not represent a real case scenario. The presence of a damping mechanism in most structures will bring the system to rest after excitation where the energy is dissipated through the damping system. Therefore, the damping matrix in equation (3.36) must be considered to generate a complete solution for the HISLO problem. The damping matrix will introduce difficulty in the analysis of the mathematical model due to the fact that the EOMs are coupled and tedious to solve.

The Rayleigh[2] method is used to decouple the EOMs to solve the truck vibration problem under HISLO conditions. This method approximates the damping matrix by creating the Rayleigh-equivalent viscous damping model, which is proportional to the stiffness and mass matrices, as defined in equation (3.37)

$$[C] = \alpha[M] + \beta[K] \tag{3.37}$$

The modal analysis procedure provides a response to the excitation introduced by the application of external forces. The solution of the 9-DOF system is assumed to be a combination of the normal modes $\hat{u}_i(t)$ found from the Eigenvalues problem [P] solved in Chapter 4.0 multiplied by a time-dependent generalized coordinates $q_i(t)$. The $q_i(t)$ is also known as the principal coordinates or modal participation coefficients. The solution has the form stated in equation (3.38).

---

[2] John William Strutt, Lord Rayleigh (1842-1919) was an English physicist well known for the "Theory of Sound". The method of computing approximate natural frequencies of vibrating bodies using an energy approach has become known as the "Rayleigh method".

$$\{z_i(t)\}=[P]\{q(t)\}=\sum_{i=1}^{9}\{\hat{u}_i(t)\}q_i(t) \tag{3.38}$$

$$[P]=\left[\begin{Bmatrix}\hat{u}\end{Bmatrix}_1 \quad \begin{Bmatrix}\hat{u}\end{Bmatrix}_2 \quad \begin{Bmatrix}\hat{u}\end{Bmatrix}_3 \quad \begin{Bmatrix}\hat{u}\end{Bmatrix}_4 \quad \begin{Bmatrix}\hat{u}\end{Bmatrix}_5 \quad \begin{Bmatrix}\hat{u}\end{Bmatrix}_6 \quad \begin{Bmatrix}\hat{u}\end{Bmatrix}_7 \quad \begin{Bmatrix}\hat{u}\end{Bmatrix}_8 \quad \begin{Bmatrix}\hat{u}\end{Bmatrix}_9\right] \tag{3.39}$$

The suggested solution in equation (3.38) is substituted in the set of governing equations in equation (3.36), which leads to equation (3.40) in the matrix form.

$$[M][P]\{\ddot{q}\}+[C][P]\{\dot{q}\}+[K][P]\{q\}=\{F(t)\} \tag{3.40}$$

Equation (3.40) is multiplied with the transpose of [P] (equation (3.39)), which yields equation (3.41).

$$[P]^T[M][P]\{\ddot{q}\}+[P]^T[C][P]\{\dot{q}\}+[P]^T[K][P]\{q\}=[P]^T\{F(t)\} \tag{3.41}$$

$$\begin{cases}[P]^T[M][P]=[I]\\ [I]=\text{Identity Matrix}\\ [P]^T[K][P]=[\Omega]\\ [\Omega]=[\text{diagonal of } \omega_i^2]\end{cases} \tag{3.42}$$

The Rayleigh damping model in equation (3.37) is used with equation (3.41) in order to generate the proportional Rayleigh viscous damping model in equation (3.43).

$$\begin{aligned}\left[P\right]^T\left[C\right]\left[P\right]\left\{\dot{q}\right\} &= \left[P\right]^T\left(\alpha\left[M\right]+\beta\left[K\right]\right)\left[P\right]\left\{\dot{q}\right\} \\ &= \left(\alpha\left[P\right]^T\left[M\right]\left[P\right]+\beta\left[P\right]^T\left[K\right]\left[P\right]\right)\left\{\dot{q}\right\} \\ &= \left(\alpha\left[I\right]+\beta\left[\Omega\right]\right)\left\{\dot{q}\right\} = \left(\alpha+\beta\omega_i^2\right)\dot{q}_i \quad \text{i=1...9}\end{aligned} \tag{3.43}$$

Decoupling the governing equations from the matrix in (3.36) yields equation (3.44) that can be solved analytically.

$$\ddot{q}_i+\left(\alpha+\beta\omega_i^2\right)\dot{q}_i+\omega_i^2 q_i = N_i(t) \tag{3.44}$$

$$\begin{cases} N_i(t)=\sum_{j=1}^{9} u_{ji}F_j(t) \\ \left(\alpha+\beta\omega_i^2\right)\equiv 2\zeta_i\omega_i \end{cases} \tag{3.45}$$

Equation (3.44) denotes nine decoupled differential equations of second order that can be re-written as equation (3.46).

$$\ddot{q}_i+2\zeta_i\omega_i\dot{q}_i+\omega_i^2 q_i = N_i(t) \quad \text{i=1...9} \tag{3.46}$$

3.4.3. Solution of the Forced Damped Vibration. The Duhamel's integral is used to generate the different q_i (i=1...9) in equation (3.46) in the forced vibrations problem. Duhamel's integral is a linear operator that captures functions of time and produces functions of time. The general form of the solution to equation (3.46) is a function of the input, the damping frequency, and the initial conditions of the system as stated in equation (3.47).

$$q_i(t)=\frac{1}{\omega_{di}}\int_0^t N_i(\tau)e^{-\zeta_i\omega_{di}(t-\tau)}\sin\omega_{di}(t-\tau)+e^{-\zeta_i\omega_{ni}t}\left[\frac{q_i(0)}{(1-\zeta_i^2)^{1/2}}\cos(\omega_{di}t-\phi_i)+\frac{\dot{q}_i(0)}{\omega_{di}}\sin\omega_{di}t\right] \quad (3.47)$$

The damped frequency (ω_{di}) and the phase angle (ϕ_i), respectively are defined in equation (3.48).

$$\begin{cases} \omega_{di} = \omega_{ni}\sqrt{1-\zeta_i^2} \\ \phi_i = \tan^{-1}\left(\dfrac{\zeta_i}{\sqrt{1-\zeta_i^2}}\right) \end{cases} \quad (3.48)$$

The natural frequencies for the undamped free vibration, ω_{ni} in equation (3.48) are used to calculate the damped frequencies, ω_{di}, of the system. The initial displacement, velocity and acceleration of the HISLO problem are equal to zero, i.e., $q_i(0)=\dot{q}_i(0)=\ddot{q}_i(0)=0$. Using these initial conditions, equation (3.47) can be solved for the generalized displacements $q_i\ (t)$ for i =1...9 and re-written as equation (3.49).

$$q_i(t) = \frac{1}{\omega_{di}} \int_0^t N_i(\tau) e^{-\zeta_i \omega_{ni}(t-\tau)} \sin \omega_{di}(t-\tau) \tag{3.49}$$

The results are then factored in to equation (3.38) and restated as equation (3.50).

$$\{z_i(t)\} = \sum_{i=1}^{9} \left\{\hat{u}_i(t)\right\} \frac{1}{\omega_{di}} \int_0^t N_i(\tau) e^{-\zeta_i \omega_{ni}(t-\tau)} \sin \omega_{di}(t-\tau) \tag{3.50}$$

The $\{z_i(t)\}$ is a 9x1 vector describing the complete displacement response of the truck under HISLO conditions. The results give the complete solution of the set of EOMs developed in equation (3.36). The velocity and acceleration vectors are found by taking the first and second derivative of equation (3.50), respectively.

3.5. SUMMARY

The theoretical model of the truck vibrations under HISLO conditions has been presented in this Chapter. This was achieved by building a 9-DOF system and solving for the displacement, velocity and accelerations vectors of the system. The results can be used to find the vibration at each truck component under the HISLO conditions. Then it can be determined whether they are harmful to the operator and the machine. A modeling framework was established based on the necessary assumptions and limitations. This framework establishes the major truck vibration kinematic parameters, such as, the displacement, velocity and the acceleration vectors. The vibrations arise due to the high impact of the material dumped by the shovel. These high impact forces result in shockwaves propagation traveling throughout the truck body, chassis and reaching the

cabin. The input variables, such as the truck component weights, the springs and damping coefficients are related to the output variables by second order nine coupled differential equations. The findings in this chapter serve as a guideline for the complete dynamic virtual truck model under HISLO conditions. This chapter is a pioneering study of truck vibrations under HISLO conditions.

4. NUMERICAL SOLUTIONS FOR DUMP TRUCK VIBRATIONS MECHANICS

The numerical models and algorithms used for solving the set of equations of motion for the different masses of the truck model are illustrated in this chapter. The equations of motion (see Chapter 3.0) are second-order coupled differential equations. The Fehlberg fourth-fifth order Runge-Kutta (RKF 45) numerical method is used to solve the equations of motions symbolically. Furthermore, the stability, convergence and error estimates are also discussed, as well as, the numerical integration procedure. Finally, the solution of the undamped free vibration problem is obtained for the 9-DOF truck system.

4.1. NUMERICAL TECHNIQUES

Numerical models and algorithms are required to solve the second order coupled-differential equations of motions in equation (3.36). MAPLE© is chosen as a programming platform for solving the set of EOMs. The MAPLE© platform was chosen because it offers a vast library of numerical algorithms. In addition, it is efficient for numerical algorithms and can handle symbolic analysis in the development of the solution. Figure 4.1 shows the flowchart of the numerical method for this research. The input force (impulse force), mass, damping and stiffness matrices are considered as input variables for the algorithm. These input variables are used to define the kinetic, potential and dissipation energies of the truck model components. Using Lagrange's formulation, these energy terms lead to the generation of a set of nine EOMs describing the forced damped vibration problem. The first step is to solve the undamped free vibration problem. Detailed description of this process is illustrated in Figure 4.2.

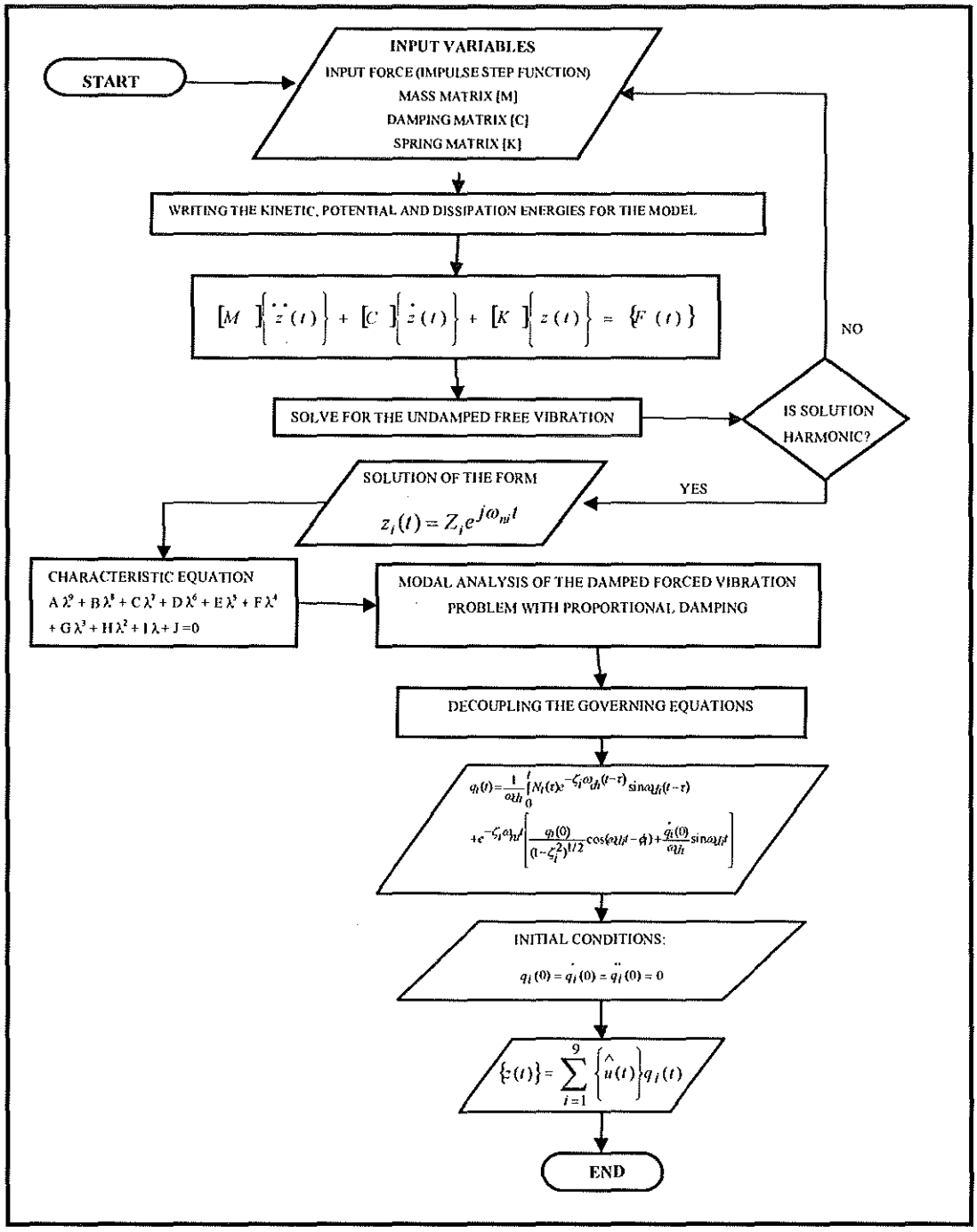

Figure 4.1. Flowchart of the Numerical Methods for the Solution

The vibration response of the undamped problem undergoes oscillatory motion that has harmonic characteristics. Thus, the solution is assumed to be harmonic with an

amplitude Z_i, and a frequency $\omega_{n,i}$. If this is true, this solution is replaced in the EOMs leading to the characteristic equation of the system. If this is false, then the input variables need to be reviewed to understand the nature of the input force and its mathematical modeling in order to select the appropriate solution form. Next, the modal analysis of the characteristic equation is conducted where the governing equations are decoupled, and Duhamel's integral is used to solve for the displacement vector $\{z_i(t)\}$ along with the initial conditions of the vibration problem.

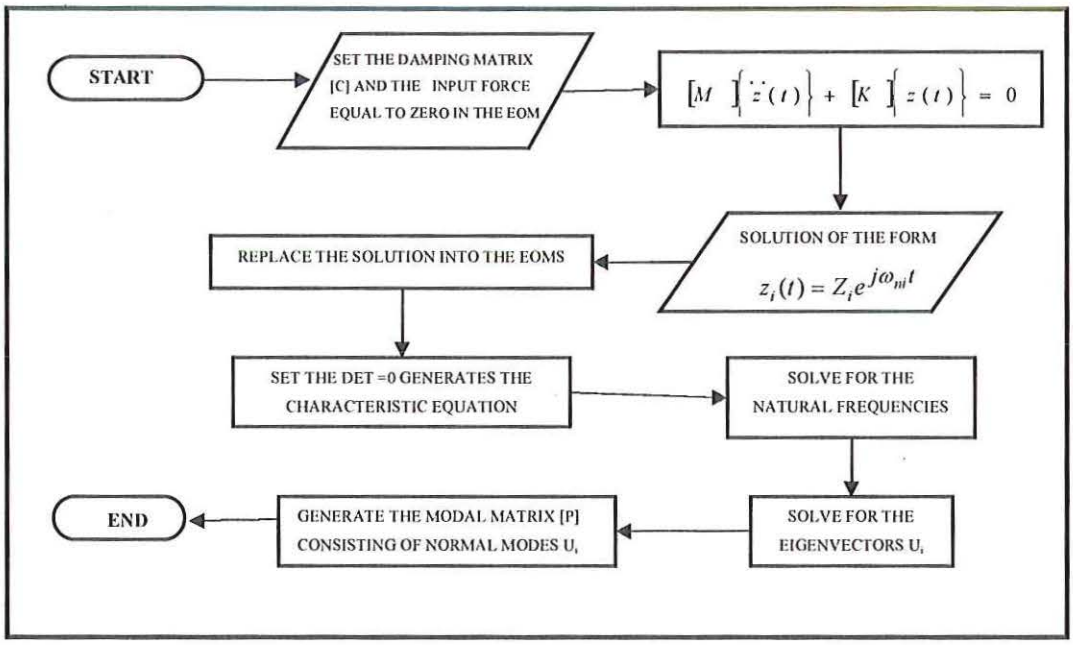

Figure 4.2. Undamped Free Vibration Solution Flowchart

Figure 4.2 describes the different steps taken to solve the undamped free vibration problem. The solution, assumed to be harmonic, is replaced in the EOMs to determine the natural frequencies of the system by solving the characteristic equation. Each natural frequency generates nine eigenvectors when replaced in the EOMs. The corresponding eigenvectors are then normalized to generate the modal matrix [P]. This modal matrix is a

9x9 matrix that includes the normal modes that describe the system behavior. The modal matrix [P] is used in finding the solution of the forced damped vibration problem.

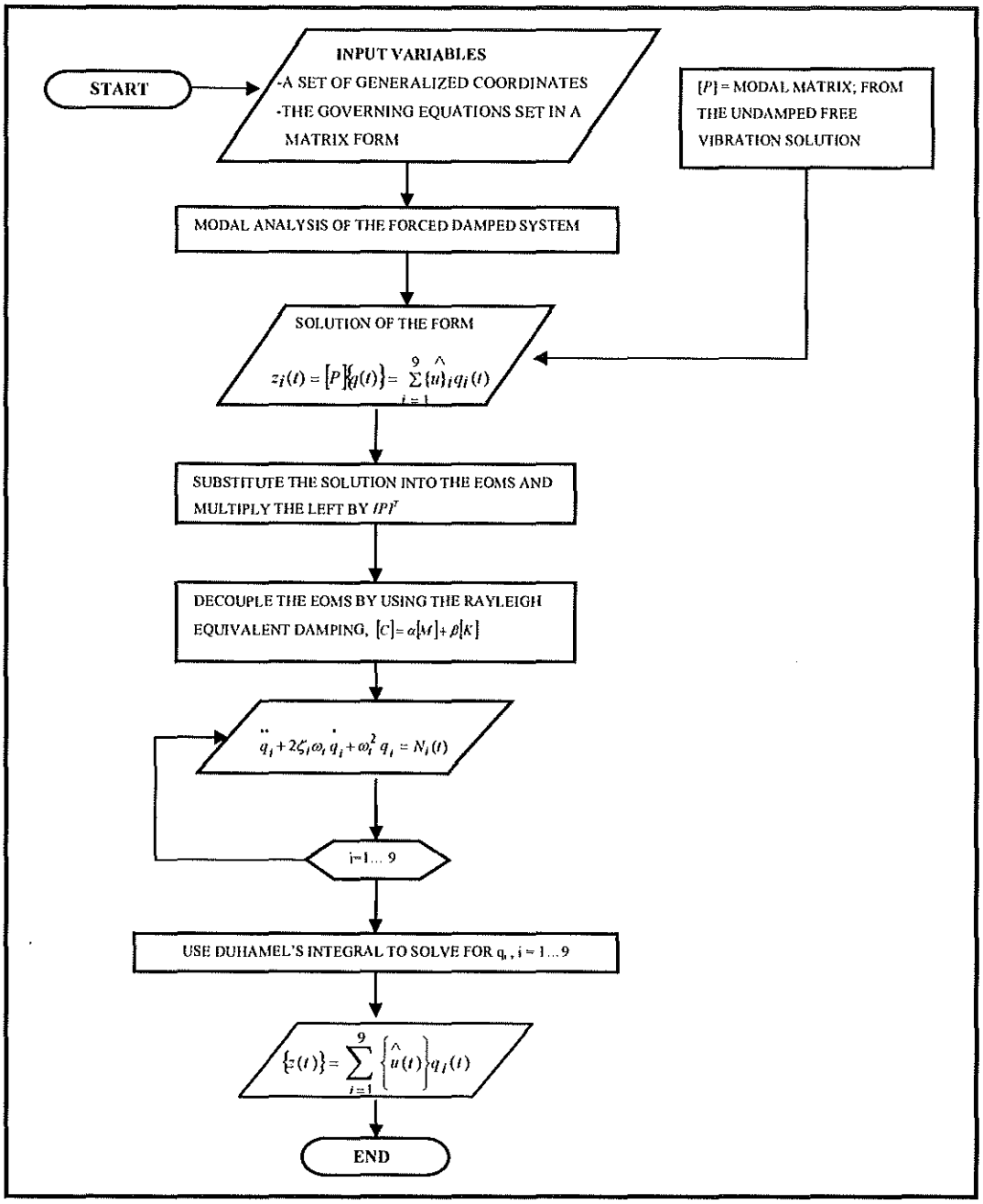

Figure 4.3. Modal Analysis Flowchart

Figure 4.3 illustrates the modal analysis process for finding the solution of the damped forced vibration problem. The solution is the product of the modal matrix, [P], and the generalized displacement vector {q(t)}. This solution is then substituted into the EOMs. The Rayleigh equivalent damping is used to decouple the EOMs. Once the EOMs are decoupled, they are solved for {q(t)} using the Duhamel's integral. The result is the displacement vector {z(t)} expressed in terms of the normal modes and the generalized displacement vector {q(t)}.

Several numerical solver algorithms for solving ODEs of the initial value kind are available in MAPLE©. Among them, the Implicit Rosenbrock, third-fourth order Runge-Kutta, the Multistep Gear, the Gear single-step extrapolation, the seventh-eighth order continuous Runge-Kutta, the Livermore Stiff ODE solver and the Taylor series methods. The RKF 45 method is used for solving the coupled differential equations since the system did not exhibit stiffness. This method is an adaptive numeric procedure for solving the initial value problem. It combines the fourth and fifth-order Runge-Kutta techniques to monitor error. The RKF 45 uses a dynamic step reduction strategy with only two function evaluations more than is used in the fixed-step fourth-order Runge-Kutta method. This algorithm requires four evaluations of the function in order to return an estimate of the dependent variable (Maplesoft, 2006).

4.2. STABILITY, CONVERGENCE AND ERRORS ESTIMATE

The error estimates of the method used for the solution were set to 10^{-7} for the absolute error and 10^{-6} for the relative error. These error tolerances are the default values

for the Fehlberg fourth-fifth order Runge-Kutta method. The initial step size i, is determined by the method taking into account the local behavior of the ODE system. The RKF 45 method solves the initial value problem (IVP) by approximating the solution successively at a discrete set of points. Using an approximation y[i] to y(x[i]), an approximation y[i+1] is computed to y(x[i+1]) with a step size h=x[i+1]-x[i]. At each step, the solver makes a truncation and/or discretization error that depend on the method and the length of the step. The cumulative effect of these errors depends on the stability of the IVP near the solution y(x). If the IVP is stable near the solution with nearby initial data that do not diverge from one another, errors are not amplified, but if the IVP is unstable near the solution, errors are amplified (Cartwright et al., 1992). Adaptive solvers estimate the discretization error at each step, and control the error by adjusting the step size. The cumulative error in the numerical solution depends on the stability of the IVP, but for moderately stable problems, the solvers are tuned so that the error is comparable to the tolerances on the discretization error.

The summation of the coefficients of the RKF 45 method is equal to one resulting in a necessary and sufficient condition for consistency. Consistency is a necessary and sufficient condition for convergence (Cartwright et al., 1992). This condition is satisfied for all Runge-Kutta methods of order one or higher. Therefore, the RKF 45 produces solutions that are stable and convergent. The Eigenvalues are computed by the QR[3] orthogonal-triangular matrix decomposition method. This method decomposes a matrix as a product of Q (orthogonal) and R (upper-triangular) matrices. The matrix is first

[3] The product QR is computed where Q is an orthonormal matrix and R is an upper-triangular matrix.

balanced and transformed into upper Hessenberg form, for computing the Eigenvalues and Eigenvectors.

4.3. NUMERICAL INTEGRATION PROCEDURES

The RKF 45 method has two distinct modes of operation. When it is used with the range option, the method computes the solution for the IVP over the specified range, stores the solution information internally, and uses that information to rapidly interpolate the desired solution value for any call to the returned procedure. In the first mode of operation, the method adjusts the step sizes at the end-points of the integration in either direction, within the boundaries of the end-points range. This method is not recommended for problems in which the solution can become singular. Many steps are taken and stored when the solution is near singular, thus the memory usage can become a significant issue.

When this method is used without the range option, the IVP solution values are not stored, but rather computed when requested. In this second mode of operation, the output solution values are computed using an interpolation method. This approach provides a more efficient continuation of the solution if multiple points are required. The computation must restart at the initial values whenever a solution point is required between the initial point and the most recently computed point because not all the IVP solution values are stored.

4.4. NUMERICAL SOLUTION OF THE 9-DOF SYSTEM

The system EOMs (in Chapter 3.0) are second-order coupled differential equations presented in a matrix form as equation (3.36). Numerical solution techniques are used to solve the 9-DOF undamped free vibration problem because the nine coupled differential equations cannot be solved analytically.

Equation (3.36) represents the EOMs of the truck vibration model in a matrix form. The damping matrix [C] causes coupled equations, which increases the complexity of the problem. The first solution step is to find the response from a free vibration system with no damping. The undamped solution results include the different natural frequencies $\omega_{n,i}$ of the system and the eigenvectors $\left\{\hat{u}_i(t)\right\}$. The natural frequencies are used to obtain the damped frequencies ω_{di} for the problem. The damped frequencies are used to derive the generalized displacement responses q_i to the vibration propagation. The EOMs for the free vibration problem are defined in the matrix form, as shown in equation (4.1).

$$[M]\{\ddot{z}(t)\}+[K]\{z(t)\}=\{0\} \tag{4.1}$$

The solution of the free vibration problem consists of multiple steps. First, equation (4.1) is multiplied by the mass inverse matrix $[M]^{-1}$, resulting in equation (4.2).

$$[I]\{\ddot{z}(t)\}+[A]\{z(t)\}=\{0\} \tag{4.2}$$

The solution of the determinant and the inverse matrices for the 9-DOF problem, with 9x9 matrices, requires the computation of 9! = 362,880 terms. MAPLE© is chosen as the programming platform for finding the determinant and, hence solving for the natural frequencies of the system numerically. The inverse mass matrix $[M]^{-1}$ is computed in the form of equation (4.3).

$$[M]^{-1} = \frac{1}{\det(M)} \cdot [M]^{T} = \begin{bmatrix} \frac{1}{m_1} & 0 & 0 & 0 & 0 & 0 & 0 & 0 & 0 \\ 0 & \frac{1}{m_2} & 0 & 0 & 0 & 0 & 0 & 0 & 0 \\ 0 & 0 & \frac{1}{m_3} & 0 & 0 & 0 & 0 & 0 & 0 \\ 0 & 0 & 0 & \frac{1}{m_4} & 0 & 0 & 0 & 0 & 0 \\ 0 & 0 & 0 & 0 & \frac{1}{m_5} & 0 & 0 & 0 & 0 \\ 0 & 0 & 0 & 0 & 0 & \frac{1}{m_6} & 0 & 0 & 0 \\ 0 & 0 & 0 & 0 & 0 & 0 & \frac{1}{m_0} & 0 & 0 \\ 0 & 0 & 0 & 0 & 0 & 0 & 0 & \frac{1}{m_0} & 0 \\ 0 & 0 & 0 & 0 & 0 & 0 & 0 & 0 & \frac{1}{I_2} \end{bmatrix} \tag{4.3}$$

Hence, the dynamic matrix $[A]$ can be found as equation (4.4).

$$[M]^{-1}\cdot[K]=[A]$$

$$\Rightarrow\begin{bmatrix}
\frac{k_1}{m_1} & \frac{-k_1}{m_1} & 0 & 0 & 0 & 0 & 0 & 0 & \frac{ak_1}{m_1} \\
\frac{-k_1}{m_2} & B^* & \frac{-k_{2r}}{m_2} & \frac{-k_{2f}}{m_2} & \frac{-k_4}{m_2} & 0 & 0 & 0 & D^* \\
0 & \frac{-k2r}{m3} & \frac{k_{2r}+k_{3r}}{m_3} & 0 & 0 & 0 & \frac{-k_{3r}}{m_3} & 0 & \frac{dk_{2r}}{m_3} \\
0 & \frac{-k2f}{m4} & 0 & \frac{k_{2f}+k_{3f}}{m_4} & 0 & 0 & 0 & \frac{-k_{3f}}{m_4} & \frac{-ek_{2f}}{m_4} \\
0 & \frac{-k4}{m5} & 0 & 0 & \frac{k_4+k_5}{m_5} & \frac{-k_5}{m_5} & 0 & 0 & \frac{-fk_4}{m_5} \\
0 & 0 & 0 & 0 & \frac{-k_5}{m_6} & \frac{k_5}{m_6} & 0 & 0 & 0 \\
0 & 0 & \frac{-k_{3r}}{m_0} & 0 & 0 & 0 & \frac{k_0+k_{3r}}{m_0} & 0 & 0 \\
0 & 0 & 0 & \frac{-k_{3f}}{m_0} & 0 & 0 & 0 & \frac{k_0+k_{3f}}{m_0} & 0 \\
\frac{ak_1}{I_2} & E^* & \frac{dk_{2r}}{I_2} & \frac{-ek_{2f}}{I_2} & \frac{-fk_4}{I_2} & 0 & 0 & 0 & F^*
\end{bmatrix} \tag{4.4}$$

The terms B^*, D^*, E^*, and F^* in equation (4.4) are defined as follows:

$$\begin{cases}
B^* = \dfrac{k_1 + k_{2r} + k_{2f} + k_4}{m_2} \\
D^* = \dfrac{ek_{2f} + fk_4 - ak_1 - dk_{2r}}{m_2} \\
E^* = \dfrac{ek_{2f} + fk_4 - ak_1 - dk_{2r}}{I_2} \\
F^* = \dfrac{a^2k_1 + d^2k_{2r} + e^2k_{2f} + f^2k_4}{I_2}
\end{cases} \tag{4.4a}$$

The required solution has a harmonic form as illustrated in equation (4.5).

$$z_i(t) = Z_i e^{j\omega_n t} \tag{4.5}$$

Z_i in equation (4.5) is the amplitude of the response (i=1…9) and ω is the frequency of oscillations. Taking the second derivative of equation (4.5) and substituting the values of z and $\ddot{z}$ in the governing equation (4.2) leads to equation (4.6).

$$\left(\left[A\right]-\omega_{ni}^{2}\left[I\right]\right)Z_i e^{j\omega_{ni}t}=\left\{0\right\} \tag{4.6}$$

A change of variables $\lambda=\omega_{ni}^{2}$ is used in equation (4.6) to simplify the computational process. The result is shown in equation (4.7).

$$\Rightarrow\left(\left[A\right]-\lambda\left[I\right]\right)Z_i e^{j\omega_{ni}t}=\left\{0\right\} \tag{4.7}$$

Equation (4.7) has a non-trivial solution only if the determinant of the coefficients equals to zero, i.e., *DET* ([*A*] – λ. [*I*]) = 0. The amplitude should be non-zero ($Z_i \neq 0$), otherwise a trivial solution will occur and there will be no motion. This determinant is a 9x9 matrix, and is set to zero as shown in equation (4.8).

$$[[A]-\lambda[I]]=0$$

$$\begin{bmatrix}
\frac{k_1}{m_1}-\lambda & \frac{-k_1}{m_1} & 0 & 0 & 0 & 0 & 0 & 0 & \frac{ak_1}{m_1} \\
\frac{-k_1}{m_2} & B^*-\lambda & \frac{-k_{2r}}{m_2} & \frac{-k_{2f}}{m_2} & \frac{-k_4}{m_2} & 0 & 0 & 0 & D^* \\
0 & \frac{-k_{2r}}{m_3} & \frac{k_{2r}+k_{3r}}{m_3}-\lambda & 0 & 0 & 0 & \frac{-k_{3r}}{m_3} & 0 & \frac{dk_{2r}}{m_3} \\
0 & \frac{-k_{2f}}{m_4} & 0 & \frac{k_{2f}+k_{3f}}{m_4}-\lambda & 0 & 0 & 0 & \frac{-k_{3f}}{m_4} & \frac{-ek_{2f}}{m_4} \\
0 & \frac{-k_4}{m_5} & 0 & 0 & \frac{k_4+k_5}{m_5}-\lambda & \frac{-k_5}{m_5} & 0 & 0 & \frac{-fk_4}{m_5} \\
0 & 0 & 0 & 0 & \frac{-k_5}{m_6} & \frac{k_5}{m_6}-\lambda & 0 & 0 & 0 \\
0 & 0 & \frac{-k_{3r}}{m_0} & 0 & 0 & 0 & \frac{k_0+k_{3r}}{m_0}-\lambda & 0 & 0 \\
0 & 0 & 0 & \frac{-k_{3f}}{m_0} & 0 & 0 & 0 & \frac{k_0+k_{3f}}{m_0}-\lambda & 0 \\
\frac{ak_1}{I_2} & E^* & \frac{dk_{2r}}{I_2} & \frac{-ek_{2f}}{I_2} & \frac{-fk_4}{I_2} & 0 & 0 & 0 & F^*-\lambda
\end{bmatrix}=0 \tag{4.8}$$

Solving equation (4.8) for λ leads to the generation of the characteristic equation to the ninth order in terms of λ as in equation (4.9). The solution of equation (4.9) yields nine different natural frequencies, $\omega_{n,i}$, of the system that describe the different modes of truck vibration in this research. The characteristic equation, in terms of λ, is shown in equation (4.9).

$$A\lambda^9 + B\lambda^8 + C\lambda^7 + D\lambda^6 + E\lambda^5 + F\lambda^4 + G\lambda^3 + H\lambda^2 + I\lambda + J = 0 \tag{4.9}$$

A, B, C, D, E, F, G, H, I and J are the coefficients of equation (4.9) corresponding to 362,880 terms that are developed numerically using MAPLE©. The coefficients reflect

the complete symbolic analysis in terms of non-defined parameters, such as masses and stiffness. The detailed expansion of these coefficients can be found in Appendix A.

Equation (4.10) represents the symbolic solution of the different natural frequencies $\omega_{n,i}$ ($\lambda_i = \omega_{n,i}^2$, i=1...9) from the polynomial in equation (4.9) generated by MAPLE©. Equation (4.10) cannot be further simplified symbolically. There are nine different solutions that lead to nine natural frequencies, $\omega_{n,i}$, representing the HISLO vibration problem. The details of equation (4.10) are presented in Appendix A.

$$\omega_{n,i} = f(m_{0...7}, k_0, k_1, k_{2r}, k_{2f}, k_{3r}, k_{3f}, k_4, k_5, a, d, e, f) \tag{4.10}$$

The natural frequencies, $\omega_{n,i}$, in equation (4.10) are then substituted in equation (4.7), in order to evaluate the corresponding eigenvectors, u_i, of the vibrating system. These nine eigenvectors corresponding to each natural frequency are then normalized to form the normalized modal matrix [P] in equation (4.11). The modal matrix is used in the development of the solution in equation (3.38) in Chapter 3.0 of the damped forced vibration problem.

$$[P] = \left[\left\{ \hat{u} \right\}_1 \quad \left\{ \hat{u} \right\}_2 \quad \left\{ \hat{u} \right\}_3 \quad \left\{ \hat{u} \right\}_4 \quad \left\{ \hat{u} \right\}_5 \quad \left\{ \hat{u} \right\}_6 \quad \left\{ \hat{u} \right\}_7 \quad \left\{ \hat{u} \right\}_8 \quad \left\{ \hat{u} \right\}_9 \right]_{9x9} \tag{4.11}$$

4.5. SUMMARY

The numerical analysis for developing the symbolic solution of the undamped free vibration problem of the 9-DOF truck system is developed, as well as, discussions on

the stability, convergence and errors estimates. The natural frequencies of the 9-DOF truck system serve as input for the modal analysis for solving the damped forced vibrations in Section 3.4.2 of Chapter 3.0. The homogeneous solution of the problem generates the natural frequencies of the system and hence, the normal modes that forms the modal matrix of the undamped system. These normal modes in the Eigenvalue problem are multiplied by time-dependent generalized coordinates, $q_i\ (t)$, to form the complete solution of the forced damped vibrations problem.

5. VIRTUAL PROTOTYPE SIMULATION OF TRUCK VIBRATIONS IN HISLO

This chapter presents the development of the virtual prototype simulator of the truck vibrations under HISLO conditions. It contains a complete methodology and procedure for building the complex dynamic model, with multi-degrees of freedom that best captures the actual truck under the HISLO conditions. The detailed steps and methodologies for building the virtual model using MSC.ADAMS are also discussed in this chapter. The constraints, dimensions and control environments of this virtual model are described. This chapter also focuses on the methods used in MSC.ADAMS to build the complex dynamic model, and their limitations for developing and simulating the virtual prototype simulators.

5.1. BUILDING THE VIRTUAL MODEL

The dump truck comprises rigid-body components linked together to form one entity. This virtual prototype model is created by connecting different parts or rigid bodies together via joints. The rigid body components of the virtual model have inertial properties and masses, and these components, cannot change in shape due to external forces. Each rigid body adds six degrees of freedom to the model, three translational and three rotational.

The virtual prototype truck model is built and simulated in the MSC.ADAMS® environment. The first step consists of creating a detailed CAD geometry of the truck that reflects the actual truck in consideration by using any commercial CAD software. This CAD model maintains the shape and dimension of the different components forming the

truck, as well as, the relative location of the components with respect to each others. The CAD geometry is imported into MSC.ADAMS/View, and each component is assigned a mass and a corresponding density in order to retain its material properties. Each truck component is linked to the appropriate component in order to create one entity that satisfies the equilibrium state. This is achieved by attaching different rigid bodies together to replicate the physical attachment between the different parts of the actual truck using spring-damper systems and joints.

In the MSC.ADAMS environment, the applied forces are input into the model. These forces are the external excitations on the truck system under the HISLO conditions, and thus, they correspond to the load dumped by the shovel under gravity. These input forces acting on the truck body are impulsive and time dependent. They fall under the "Custom Forces" category in MSC.ADAMS. The magnitude of these forces is a user-written subroutine that defines a non-standard input into ADAMS, using the AKISPL data access subroutine. AKISPL uses the Akima cubic-curve fitting method of interpolation to create a spline function across a set of data points. The data points to be interpolated are defined by a SPLINE statement in the ADAMS/Solver dataset. The user-defined SPLINE in the dataset represents the impulse force that changes with respect to time. The ADAMS/Solver uses the cubic polynomial to interpolate between points. The AKISPL function is very fast, and always produces accurate results for the value of the approximated function.

AKISPL returns estimates for the first derivative of the approximated function with evenly spaced data points. After assigning the input forces, MSC.ADAMS/View evaluates the reactive forces on the structure that corresponds to the spring-damper systems. It also evaluates the reactions in the joints connecting different components due to the dynamic motion of the structure under the input force. Once the virtual model is built and validated, a static simulation is performed to configure the model under equilibrium conditions. This is then followed by a dynamic simulation, which reduces some of the initial, transient system responses. During the static equilibrium simulation process, the Adams/Solver iteratively adjusts the spatial geometry of all the parts to balance all the forces on the system. A static simulation is performed with initial conditions to check and correct any geometric inconsistencies in the model. The corrected model becomes an input for a nonlinear or linear simulation.

Dynamic simulation is carried out after the static simulation. During the simulation process, Adams/View (i) sets the initial conditions for all the model objects, (ii) formulates appropriate EOMs based on the laws of Newtonian mechanics. The EOMs control objects motions given the set of forces and constraints acting on them, (iii) solves the EOMs for component displacements, velocities, acceleration, and the applied and constraint forces to within the specified accuracy tolerance, (iv) temporarily saves the results for later animations, plots, and numerical signal processing. The animations provide graphical illustration of the overall behavior of the model for pinpointing specific problems, such as improper connectivity or misapplied motions or forces. ADAMS/View can display this information in strip charts through measures. ADAMS/Post Processor

displays the results for more in-depth investigation and manipulation. Figure 5.1 illustrates the stages and procedures for developing and simulating the virtual prototype simulator of the HISLO problem. After importing the CAD geometry into the MSC.ADAMS environment, the first step consists of connecting the elements together and adding the constraints to the model that mimics the physical constraints of the actual truck. Then, the static equilibrium simulation is performed to verify the stability of the model. The third step is to perform a dynamic simulation by defining the simulation end time and the step size. If the simulation is successful, the results are viewed in ADAMS/Postprocessor. If the simulation fails, the model is verified again for stability, constraints and proper joints selection.

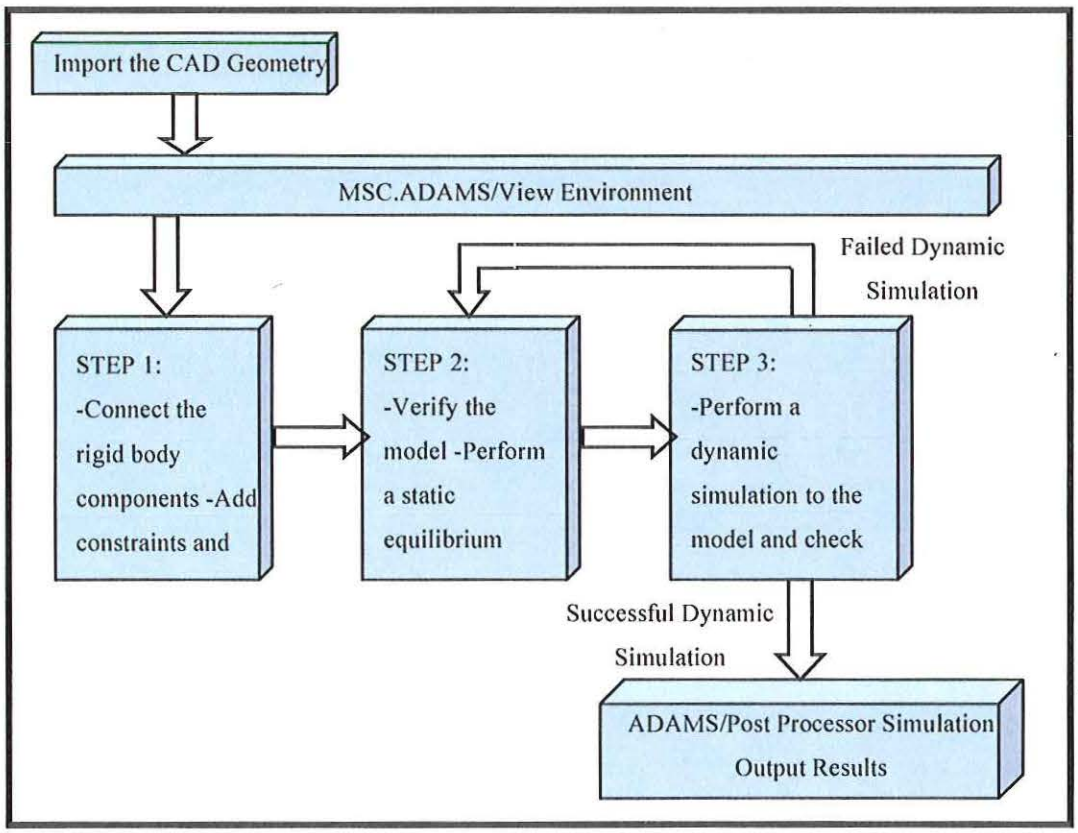

Figure 5.1. ADAMS Virtual Modeling and Simulation Process

Figure 5.2 shows different views of the 3D virtual prototype model of the CAT 793D developed in ADAMS/View. It also shows the connections between the different parts via springs and dampers. The ground is showed as a plate with unit thickness. The operator is modeled as two elements, his neck and body are connected via spring-damper system.

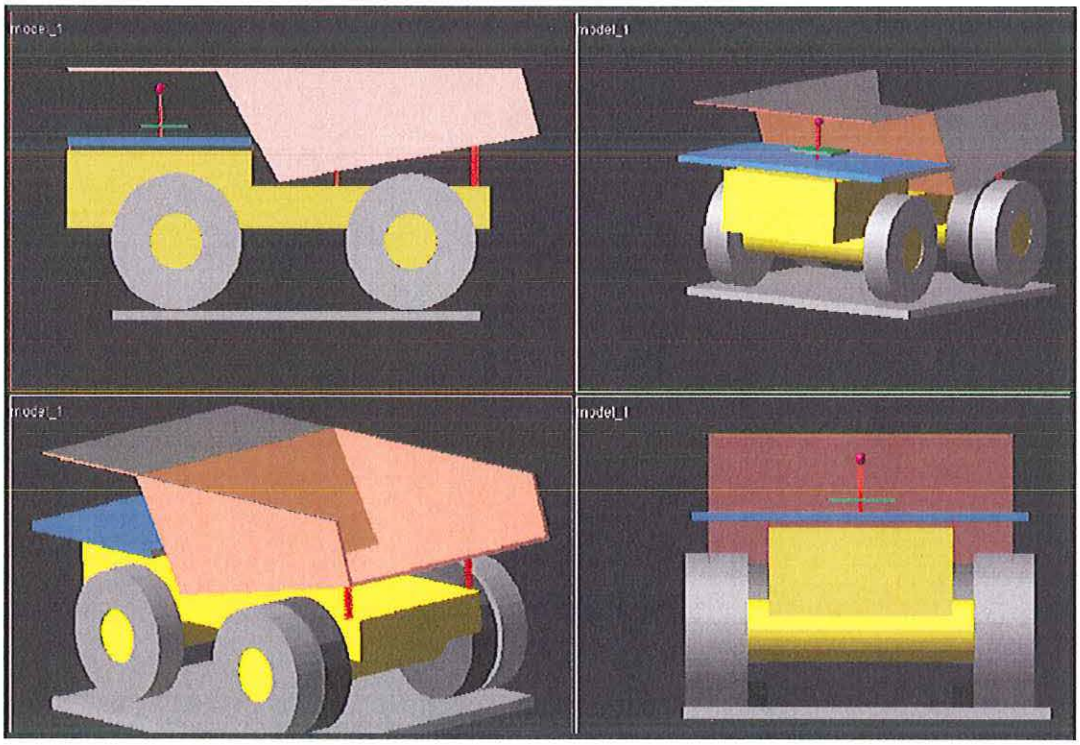

Figure 5.2. Truck Model in MSC.ADAMS Environment

5.2. CONSTRAINTS-DIMENSIONS AND CONTROL ENVIRONMENT

The attachments serve as the physical bearings and bolts in the truck. These attachments, or joints in MSC.ADAMS, add constraints to the overall model by defining the geometric relationships (i.e., joints) and the relative motions of the system components. These joints allow motion in any of the six axes, three for translation and

three for rotation. The joint motions and their impact on the different rigid components of the truck model determine the overall number of degrees of freedom of the truck. For instance, the body of the truck is attached to the chassis and rotates around the y-axis while it is constrained in the three translational and the other two rotational axes. The dimensions of the different components are set in the CAD environment, while constructing the geometry of the truck. These dimensions are unchanged in MSC.ADAMS. However, the mass properties, such as densities and Poisson's ratio, must be modified in order to maintain similar properties as the physical components in the truck. This is required to create a solid geometry that mimics the actual truck instead of a shell with no properties.

The control environment for the virtual model consists of maintaining static equilibrium by connecting all parts to each other with one part connected to a fixed reference. This fixed reference is essential for successful simulation and to avoid free falling parts due to the presence of gravity. Thus, the connections between the parts are achieved by adding spring and damping controls to the model. These controls introduce forces that resist the motion. The characteristics of these forces, created by MSC.ADAMS/View, are based on the stiffness and damping coefficients specified by the user. In this case, MSC.ADAMS/View automatically generates forces with magnitudes proportional to the distance and velocity between two points. The coefficients specified by the user represent the proportionality constants. Moreover, the joints return a reactive force on one of the two bodies connected by the joint object. Also, the impulsive force generated under the HISLO conditions is input as a SPLINE data element function that

defines a curve defining the force magnitude with respect to time. This force has a single component in the vertical direction and is constrained in the other five directions (two translational and three rotational).

5.3. METHODS IN MSC.ADAMS ENVIRONMENT

The MSC.ADAMS/Vibration environment is a plugin to MSC.ADAMS/Solver, and MSC.ADAMS/View that allows the performance of the frequency-domain analysis of forced vibrations over different operating points in order to compute the system response. MSC.ADAMS/Vibration plugin evaluates the frequency response functions for magnitude and phase characteristics and solves for the system modes over the frequency range of interest. It also tabulates the contribution of the model elements to the kinetic, potential, and dissipative energy distribution in the system modes.

The two types of analyses used in this research are the normal mode analysis and the forced response analysis. The normal mode analysis computes the Eigenvalues and Eigenvectors of the model at a specified operating point by the user. This analysis is effective in understanding the natural modes of vibration for the model and to determine the basic dynamic characteristics of the model. Although the results of the Eigenvalues analysis are independent of the external excitation, they are useful in predicting the effects of applying dynamic loads to the model. The normal mode analysis is relevant in the determination of the natural frequencies of the truck model. On the other hand, the truck vibration problem, under the HISLO conditions, consists of a forced vibration problem. Therefore, the forced response analysis is performed for the virtual prototype

dynamic analysis. The forced response analysis is the response of the model to vibration input channels that describes the input excitation on the system. This forced response analysis consists of a collection of input and output channels, the operating point specification, the frequency range and number of steps in this range. Details of the forced response analysis are described below in Section 5.3.1.

5.3.1. Forced Response Analysis in MSC.ADAMS. ADAMS/Vibration requires the definition of a collection of input and output channels, the operating point, the frequency range and the number of steps in this range in order to perform a forced-response vibration analysis. A vibration input channel defines the location, orientation, and the type of the applied forced function. The type of input channels that corresponds to the HISLO conditions specified in ADAMS/Vibration is the force-type input channel. The vibration output channels are defined using run-time expressions (MSC.ADAMS, 2007). These expressions can consist of kinematic or forced expression or some combination of the state variables defined by the user. The system of differential and algebraic equations is linearized about an operating point z_0. An operating point is defined by an initial-conditions analysis or static or dynamic analysis (Sohoni, 1986).

The Eigenvalue problem is solved in ADAMS/Vibration using the well-known QR method (Press et al., 1994) for computing Eigenvalues and Eigenvectors. The integrator statement controls the numerical integration of the EOMs for a dynamic analysis. ADAMS/Solver (FORTRAN) uses an iterative, quasi-Newton-Raphson algorithm to solve the difference equations and obtain the values of the state variables.

This algorithm ensures that the system states satisfy the EOMs. The Newton-Raphson iterations require the Jacobian matrix, which are the partial derivatives of the equations being solved with respect to the solution variables. The GSTIFF (Gear integrator) is the default integrator used by ADAMS/Solver (FORTRAN) for integrating the differential EOMs. The GSTIFF default integrator uses Newton-Raphson iterations to solve the nonlinear Differential-Algebraic Equations (DAE) of motion. It is a variable-order, variable-step and multi-step integrator with a maximum integration order of six. The backward-difference formulae (BDF) coefficients are calculated by assuming that the step size of the model is mostly constant. Thus, when the step size changes in this integrator, a small error is introduced in the solution. The RKF 45 method is chosen as the integrator used by ADAMS/Solver because it is suitable for solving non-stiff vibration problems and gives accurate results for the acceleration fields.

5.3.2. Numerical Method Used in MSC.ADAMS. The RKF 45 method is used to integrate the differential equations governing the system. It is a single-step method, which is primarily designed to solve non-stiff and mildly stiff differential equations when derivative evaluations are not expensive or time consuming. Internally, RKF 45 uses the DDERKF code, which is a driver for a modification of the RKF 45 code by Shampine and Watts (1979). The RKF methods are an extension of the traditional Runge-Kutta (RK) methods. The local truncation error per step for the RKF method is computed by comparing the calculated result, y_{n+1} (at $t = t_{n+1}$), with the result of an associated higher order RK formula. Therefore, in a fourth-fifth order method, the error in the fourth-order

RK method is estimated by subtracting it from the value obtained by a fifth-order RK method. In its formulation in ADAMS/Solver, the derivative evaluation is time consuming; thus, RKF 45 is usually not very fast. The RKF 45 is about five times slower than the default GSTIFF for most models. However, RKF 45 is a good addition to the suite of integrators in ADAMS, because, unlike all the others, it is a single-step integrator. It can only handle ODEs and not differential algebraic equations (DAE). Therefore, the DAE equation of the model needs to be transformed into ODE.

The RKF 45 uses coordinate partitioning to convert the DAE into ODE. This is achieved by using the coordinate partitioning, which is a method of eliminating constraint equations, such as the ones induced by joints, from the EOMs. This method reduces the entire system of DAEs to a condensed set of ODEs. It does so by selecting the degrees of freedom that will change the most during the simulation constraints. After each successful integration step, the coordinate-partitioning algorithm computes the dependent displacements, their time derivatives, and the accelerations and Lagrange multipliers (constraint reactions). During this process, ADAMS/Solver (FORTRAN) holds the independent coordinates constant and employs a Newton-Raphson iteration scheme to find the dependent coordinates. After computing the dependent velocities from the independent values, the ADAMS/Solver uses the Newton-Raphson algorithm again to find the full set of accelerations and Lagrange multipliers.

The different stages for solving the complete vibration problem of the truck model under HISLO conditions are by using ADAMS/View for dynamic simulation analysis;

followed by a modal and forced response analyses using MSC.ADAMS/Vibration. Finally, MSC.ADAMS/Post Processor is used to post-process the results, such as debugging, validating, improving and presenting the results. Post-processing involves animating forced vibrations and plotting frequency response functions, generating modal coordinates, and displaying other time and frequency data.

5.4. LIMITATIONS OF THE VIRTUAL MODEL

The virtual model of the truck vibrations simulator has limitations in the input parameters, as well as the simulation process.

5.4.1. Input Parameters Limitations. The input parameters introduce limitations in the overall solution of the HISLO vibrations problem due to the data unavailability. There is no published data for the stiffness and damping coefficients for the 793 truck series. These coefficients are approximated based on the available literature for heavy machinery and farming trucks (Trangsrud et al., 2004), as well as, data from Caterpillar (2007). These parameters, once defined for a specific dump truck, such as the CAT 793 and the CAT 797 series, can be input into the generic simulator for formulating the model under HISLO conditions.

5.4.2. Simulation Limitations. The RKF 45 integrator is used to solve the multi-degrees of freedom vibration problem under the HISLO conditions. Thus, the simulation is five times slower than the default MSC.ADAMS/Solver. The computation time might be too costly for solving the 38-DOF truck model in industrial applications. Also, the RKF 45 can only handle ODEs, and not DAE. Therefore, the DAE corresponding to the model needs to be transformed to ODE. The RKF 45 is suitable for the vibration analysis but is only supported by the FORTRAN77 solver. Therefore, kinematic analysis on critical models cannot be performed. This type of analysis is supported by the C++ Solver because it uses a more advanced quadrature scheme to integrate the motion function. This is a potential source of difference in the results produced by the two solvers.

5.4.3. Confidence in the Simulated Results. The confidence level is the measure of how reliable are the simulation results compared to the real-world scenario. The results are expected to be at 95% confidence level. Due to the fact that the stiffness and damping coefficients are approximated based on the suspension cylinder stroke, the simulation results will be different than the experimental results. Comparing the simulation results with the experimental data, the differences are in the range of 1% to 9% (Table 6.9).

5.5. SUMMARY

A detailed description of the techniques and methods has been provided for building the virtual model in the MSC.ADAMS environment. The process begun by exporting the CAD geometry of the truck into ADAMS. The system constraints were added to the ADAMS model in order to replicate the physical behavior of the truck model under the HISLO conditions. The Akima cubic-curve fitting method of

interpolation was used to create a spline function using a set of data points. This spline function generates a curve that models the high material impact into the truck body under gravity. Static equilibrium simulation was performed to verify the model's consistency before carrying out the dynamic simulation. The dynamic simulation of the 38-DOF truck model, under the HISLO conditions, is carried out by using the RKF 45 algorithm and the FORTRAN solver.

This chapter also highlights the limitations encountered during the development and simulation of the truck model. These limitations fall under two categories, the input parameters and the simulation limitations. The input parameters limitations occur due to the unavailability of truck stiffness and damping coefficients. However, the generic model can be used to simulate the vibration of any truck provided that the masses, stiffness and damping coefficients are available. The simulation limitations consist of the slow computation of the solution using RKF 45 integrator that is only supported by FORTRAN solver, but is suitable for the vibration analysis of the truck model under HISLO conditions.

6. MODEL VALIDATION AND EXPERIMENTAL RESULTS

6.1. VALIDATION OF THE VIRTUAL PROTOTYPE SIMULATOR

Validation is the process of checking the designed model against a real-world model. In this study, the validation of the virtual prototype simulator is done by comparing the simulation results to field results conducted by Kumar (1999) at Syncrude in Canada during the Spring of 1999. The significance of this validation process is to ensure that: (i) the models are reliable for explaining a real-world phenomenon; (ii) the models are robust enough to provide solutions in prescribed parametric domains; (iii) the simulation results can be reproduced under similar conditions within different paradigms.

The validation steps consist of re-creating the experiment in MSC.ADAMS virtual environment by maintaining the same ground conditions, as well as, data collection and sensors location. This validation process is achieved by replacing the truck component characteristics, such as stiffness and damping coefficients of the cabin, seat and tires with actual values from truck manufacturers (Trangsrud et al., 2004). The stiffness and damping coefficients of the suspension system are calculated based on the maximum allowable effective suspension piston stroke for the rear and front suspension (Caterpillar, 2007). The body, sprung weight, cabin, seat and tire/wheel assembly weights of the CAT 793D truck used in the analysis are defined in Caterpillar's handbook.

6.1.1. Model Dimensions. Figures 6.1 and 6.2 illustrate the 2D schematic diagrams of the left and front views of an empty Caterpillar 793D dump truck, respectively. The CAT 793D truck data is used to validate the virtual models under HISLO conditions. Tables 6.1 and 6.2 describe the different dimensions in metric and imperial units for the left and the front configurations.

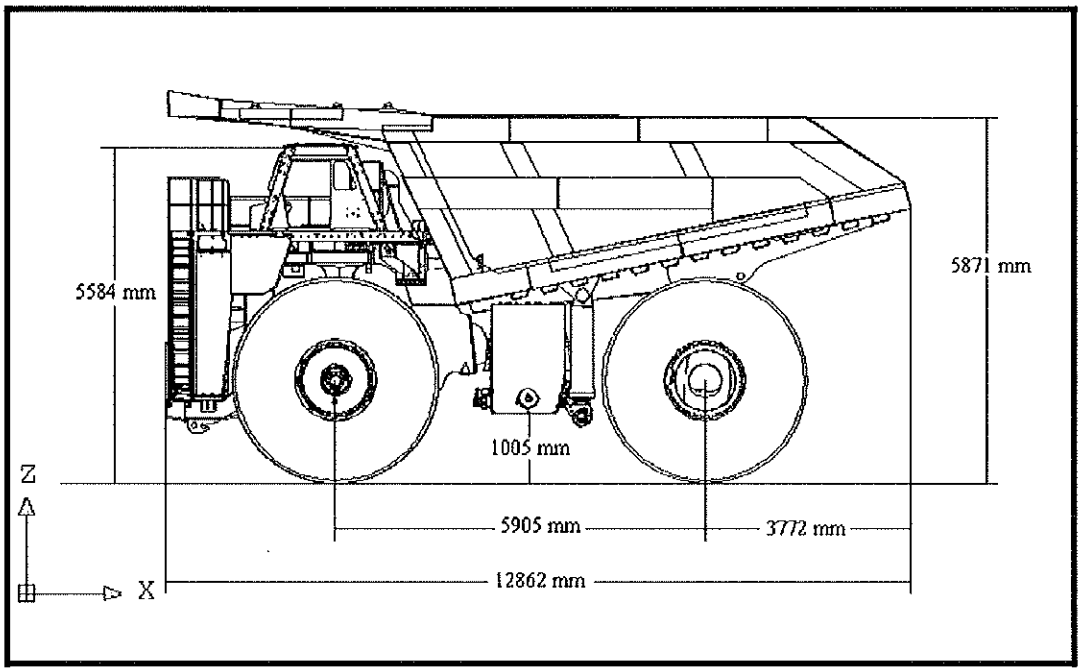

Figure 6.1. CAT 793D Left View with Dimensions

Table 6.1. CAT 793D Left View Dimensions Descriptions

Descriptions	Dimensions (mm)	Dimensions (in)
Height to Top of ROPS – Empty	5584	220
Overall Length	12862	507
Wheelbase	5905	233
Rear Axle to Tail	3772	149
Ground Clearance – Empty	1005	40
Loading Height – Empty	5871	232

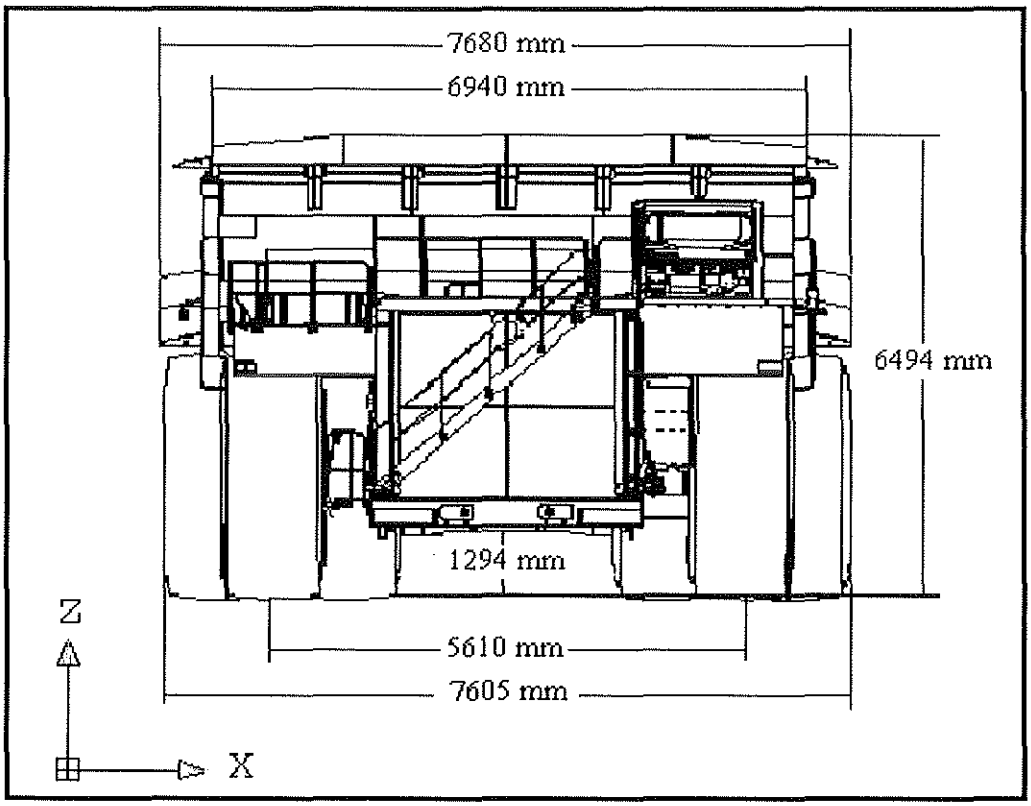

Figure 6.2. CAT 793D Front View with Dimensions

Table 6.2. CAT 793D Front View Dimensions Descriptions

Descriptions	Dimensions (mm)	Dimensions (in)
Overall Tire Width	7605	299
Centerline Front Tire Width	5610	221
Engine Guard Clearance – Empty	1294	51
Front Canopy Height	6494	256
Inside Body Width	6940	274
Overall Canopy Width	7680	303

The specifications of the CAT 793D truck fall into four major categories: (i) general information about the power, capacity and weight; (ii) suspension system; (iii) frame; and (iv) body structures (Caterpillar, 2007). These four categories are reviewed in detail to fully understand the geometric design of the CAT 793D and their role in vibration propagation under the HISLO conditions. Table 6.3 contains a summary of the general information of the 793D truck.

Table 6.3. CAT 793D Engine and General Info

CAT® 3516B High Displacement Electronic Unit Injection (16 Cylinders, 4 stroke)		
Gross Power at 1750 RPM	1801 KW	2415 hp
Flywheel Power at 1750 RPM	1743 KW	2337 hp
Body Capacity (SAE 2:1)	Customized	Customized
Gross Machine Operating Weight	383,749 kg	846,000 lb
Payload Weight, Standard Configuration	218 metric tons	240 tons
CAT 793D General Info		
Transmission	6–speed planetary power shift	
Weight Distribution (Empty)	46% Front Axle and 54% Rear Axle	
Standard Tires	40R57	

The suspension system is designed to dissipate haul road and loading impacts for longer frame life and a more comfortable ride. The system is made up of four independent, self-contained, hybrid hydraulic-pneumatic suspension cylinders. It features: (a) a variable rebound rate that reduces impacts and smoothens the ride; (b) front cylinders with preset caster and camber that are mounted to the frame and serve as steering kingpins for a tight turning radius with excellent maneuverability and low

maintenance; and (c) rear cylinders that allow axle oscillation for absorbing bending and twisting stresses caused by uneven and rough haul roads rather than transmitting them to the main frame. The frame uses a box-section design, incorporating two forgings and twenty four castings in highly stressed areas. It has deep penetrating and continuous wrap-around welds to resist damage from twisting loads without adding extra weight. A rollover protective structure (ROPS) is resiliently mounted to the main frame to reduce vibration and sound wave propagation. The ROPS structure is designed as an extension of the truck frame, with five-sided protection for the operator.

The body structures consist of three different body styles (a) dual slope; (b) flat floor; and (c) mine specific design (MSD II). These bodies are designed for optimal strength, capacity and durability. Wear surfaces are equipped to handle the toughest impact and abrasion over the long haul without diminishing capacity. Five-sided beams tie in the sidewall and floor junctions to increase the body rigidity and strength. Wide ribs in body floor provide increased durability and impact support. Full-length stringers create strength and rigidity throughout the body. The box section beams offer increased durability in the floor, sidewall, top rail, corner, and cab canopy areas. A variety of bodies specifically designed for each unique application, are available, but the standard flat floor design configuration data is used to validate the models in the study.

6.1.2. Model Parameters Determination. Table 6.4 contains the body, sprung mass, tires/wheels assemblies, cabin and seat weights of the CAT 793D truck used in building the ADAMS virtual model.

Table 6.4. CAT 793D Components Characteristics

Component	Weight (kg)
Gross Machine Weight	383,749.00
Body	54,431.00
Sprung Mass	116,707.00
Cabin	2,772.72
Tire/Wheel Assembly	8,651.83
Seat	15.97

The stiffness constants of the suspension system are derived from the assumption that the coil springs are designed with a deflection due to the weight of the truck equal to the effective cylinder stroke (Gillespie, 1992). Thus, the stiffness constants for the front and rear suspension systems are derived by using Hooke's Law in equation (6.1).

$$F = K\Delta z \tag{6.1}$$

$F=Mg$ is the force due to the weight of the sprung mass. Δz is equal to the effective cylinder stroke, which are equivalent to 130.5 mm and 105.5 mm for the front and rear suspension cylinders, respectively. Replacing each term in equation (6.1) with its corresponding value leads to the stiffness constants for the front and rear of the

suspension system. The results of the calculations are listed in Table 6.5. On the other hand, the damping coefficients are found by considering the damping ratio equal to 0.4 (Gillespie, 1992), which is true for most cars and trucks. Thus, the damping coefficients C_{2r} and C_{2f} for the front and rear suspension are calculated using equation (6.2).

$$C = 2\xi\sqrt{KM} \tag{6.2}$$

The body and cabin stiffness constants are calculated using equation (6.3). In this equation, the natural frequency, f_n, is equal to 1 Hz for optimum vehicles design according to Gillespie (1992).

$$f_n = \frac{1}{2\pi}\sqrt{\frac{K}{M}} \tag{6.3}$$

Similarly, the damping coefficients are found by using equation (6.2). The tire stiffness constants are also calculated using equation (6.3). The tire damping coefficients are very small compared to the stiffness constants and are neglected in the analysis. The seat stiffness constant and damping coefficient are equal to k_5 = 3403 N/m and C_5 = 1329 Ns/m according to Trangsrud et al. (2004) for commercial trucks. The ground conditions are defined for a unit weight of the oil sands, where the stiffness constant represents the elastic modulus of the oil sands (Frimpong et al., 2006). The operator weight is considered to be 100 kg. The human muscles, tissues and organs act as a natural spring-damper system with stiffness constant of 45005.3 N/m and damping coefficient of 1360

Ns/m (Rosen et al., 2003). All the stiffness and damping coefficients used in the truck model are illustrated in Table 6.5.

Table 6.5. Truck Model Stiffness and Damping Coefficients

Component	Stiffness (N/m)	Damping Coefficient (Ns/m)
Human Body	$K_{human} = 45005.3$	$C_{human}=1360.0$
Body	$K_1 = 2.15x10^6$	$C_1 = 2.737x10^5$
Rear Suspension	$K_{2r} = 1.927x10^7$	$C_{2r} = 1.596x10^6$
Front Suspension	$K_{2f} = 1.327x10^7$	$C_{2f} = 1.224x10^6$
Rear Tires	$K_{3r} = 8.945x10^4$	$C_{3r} \sim 0$
Front Tires	$K_{3f} = 8.945x10^4$	$C_{3f} \sim 0$
Cabin	$K_4 = 1.1x10^5$	$C_4 = 1.4x10^4$
Seat	$K_5 = 3403.0$	$C_5 = 1329.0$

6.2. EXPERIMENTAL RESULTS FROM KUMAR (1999)

Experimental results are used to test the accuracy of the MSC.ADAMS virtual prototype for the validation process. Kumar (1999) conducted experiments at Syncrude in Canada during the Spring of 1999. The purpose of these experiments was to study the effect of vibration and impact experienced by truck drivers during the loading process. The CAT 793 series was used to perform the impact loading test in these experiments. The data was collected in the early Spring season with hard frozen ground conditions. These conditions resulted in low rolling resistances, with relatively comfortable operations compared to the soft ground conditions due to the thinning viscous bitumen in the summer conditions.

The impact test was performed on the CAT 793 truck by using a shovel to dump a load of 100 tons into the empty truck body. A full size human dummy in the driver's seat was used during this test. The vibration at the seat pan, drivers back and neck was measured in fore-aft (x-axis), side to side (y-axis), and up and down vertical (z-axis) axes. The accelerations were measured in terms of m/s^2 RMS values, as well as, in terms of gravity, g. These acceleration values were measured using three high performance tri-axial accelerometers. Two accelerometers, with a vibration range of ± 5g were mounted on the cervical and lumbar regions of the dummy operator. The third accelerometer, with a vibration range of ± 25g was mounted on the driver's seat. Data was collected for the first, second and third shovel passes. The durations for which the signals were analyzed ranged between 5.6 seconds for the first pass to 9.7 seconds for the third pass.

The RMS accelerations experienced during the first impact ranged between 0.35 to 0.84 m/s^2 for the cervical region. The x and y components of the acceleration were 0.35 m/s^2 and 0.52 m/s^2, respectively. The vertical axis had an acceleration of 0.84 m/s^2. At the lumbar region, the accelerations ranged between 0.38 m/s^2 in the x axis, to 0.41 m/s^2 in the y axis and 1.09 m/s^2 in the z axis. At the operator's seat, the acceleration in the x axis was 1.47 m/s^2, y axis 1.19 m/s^2, and the z axis 3.49 m/s^2. The frequencies in the cervical region were generally under 0.8 Hz for the x, y and z axes, with a maximum of 1.4 Hz in limited cases. In the lumbar region, the frequencies were generally lower than 0.7 Hz in both the x and y axes. However, in the vertical axis, the frequencies were 6.5 and 7.5 Hz for the first and second pass, respectively. The frequencies at the operator's seat were generally between 2.4 and 2.7 Hz for the impacts in all three axes. However,

the frequencies were 8.1 Hz in the y and z axes for the first pass only. Tables 6.6 and 6.7 summarize the accelerations in the three regions cervical, lumbar and operator's seat, and the frequencies at the seat pan, respectively.

Table 6.6. RMS Accelerations Recorded During the Impact Testing

		X (front-back)	Y (left-right)	Z (up-down)
Passes	Truck	Acceleration at Cervical Region (m/s^2)		
1st	CAT	0.35	0.52	0.84
2nd	CAT	0.41	0.50	0.34
3rd	CAT	0.23	0.64	0.62
		Acceleration at Lumbar Region (m/s^2)		
1st	CAT	0.38	0.41	1.09
2nd	CAT	0.48	0.40	0.79
3rd	CAT	0.32	0.82	0.70
		Acceleration on the Operator Seat (m/s^2)		
1st	CAT	1.47	1.19	3.49
2nd	CAT	1.24	1.29	1.43
3rd	CAT	1.47	0.81	1.55

Table 6.7. Frequencies at the Operator's Seat

		Frequency (Hz)		
Passes	Truck	X (front-back)	Y (left-right)	Z (up-down)
1st	CAT	2.6	8.1	8.1
2nd	CAT	2.8	2.8	2.6
3rd	CAT	2.6	2.7	2.6

6.3. COMPARISON OF SIMULATION AND EXPERIMENTAL RESULTS

The simulation results of the virtual prototype model are compared to the experimental results for the oil sands mining operations presented in the pervious section. In order to have a rational comparison, the ADAMS model is built to re-create a virtual representation of the physical environment. This is achieved by using the same ground characteristics and weather conditions in the virtual model as the physical experiments. The virtual model generates the complete vibration solution of the 38-DOF system, as well as, the dynamics of the different truck components. The components of interest are the operator lumbar and cervical region and his seat. These three major components are compared by using the RMS acceleration in 3D, the x-, y- and z-axes. Table 6.8 summarizes the ADAMS virtual prototype simulation findings.

Table 6.8. RMS Accelerations of the ADAMS Truck Model Simulation

	X (front-back)	Y (left-right)	Z (up-down)
Passes	Acceleration at Cervical Region (m/s^2)		
1^{st}	0.36	0.53	0.90
2^{nd}	0.23	0.36	0.39
	Acceleration at Lumbar Region (m/s^2)		
1^{st}	0.40	0.42	1.12
2^{nd}	0.23	0.38	0.56
	Acceleration on the Operator Seat (m/s^2)		
1^{st}	1.49	1.08	3.56
2^{nd}	0.71	0.82	1.32

The comparison between the simulation and experimental results is tabulated in Table 6.9. The percent differences between these two results are also calculated as illustrated in Table 6.9. Only the accelerations resulting from the first shovel pass are used because of their predominance in the overall truck vibration analysis. This is true for both, the virtual prototype simulation results and the Kumar's experimental results.

Table 6.9. RMS Accelerations Comparison between ADAMS and Experimental Results

RMS Acceleration (m/s^2)	Virtual Prototype Results	Kumar's (1999) Results	Percent Difference (%)
Cervical Region			
a_x	0.36	0.35	2.8
a_y	0.53	0.52	1.9
a_z	0.90	0.84	6.7
Lumbar Region			
a_x	0.40	0.38	5.0
a_y	0.42	0.41	2.4
a_z	1.12	1.09	2.7
Operator Seat			
a_x	1.49	1.47	1.3
a_y	1.08	1.19	9.2
a_z	3.56	3.49	2.0

The simulation results of the virtual prototype model showed strong agreement with the results from Kumar's study. The first shovel pass results of the virtual simulation are compared to the experimental results as showed in Table 6.9. These results consist of the RMS values for the operator's lower back and neck, as well as his seat. The

difference in these values ranged between 1.3% and 6.7%; with only one exception of 9.2% for the operator's seat in the y-direction (left-right).

6.4. SUMMARY

The CAT 793 truck is used as the subject for research study. Experimental results from oil sands mining operations by Kumar (1999) have been presented and discussed in detail. The virtual prototype simulation results are validated with these experimental results. The results show that the virtual truck simulator simulates the physical behavior of the truck under the HISLO conditions with minimal deviation from the experimental results. Detailed model dimensions and characteristics of this truck have also been presented in this chapter. The model parameters, such as the stiffness and damping coefficients and the weight of the components are determined based on design parameters and from literature.

7. VIRTUAL PROTOTYPE SIMULATION RESULTS AND DISCUSSIONS

This chapter presents the simulation results of the 38-DOF truck model under the HISLO conditions. The acceleration vectors for the operator's seat, lumbar and cervical regions are presented, with detailed discussion of the simulation results. The purpose and significance of this chapter to the overall work is to emphasize the presence and the effects of high vibration levels, in excess of the ISO 2631 limits, under the HISLO conditions. These vibration levels might cause operator's health problems and permanent injuries over long-term exposure.

7.1. VIRTUAL PROTOTYPE SIMULATION RESULTS

The virtual truck model in Chapter 5.0, validated in Chapter 6.0, is simulated in MSC.ADAMS/View and MSC.ADAMS/Vibration, successfully. The virtual prototype simulator captures the complete truck vibration dynamics under HISLO conditions using a 38-DOF system in the MSC.ADAMS environment. The results of the 38-DOF model allow the expansion of the analysis to integrate severe operating conditions and detailed multi-degree-of-freedom truck models.

These simulation results are also compared to the ISO standards to check the severity of the vibration that the operator is exposed to under the HISLO conditions. The virtual truck model is used to generate solutions of the HISLO vibrations without the need for physical experiments on the field that can be very costly. Thus, the complete virtual analysis does not affect the operator's health while testing for different scenarios and is less time consuming compared to field tests. These simulation models capture the

3D multi-body dump truck vibrations under the HISLO conditions and create the basis for understanding truck vibrations generation and propagation.

The virtual prototype simulation results include the acceleration, velocity and displacement vectors of the truck under the HISLO conditions. The results also include the relative motion of the truck components with respect to each other due to the excitation force. The object of these virtual experiments is to detect the acceleration peaks, under the HISLO conditions, and their corresponding times and durations. In addition, there is also a need for finding the natural frequencies that the system experiences under the high impact forces. This 38-DOF model allows such inspection of the acceleration fields for the three major components of interest, including the operator's seat, cervical and lumbar regions. Thus, the RMS values for the acceleration fields of the operator's seat, as well as, the human body at the cervical and lumbar regions are the main focus of this analysis. The actual accelerations of the operator's seat, cervical and lumbar regions are also presented in this study. The displacement, velocity and acceleration fields of each component of the virtual model are illustrated in Appendix B.

The vertical acceleration component is the predominant component of the acceleration fields, and hence, the highest RMS value compared to the x- and y- RMS acceleration components. This is mainly due to the fact that the excitation force under the HISLO conditions is acting downward in the vertical direction. Figure 7.1 shows the RMS vertical acceleration (the z-direction) of the operator's seat. This vertical acceleration has an RMS value of 3.56 m/s^2, and it oscillates for about ten seconds due to

the first shovel pass then diminishes to zero. The highest acceleration spectrum occurs when the external force is applied to the truck body, which explains the peak of the acceleration at *t=0.1 sec*. The same pattern is repeated for the second pass but on a lower scale as illustrated in Figure 7.2.

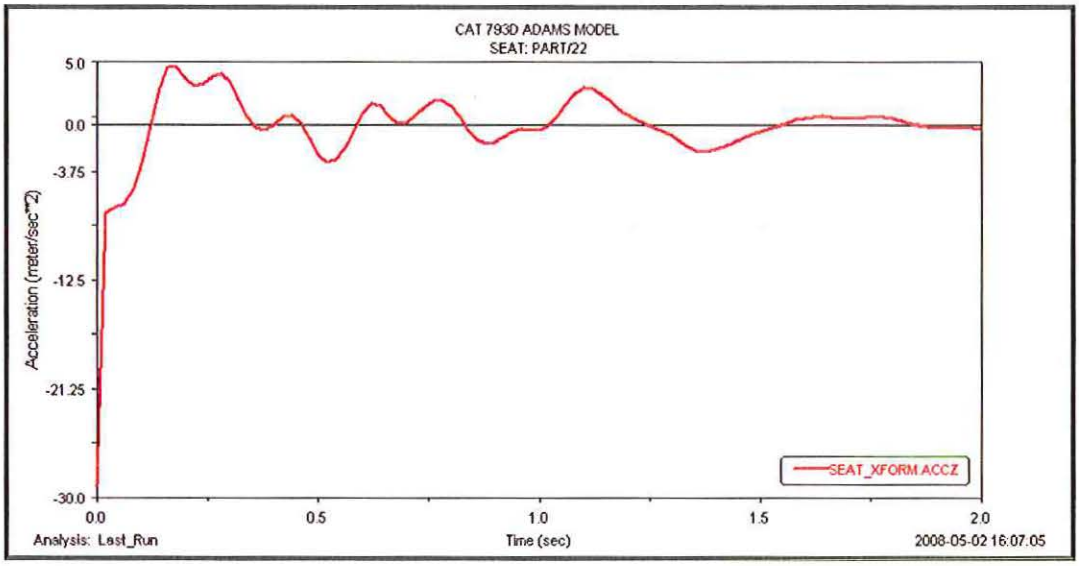

Figure 7.1. Operator's Seat Vertical RMS Acceleration in the z-direction

Figure 7.2 shows the actual vertical acceleration of the operator's seat. The highest acceleration occurs when the first load is dumped. From the results, it can be clearly noticed that the second shovel pass has lower effects on the operator's seat compared to the first pass. The vibration propagates quickly through the truck. There is no time lag between the application of the input force on the truck body and the behavior of the operator's seat in the vertical direction as a response to this excitation.

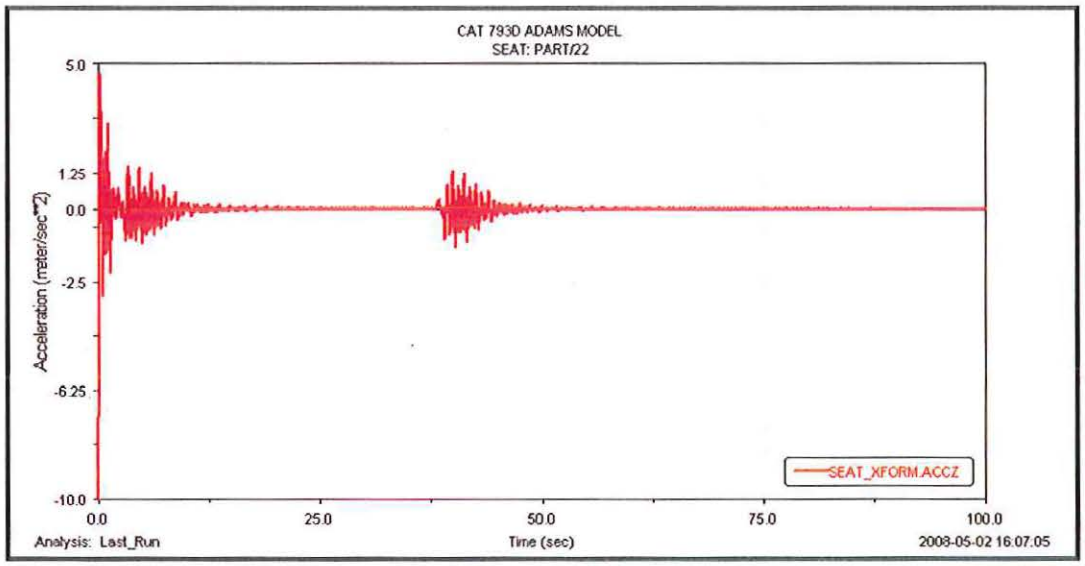

Figure 7.2. Operator's Seat Vertical Acceleration in the z-direction

The simulation is performed until time *t=100 sec* in order to determine the duration required for the structure to come to complete rest after the forced excitation. Two shovel passes are applied at time *0.1 sec* and *38 sec*, respectively. These loads are applied for *3 sec*. There is a *35 sec* lag in between the two passes allowing the shovel to swing, load, and swing back before dumping.

The results showed that there are significant accelerations in the x and y components but not as severe as in the vertical direction. Therefore, these two directions need to be incorporated in the study for a complete 3D vibration analysis.

Figures 7.3 and 7.4 illustrate the RMS and actual accelerations in the y-direction that induce lateral motion. The RMS value of the acceleration in the y-direction in Figure 7.3 is equal to 1.08 m/s^2, over a period of two seconds, for the first shovel pass. This acceleration peaks at *t=0.7 sec* after the load has been dumped into the truck body.

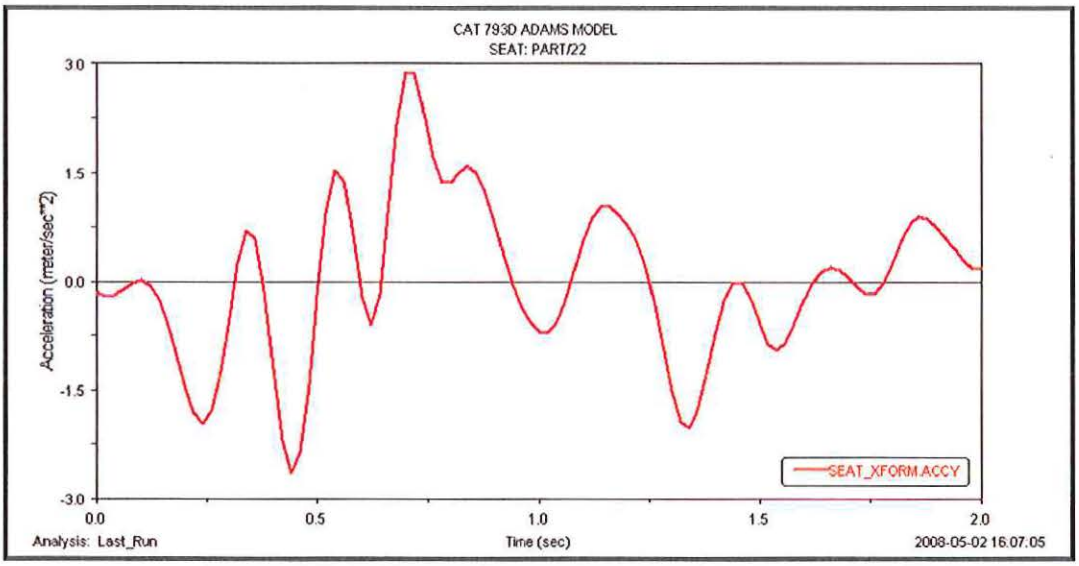

Figure 7.3. Operator's Seat RMS Acceleration in the y-direction

Figure 7.4 shows the actual acceleration distribution in the y-direction for the first and second shovel passes. The acceleration associated with the first shovel pass is predominant and takes more time to diminish to zero compared to the second shovel pass. The excitation force, due to the first shovel pass lasts for 3 seconds, is clearly shown in Figure 7.4 with the acceleration peak values occurring during that time. However, the structure dissipates the energy due to the first shovel pass by oscillating for another fifteen seconds before the acceleration diminish to zero.

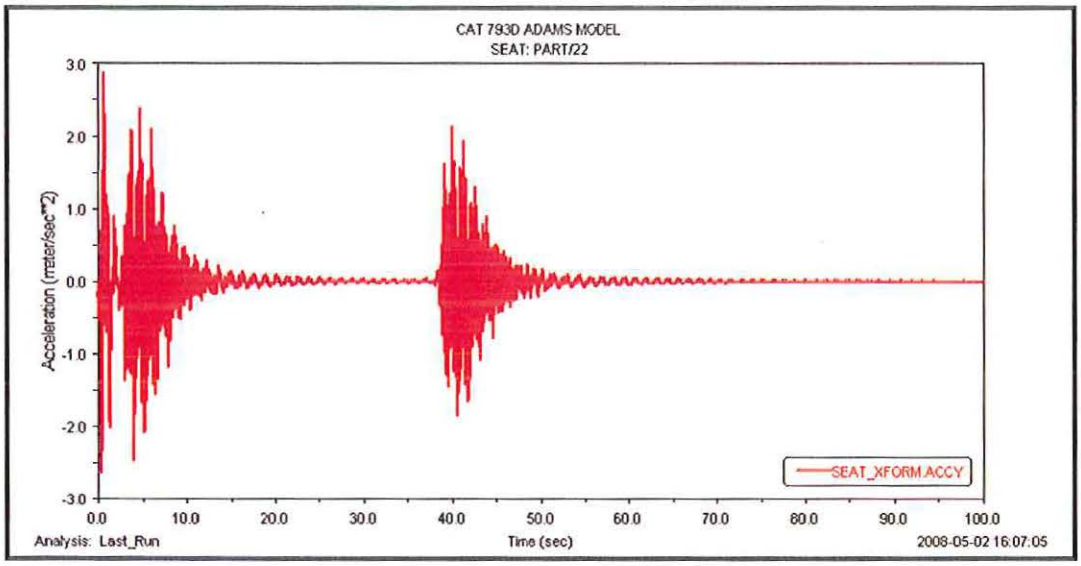

Figure 7.4. Operator's Seat Acceleration in the y-direction

At time *t=39 sec,* the second shovel pass is dumped, and the seat starts to oscillate in the y-direction after one second of the application of the second load. This is due to the fact that the material in the truck body from the first pass acts as a cushion and delays the vibration propagation. This second load excites the seat until *t=55 sec* where the oscillation ceases and the structure returns to complete rest.

The acceleration in the x-direction of the operator's seat is illustrated in Figures 7.5 and 7.6 for the RMS and actual values, respectively. The x-direction is described by the front-back motion that creates a shaking effect on the operator and the truck due to the vertical input force under the HISLO conditions. The acceleration in the x-direction at the seat has an RMS value of 1.49 m/s^2.

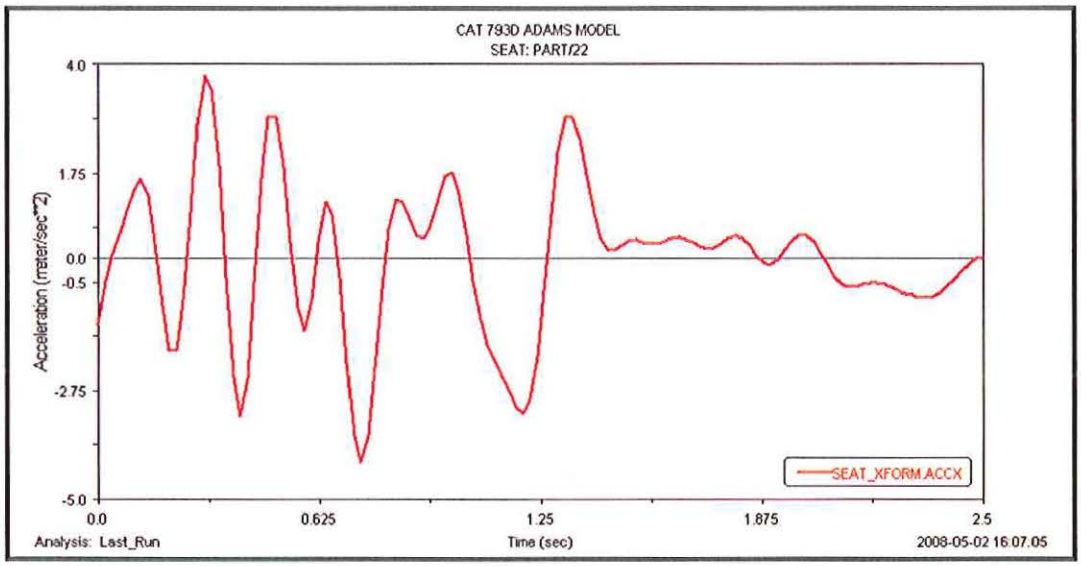

Figure 7.5. Operator's Seat RMS Acceleration in the x-direction

This RMS value is captured for the first three seconds when the first load is dumped where the seat experiences the highest vibration levels. After three seconds, the structure oscillates for another ten seconds until the seat comes to complete rest before the application of the second load. The second shovel pass induces vibrations in the seat from time *t=38 sec* until time *t=48 sec,* where the acceleration completely diminish to zero afterward. Although the second pass induces acceleration in the seat allowing it to oscillate for ten seconds, its corresponding RMS and actual accelerations are lower than the accelerations due to the first shovel pass. The acceleration due to the first shovel pass takes longer to diminish to zero compared to the second pass, as illustrated in Figure 7.6. This explains the predominance of the first load dumped under the HISLO conditions, as well as, the material cushioning effect in the truck body after the first pass that absorbs part of the shock waves.

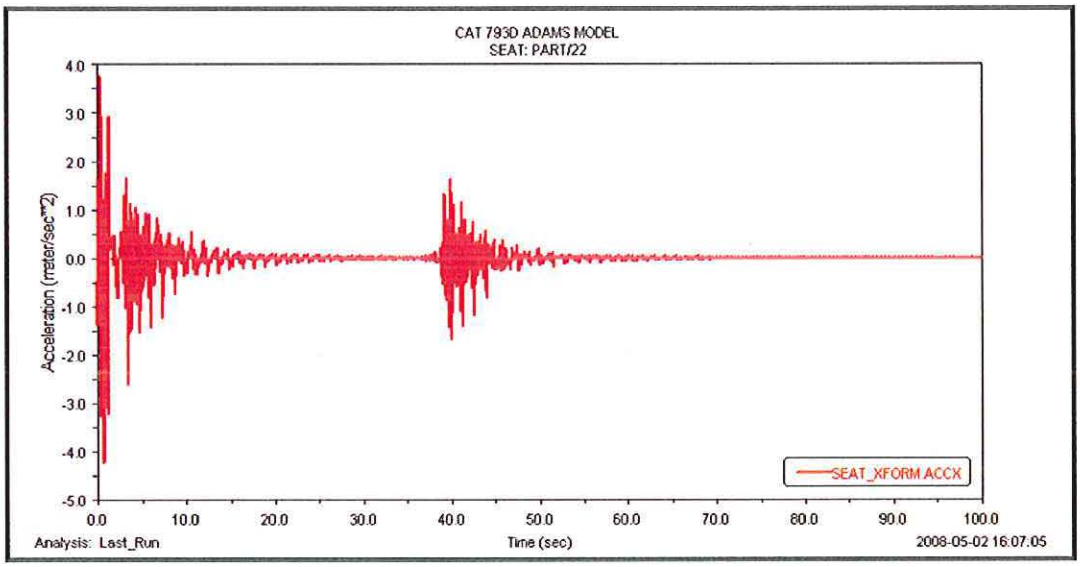

Figure 7.6. Operator's Seat Acceleration in the x-direction

The acceleration fields at the lumbar and cervical regions are studied to investigate the effects on the operator. The operator is modeled in ADAMS as two lump masses connected with a spring-damper system that reflects the stiffness and damping characteristics of the muscles, the internal organs and the bones (Rosen et al., 2003). These two lump masses correspond to the neck and head with a mass of 30 kg, and the shoulders and below with a mass of 70 kg. The RMS and actual accelerations in the x-, y- and z-directions are generated for detailed analysis. The vertical acceleration component is predominant compared to the x- and y- components.

Figure 7.7 illustrates the vertical RMS acceleration in the z-direction at the lumbar region under the HISLO conditions with a value equal to 1.12 m/s^2. Again, the first three seconds contribute the most to the RMS acceleration due to the vertical load applied to the truck body during the first shovel pass.

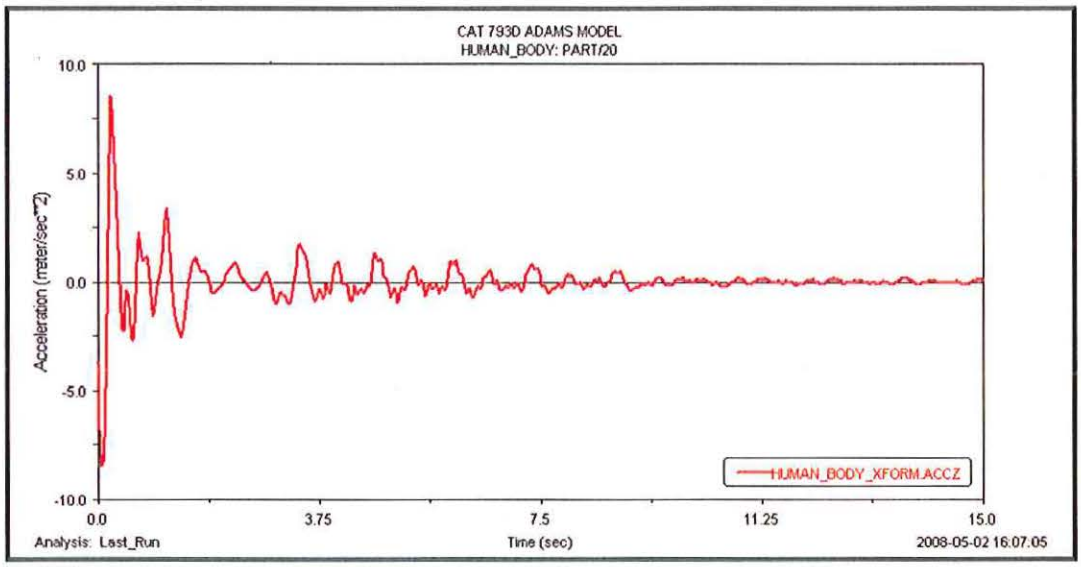

Figure 7.7. Human Lumbar Region RMS Acceleration in the z-direction

This first load excites the human lumbar region for almost ten seconds before the oscillations diminish to zero. However, it can clearly be noticed that the acceleration is lower for the second pass and it becomes insignificant after about 15 seconds, as illustrated in Figure 7.8.

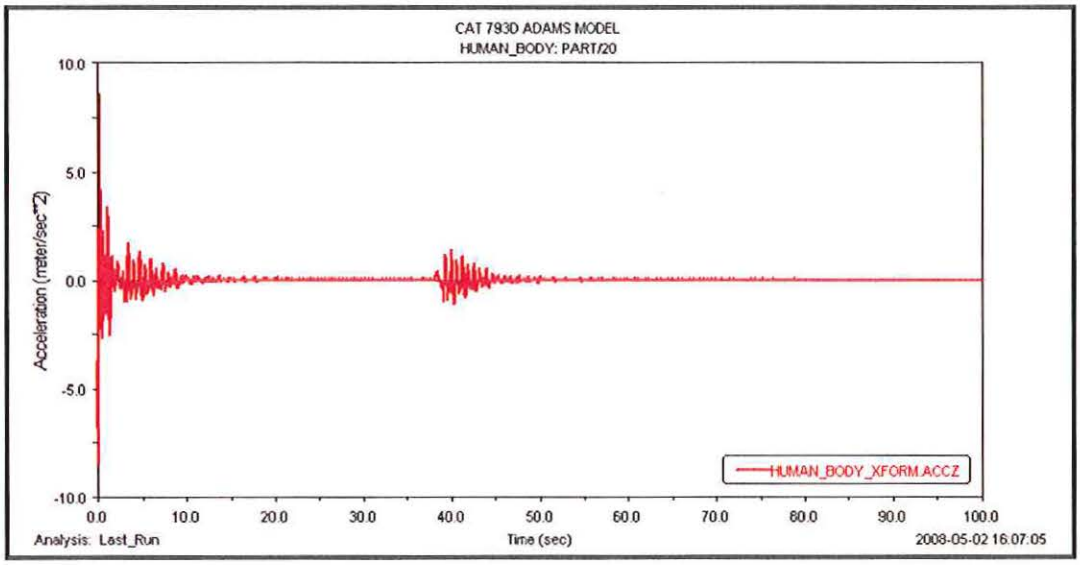

Figure 7.8. Human Lumbar Region Acceleration in the z-direction

Similar to the operator's seat behavior, there are significant accelerations in the x- and y- components that contribute to the complete truck vibration. Figure 7.9 shows the RMS acceleration at the human lumbar region in the y-direction with a value equal to 0.42 m/s^2.

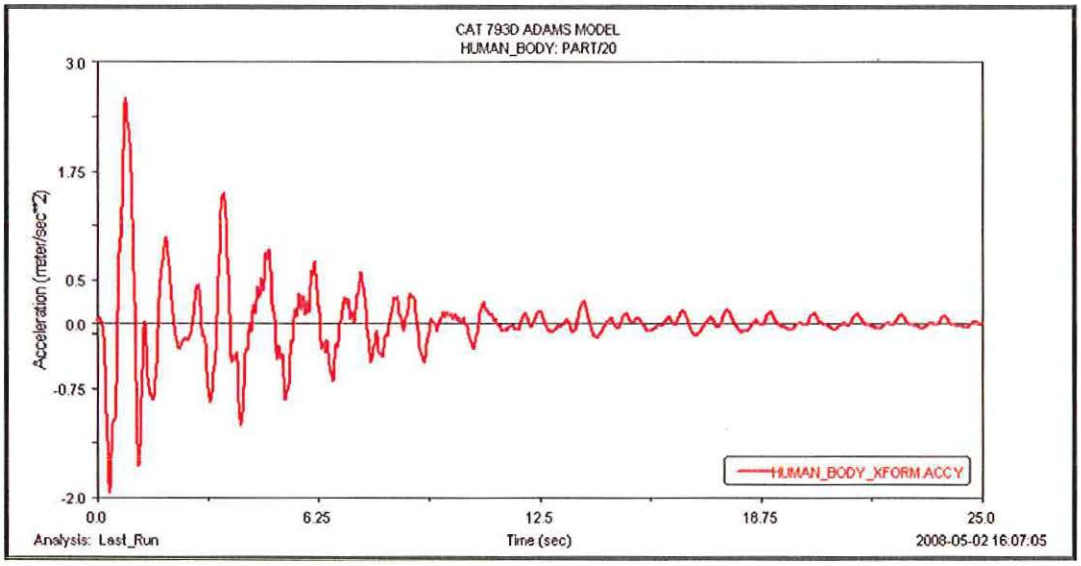

Figure 7.9. Human Lumbar Region RMS Acceleration in the y-direction

This acceleration oscillates for 12 seconds before it diminishes to zero for the first shovel pass. The second pass affects the lumbar region with an acceleration spectrum lasting for 12 seconds but with lower acceleration magnitudes, as illustrated in Figure 7.10. This figure shows the actual acceleration spectrum at the human lumbar region in the y- direction.

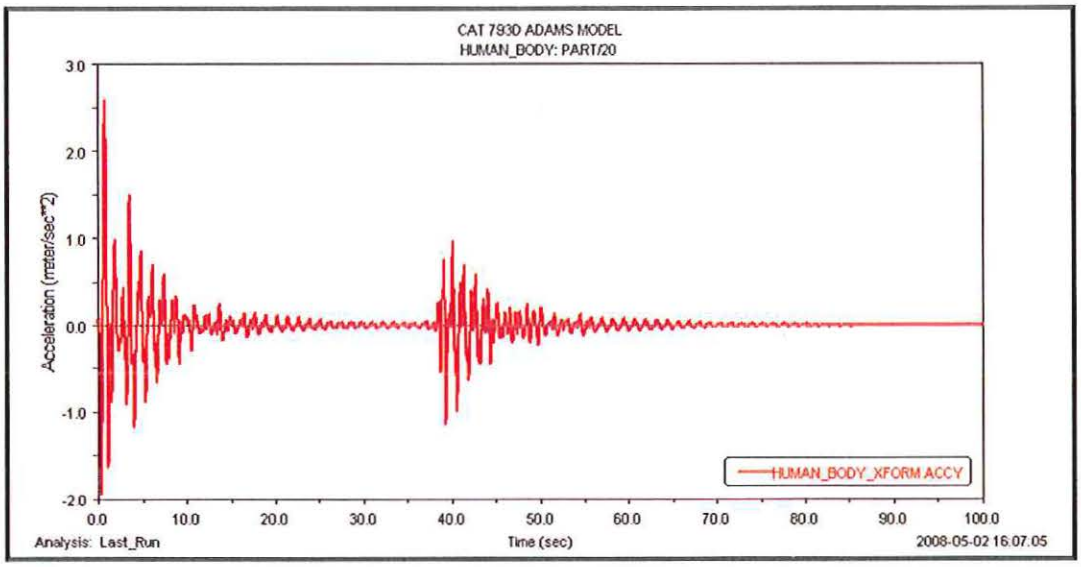

Figure 7.10. Human Lumbar Region Acceleration in the y-direction

The front-back motion (x-direction) of the human body at the lumbar region is illustrated in Figures 7.11 and 7.12 for the RMS and actual accelerations, respectively. The RMS acceleration is equal to 0.40 m/s^2 and its distribution with respect to time is shown in Figure 7.11.

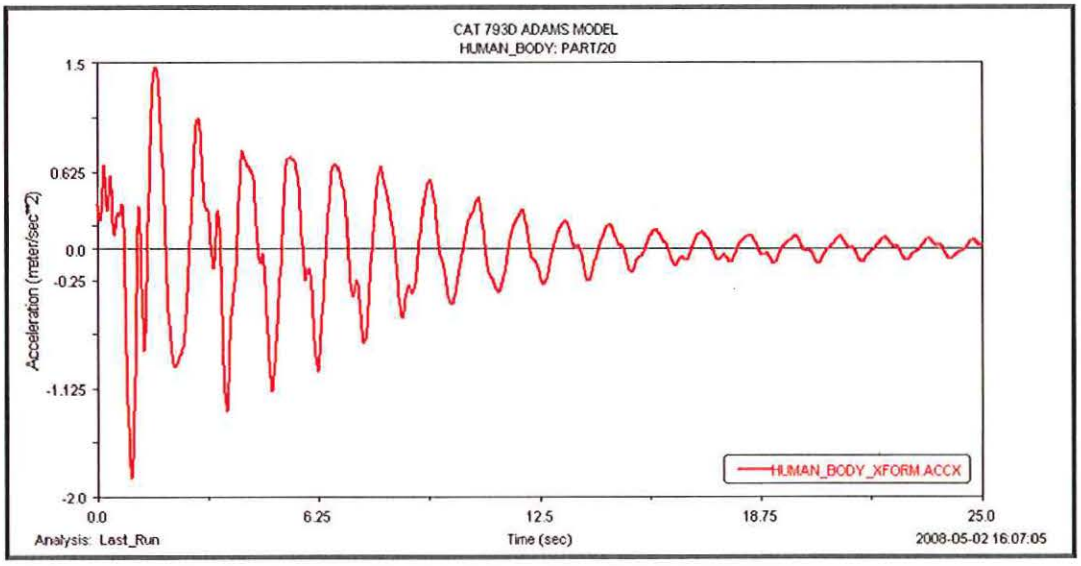

Figure 7.11. Human Lumbar Region RMS Acceleration in the x-direction

The complete acceleration at the human body lumbar region under the HISLO conditions is shown in Figure 7.12. The acceleration peaks occur at time $t = 3\ sec$ exactly during the period the first load is applied. The second shovel pass has minor effects on the human lumbar region in the x-direction.

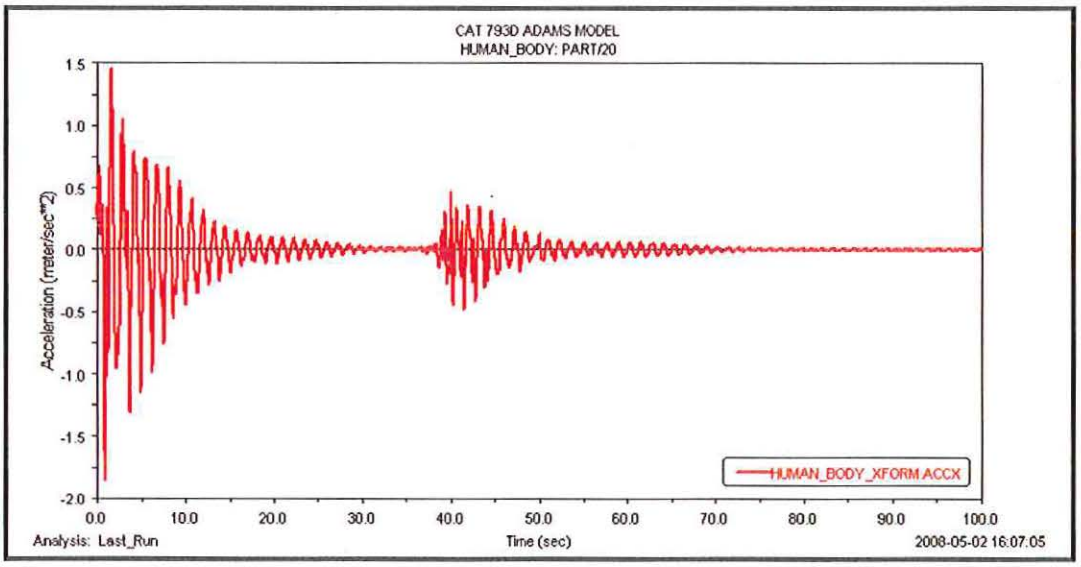

Figure 7.12. Human Lumbar Region Acceleration in the x-direction

The results of the human cervical region showed similar acceleration spectra to the human lumbar region with slightly different acceleration magnitudes. Similarly, the first shovel pass is predominant in its effect on the human cervical region.

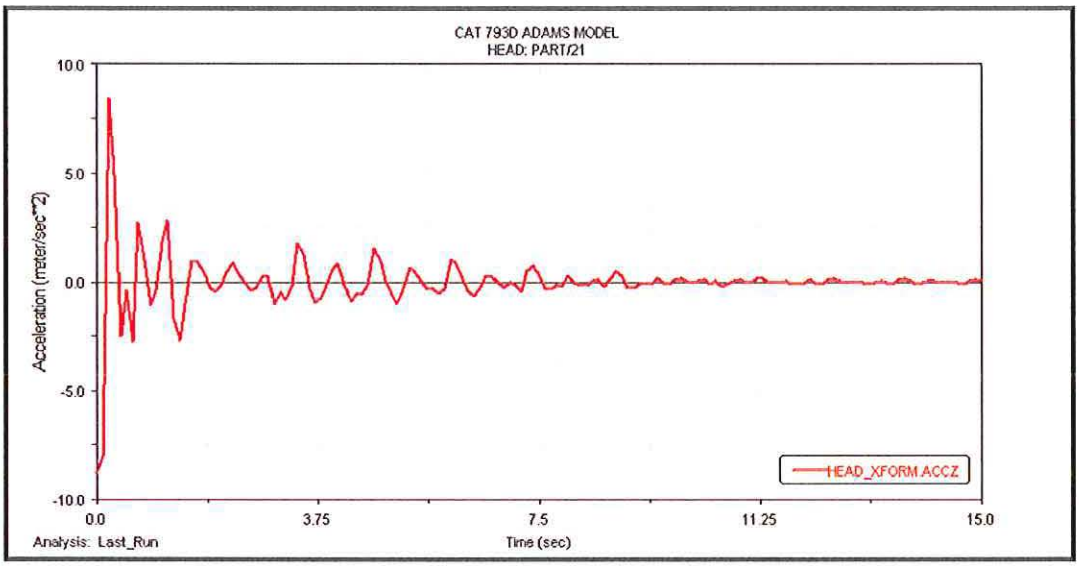

Figure 7.13. Human Cervical Region RMS Acceleration in the z-direction

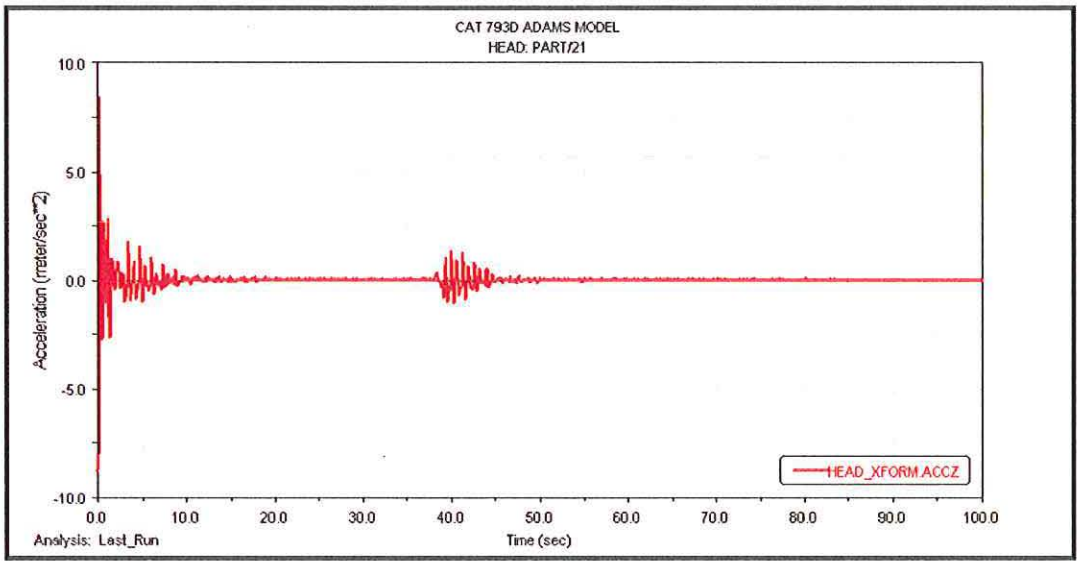

Figure 7.14. Human Cervical Region Acceleration in the z-direction

Figures 7.13 and 7.14 illustrate the RMS and the actual accelerations at the human cervical region in the z-direction, respectively. The RMS acceleration magnitude is equal to 0.90 m/s^2. The human cervical region oscillates vertically due to the first shovel pass for about ten seconds before it diminish to zero. This vertical acceleration lasting ten

seconds on the human cervical region can cause health problems over long-term exposure.

The results of the RMS and actual accelerations at the human cervical region in the y-direction are presented in Figures 7.15 and 7.16, respectively. The RMS acceleration value of the human cervical region in the y-direction is equal to 0.53 m/s^2. Similar trend is followed by the human cervical region in the y-direction compared to the z-direction.

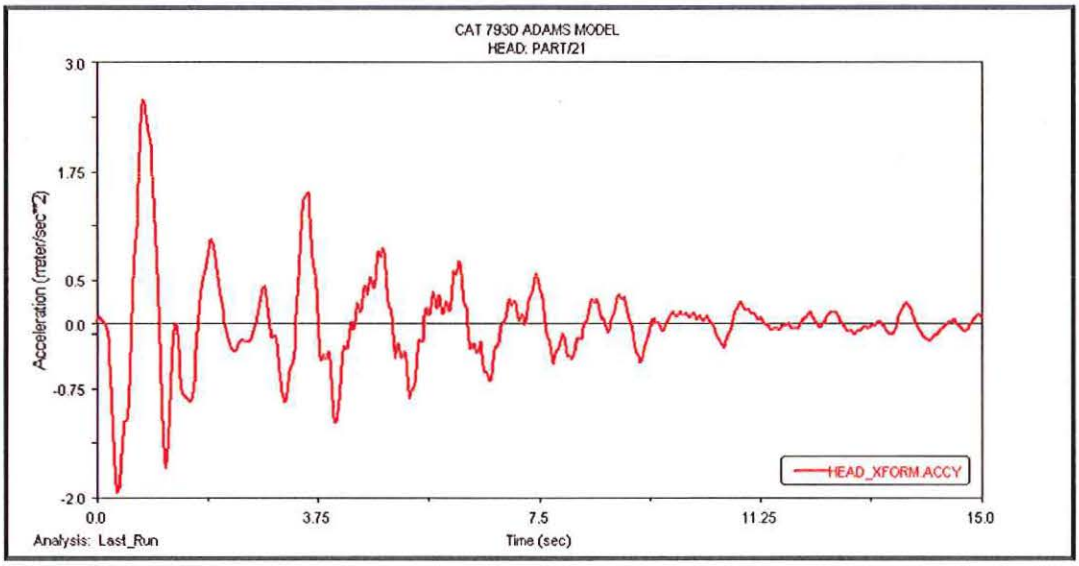

Figure 7.15. Human Cervical Region RMS Acceleration in the y-direction

Figure 7.16 presents clearly the effect of the HISLO on the human cervical region during the first and second shovel passes. The second shovel pass has lower effects on the human cervical region compared to the first shovel pass.

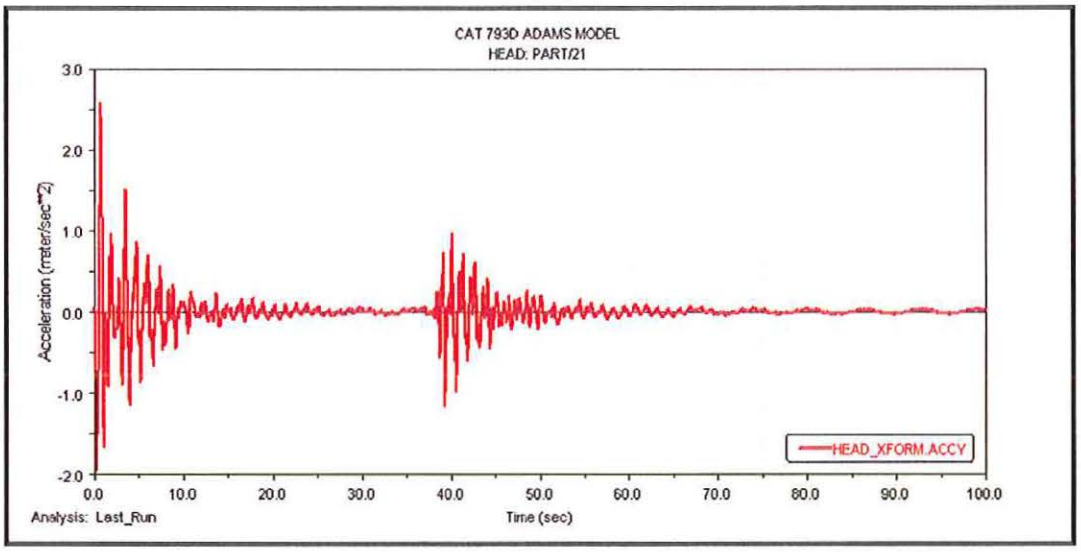

Figure 7.16. Human Cervical Region Acceleration in the y-direction

Figures 7.17 and 7.18 present the results of the RMS and the actual acceleration fields felt by the operator at the cervical region in the x-direction. The RMS acceleration is equal to 0.36 m/s^2.

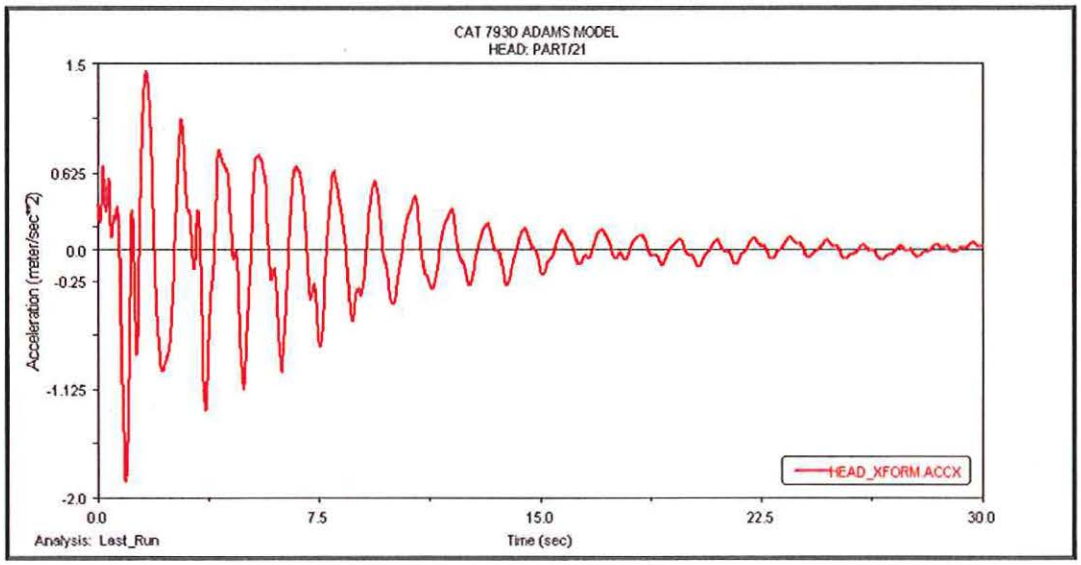

Figure 7.17. Human Cervical Region RMS Acceleration in the x-direction

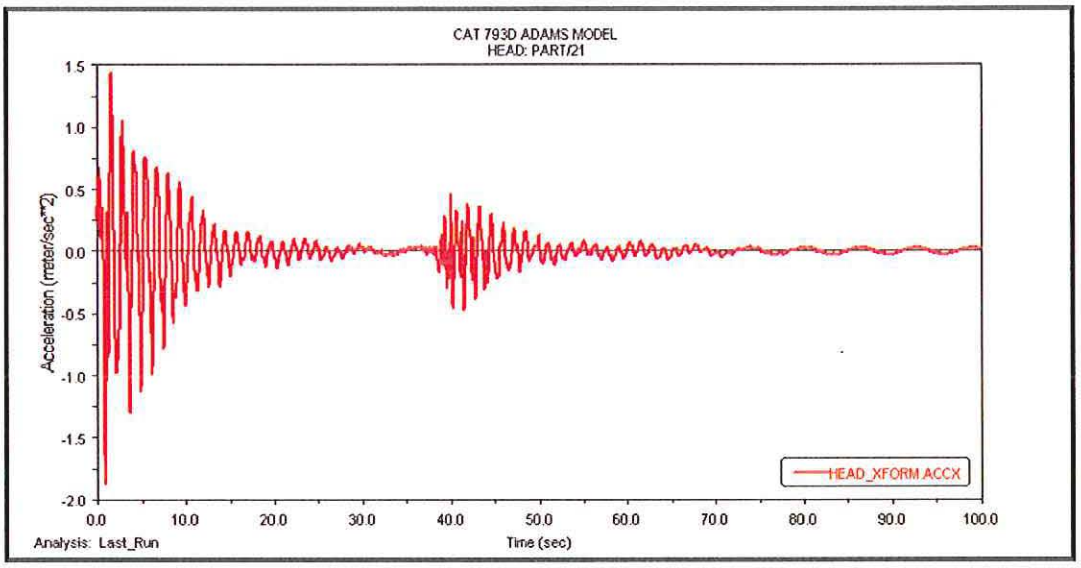

Figure 7.18. Human Cervical Region Acceleration in the x-direction

The vertical acceleration fields that the truck cabin experiences are presented in Figures 7.19 and 7.20. The RMS acceleration is equal to 4.19 m/s^2 as illustrated in Figure 7.19. The vertical acceleration peaks at *t=0.1 sec.*, and lasts for two seconds due to the first shovel pass.

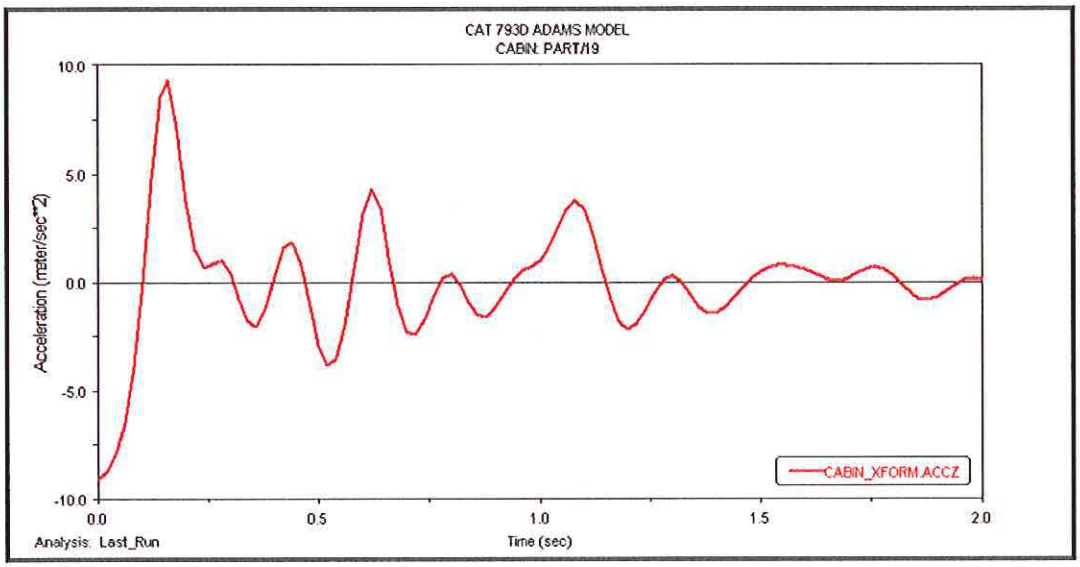

Figure 7.19. Cabin RMS Acceleration in the z-direction

Then, the cabin oscillates for about ten seconds before the acceleration diminishes to zero, as illustrated in Figure 7.20. The second shovel pass occurs at *t=38 sec.* resulting in a lower acceleration field that affects the truck cabin. This corresponding acceleration field excites the cabin forcing it to oscillate for about six seconds before its value diminishes to zero. Only the vertical acceleration component is presented because of its predominance compared to the x- and y- components.

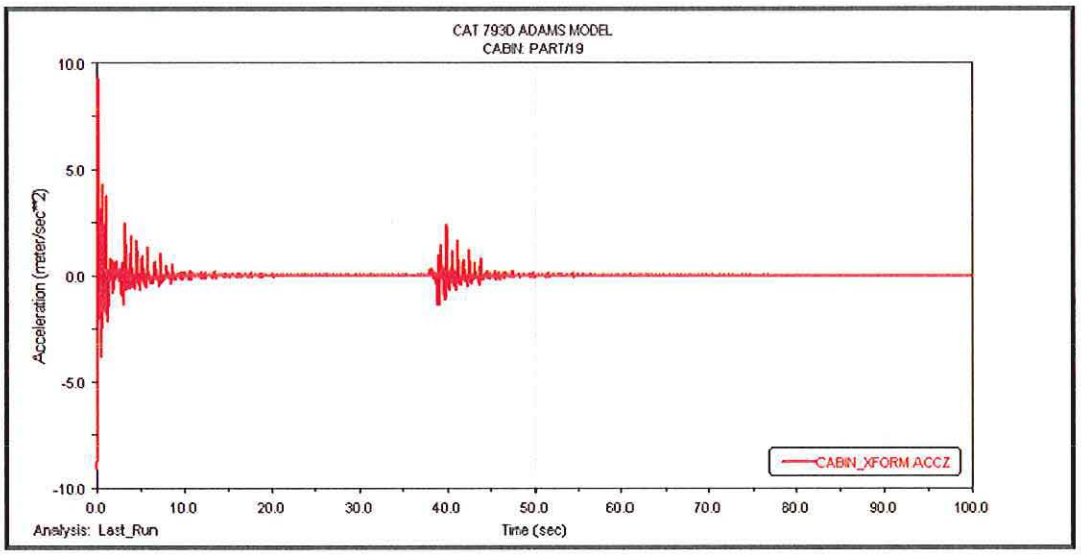

Figure 7.20. Cabin Acceleration in the z-direction

Figure 7.21 shows the RMS acceleration of the truck chassis. This RMS acceleration has a value equal to 1.65 m/s^2, and is significantly lower than the RMS accelerations of the truck cabin and operator's seat. This lower acceleration was expected because the chassis is about forty-three times heavier than the truck cabin, which makes it harder to oscillate under the excitation forces generated by the HISLO conditions.

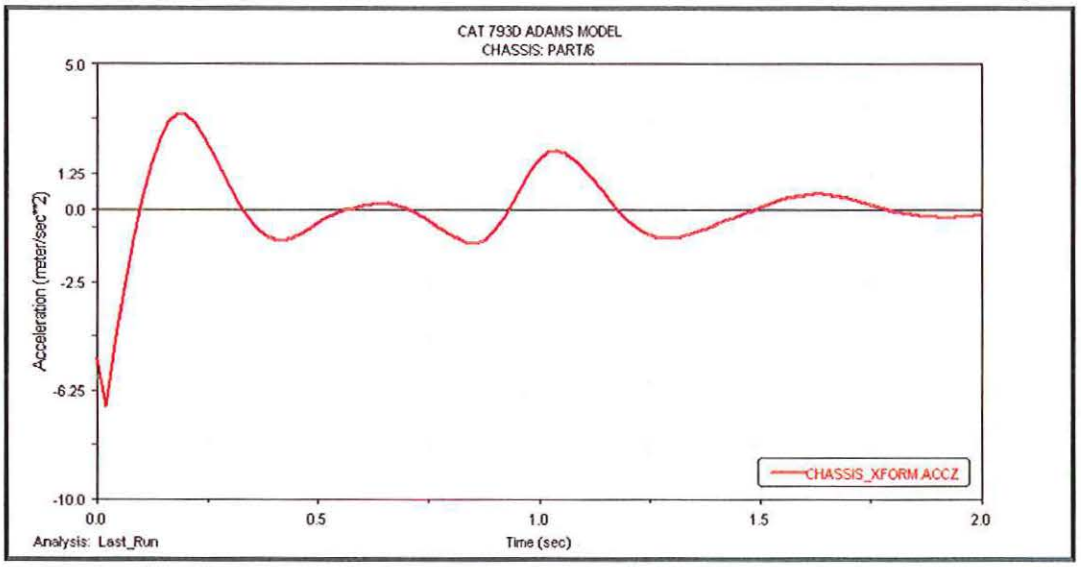

Figure 7.21. Chassis RMS Acceleration in the z-direction

Figure 7.22 presents the chassis acceleration due to the first and second shovel passes. It can be clearly noticed that the severity of the acceleration is lower for the chassis compared to the truck cabin. The oscillation of the chassis lasts about eight seconds for the first shovel pass and seven seconds for the second shovel pass.

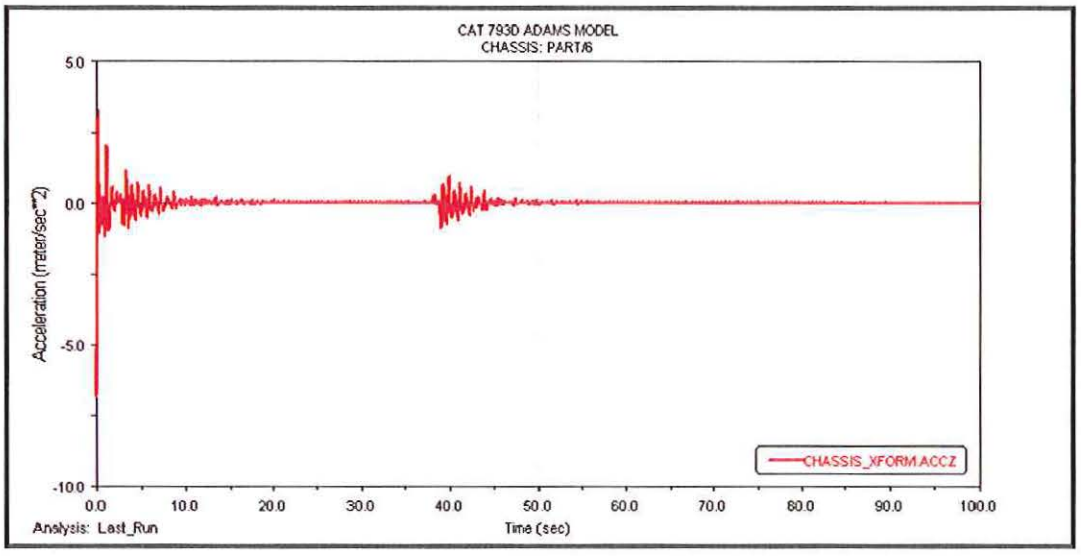

Figure 7.22. Chassis Acceleration in the z-direction

Figures 7.23 and 7.24 show the RMS and actual acceleration fields of the truck body, respectively. The RMS acceleration is equal to 2.45 m/s^2, which is lower than the cabin RMS acceleration due to the fact that the truck body weight is about twenty times heavier.

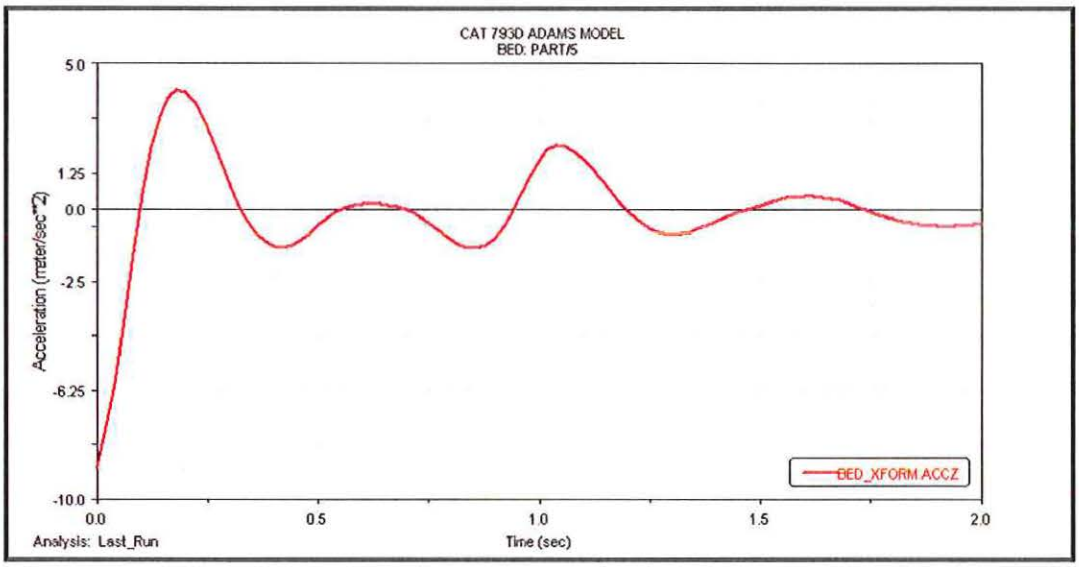

Figure 7.23. Body RMS Acceleration in the z-direction

Figure 7.24 shows the acceleration of the truck body which peaks when the first load is dumped; therefore, forcing the structure to oscillate for about fifteen seconds before it diminishes to zero. The second shovel pass dumped at *t=38 sec.* introduces oscillations that lasts for twelve seconds with a lower magnitude than the accelerations due to the first shovel pass. Only the vertical acceleration fields are presented because of their predominance and their major contribution to the overall truck vibrations. The displacements and velocities of the truck body, as well as, the chassis and cabin are presented in Appendix B.

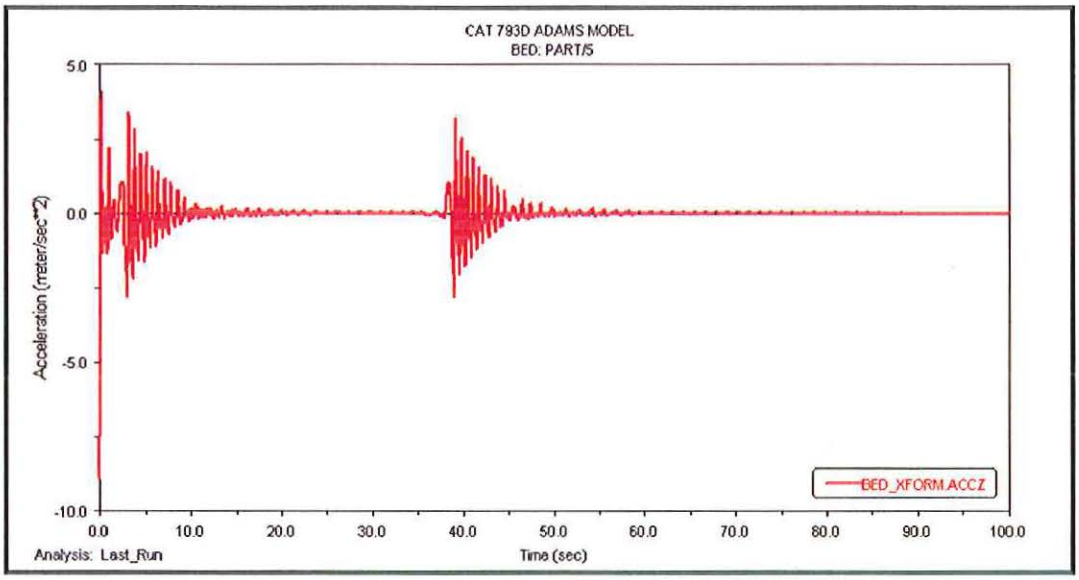

Figure 7.24. Truck Body Acceleration in the z-direction

7.2. DISCUSSION ON THE EFFECTS OF VIBRATION

This research points out the severity of truck vibrations under HISLO conditions as shown by the virtual prototype simulation results. These results show that the virtual truck simulator simulates the physical behavior of the truck under the HISLO conditions with minimal deviation from the field experimental results. The virtual truck simulator is a very powerful tool for simulating truck vibrations in severe operating conditions to examine an operator's exposure to vibration levels. This virtual model eliminates the costly and sometimes dangerous field tests. It provides a complete range of results from dynamic analysis such as the displacement, velocity and acceleration fields, as well as, the kinetic and potential energies of each truck component.

The simulation results of the 38-DOF truck model, under the HISLO conditions, showed that the operator is subjected to high levels of vibrations over a significant period

of time ranging between 3 to 25 seconds. The vibrations propagation throughout the truck structure in the three dimensions are transmitted to the operator's back and neck with RMS acceleration values significantly higher in the vertical direction (1.12 and 0.90 m/s^2, respectively). This creates a compressive effect on the operator's back that may result in injuries over long-term exposure.

The predominance of the vertical acceleration field is clearly demonstrated by values that are more than double that of the x- and y- acceleration components. Comparison of these RMS acceleration values to the comfort regions defined by the ISO 2631 standards reveals that the accelerations felt by the operator's lower back and neck are in the fairly uncomfortable to the uncomfortable comfort zone, respectively. The magnitudes of the accelerations from the simulation model generate forces that are smaller than the failure strength of the human lumbar vertebra (1.7 MPa) to cause fracture of lumbar vertebra (Campbell-Kyureghyan et al., 2007). However, long-term exposures to these WBV levels can cause health problems to operators. The seat is subjected to higher RMS accelerations between 1.49 and 3.56 m/s^2. These acceleration values are significantly higher than the exposure values compared to the ISO 2631 standards. The RMS accelerations range in the seat compartment lies within the very uncomfortable and extremely uncomfortable comfort zone defined by ISO 2631 in Table 2.2.

The vibration of the truck model, under HISLO conditions, is tri-axial, as shown in the simulation results. The vertical acceleration is responsible for the compressive and

stretching effect of the spine, whereas the x- and y- vibrations cause significant postural instability. Therefore, the injury potential of the combined acceleration fields in the x-, y- and z-directions would probably be greater than the injury potential due to accelerations applied in any one axis.

The CAT 793 truck series modeled and analyzed in this study is widely used in industry where it showed strength in various weather conditions. For instance, Freeport-McMoRan Morenci's copper mine uses more than 80 CAT 793 truck (Freeport-McMoRan, 2007) in the operation. Therefore, the practical use of this truck series in the industry is well recognized and, thus, the theoretical and simulation models developed in this study will help solving major operators' health problems.

The environmental conditions for truck loading in the industry ranges between solid ground conditions, in the Arizona copper mines for example, to soft ground conditions in northern Canada during the summer. These ground conditions behave differently under HISLO conditions and affect the vibration propagation throughout the truck structure reaching the operator. Even though this study focused on the oil sands ground conditions, it can be extended to cover the different ground conditions present in the industry. This can be done by using the theoretical and virtual models with the appropriate boundaries representing the ground conditions of interest to find the vibration levels that the operator and the truck structure experience. The models developed in this research cover the whole envelope of different environmental conditions encountered in the surface mining industry.

The vibrations experienced by the truck operator under HISLO conditions must be considered by MSHA for creating a safe work environment. MSHA regulations have setup strict guidelines for hand vibrations using hand tools, but have not considered the WBV under the HISLO conditions.

7.3. SUMMARY

The virtual truck model under the HISLO conditions is simulated in ADAMS environment successfully. The virtual truck model is built based on the CAT 793 series that is widely used in surface mining operations. The oil sands environmental ground conditions were used in the simulation; however, the study can be expended to cover the complete environmental ground conditions envelope encountered during loading in the industry. This is done by changing the ground conditions parameters in the simulator. The simulation results showed that the operator is subjected to high levels of vibration compared to the ISO 2631 exposure limits. These high acceleration values can cause long-term lower back and neck injuries, musculoskeletal disorder and health problems over long-term operator exposure.

8. SUMMARY, CONCLUSIONS AND RECOMENDATIONS

8.1. SUMMARY

The shovel-truck mining system is used widely in surface mining operations for achieving production targets. The system constitutes a major component in surface mine production cost. Truck haulage and shovel loading costs range between 3% and 35% of the overall production cost based on statistical data from surface mining operations (Hustrulid et al., 1995). Over the last two decades, there has been an increased demand for large capacity shovels and trucks for achieving high production and low cost operations. These large shovels, with dipper capacities in excess of 100 tons, are matched with large capacity haul trucks. The resulting impact force, from high-impact shovel loading operations (HISLO), causes significant vibrations that are propagated through the truck structure to the operator's cabin. Truck operators are, thus, exposed to high levels of WBV that may cause operator health problems over time. Thus, efforts must be made to minimize or eliminate the impact of the vibrations, and prevent operator health problems under HISLO conditions.

Research studies in machinery design have focused on methods to control and monitor the amount of vibrations to maintain the frequency levels within the ISO limits. No fundamental research studies have yet been carried out on machinery vibrations and WBV exposures for large mining trucks. This research study provides an effort in developing the mechanics of truck vibrations, under HISLO conditions, using Lagrangian formulation for a 9-DOF system. Furthermore, a 3D virtual truck prototype model with 38-DOF, is built and simulated in MSC.ADAMS in this research. The virtual 3D

dynamic model and simulator provide a powerful tool for predicting vibration levels for different truck configurations and other machinery for understanding operators WBV exposure levels under the HISLO conditions. The information gained from the dynamic truck simulator model will be used to design better shovel loading methods, truck suspension and control methods for reducing the operator's WBV exposure levels. Thus, the 38-DOF truck model is the frontier study of the truck vibrations under the HISLO conditions. The sections below summarize the detailed procedures used to achieve the objectives of the study (in Chapter 1.0).

1. The introduction provides the underlying HISLO problems in large scale surface mining operations, as well as, the objectives and scope of the research study. It also outlines the importance of this research and its scientific and industrial contributions.

2. An in-depth literature survey was carried out to examine the contributions and limitations of the previous and current body of knowledge on the WBV, machinery vibration and dynamic modeling. Many researchers have focused on the WBV as one aspect of machinery vibration. Other vibration studies focused on seat ergonomics and seat design that eliminate or minimize the operator's exposure to vibrations. Virtual prototyping and dynamic modeling techniques have been used in the automotive industry, and literature shows their extensive use in the vibration area, as well as, the fatigue life expectation. The literature survey had limitations pertaining haul truck vibrations analysis. A 3D dynamic

modeling and vibration analysis of the haul truck has not yet been studied. No fundamental researches have been carried out on vibrations propagation and WBV exposures for large mine trucks. Additionally, a virtual truck model using MSC.ADAMS has not been developed and simulated yet.

3. The mechanics of truck vibrations under the HISLO conditions have been successfully developed in 3D. The theoretical analysis of truck vibrations has been achieved by applying the Lagrangian method on a 9-DOF truck model to develop an understanding for the basis of vibration problems. The corresponding EOMs of the 9-DOF system have been generated in order to describe the truck behavior under the HISLO conditions.

4. The numerical techniques for developing the symbolic solution of the undamped free vibration problem of the 9-DOF truck system is developed, as well as, discussions on the stability, convergence and errors estimates. The natural frequencies of the 9-DOF truck system are found and served as an input for the modal analysis for solving the damped forced vibrations.

5. The virtual prototype simulator consisting of 38-DOF has been developed in MSC.ADAMS. This 3D model captures the vibrations propagation for the multi-degree of freedom system in a software environment without the need to conduct physical experiments at the field.

6. The CAT 793 truck is used as the subject for research study. The model parameters, such as the stiffness and damping coefficients and the weight of the components are determined based on design parameters and from literature. Experimental results from the oil sands mining operations by Kumar (1999) have been presented and discussed in detail for validating the virtual prototype simulation results.

7. The 38-DOF virtual model in Chapter 5.0 is simulated successfully. Several experiments are conducted using the using the developed virtual prototype simulator. These experiments included analysis of the operator's seat, his lumbar and cervical regions, as well as, the truck cabin, chassis and body. Medium-hard ground conditions are set for these experiments.

8.2. CONCLUSIONS

This research study is limited to the high impact shovel loading operations in surface mining. The study focuses on the CAT 793 series and their corresponding shovel excavators. However, the theoretical underpinnings of this study can be applied to other mining trucks and equipment. The results of this research will allow the development of a dynamic model that will serve as a guidance to modify the truck design to absorb the shockwaves beyond the ISO standards and maintain a safe workplace. Hence, the research objectives stated in Section 1.3 have been achieved within the research scope.

From the literature surveys, the following conclusions can be drawn.

1. The 3D dynamic modeling and virtual simulation of dump truck vibration under the HISLO conditions has never been studied. This is the first fundamental research study on dump trucks vibrations in surface mining operations. This research has created a frontier in the mechanics of dump truck vibrations by modeling the shockwaves and their propagation through the truck structure.

2. This research endeavor provides contributions and understanding into the body of knowledge of truck vibrations. Therefore, the effects on operator's health, under the HISLO conditions, will be a significant asset to truck manufacturers, as well as, mining companies and safety personnel.

3. The virtual prototyping and dynamic modeling techniques are limited in use in large scale surface mining industry, whereas they are well used in automotive and aerospace industries. Therefore, there is a need to create a virtual prototype simulator that captures the vibrations propagation for the multi-degree of freedom truck system in a software environment.

From the mechanics of dump truck vibrations under HISLO conditions analysis, the following conclusions can be drawn.

1. The mathematical model for a 9-DOF truck vibration system is solved for the undamped free vibrations problem. The vertical z-direction is considered in the analysis due to its predominance over the x- and y- directions.

2. The undamped free vibration analysis provides the natural frequencies, and hence the different mode shapes of the system under the HISLO conditions.

3. The mathematical model of the forced damped vibrations is developed and solved. This model provides a basis for truck vibrations simulation.

4. The modal analysis of the forced damped vibrations problem presents the displacement vector of the 9-DOF system.

From the research results of the truck model simulation in MSC.ADAMS, the following conclusions are drawn.

1. The discussion and analysis of the experimental results have been achieved to point out the value of the work carried out. This discussion shows how the models could be replicated for other truck models.

2. The operator's lower back (lumbar region) and neck (cervical region) vibration levels exceed the ISO 2631 exposure limits exposing the operator to high accelerations in the x-, y- and z- directions with the vertical acceleration being the

predominant. The RMS values for the a_x, a_y and a_z axes for the lumbar region are equal to 0.40 m/s^2, 0.41 m/s^2 and 1.12 m/s^2, respectively. The x, y and z RMS accelerations for the cervical region are equal to 0.36 m/s^2, 0.53 m/s^2 and 0.90 m/s^2, respectively.

3. The operator's seat experiences the highest acceleration levels due to the HISLO conditions. The accelerations (RMS) at the seat has a value of 3.56 m/s^2 in the vertical direction, 1.49 m/s^2 and 1.08 m/s^2 in the x and y directions, respectively.

4. The vibration of the operator's seat in the vertical direction affects the driver's buttocks by subjecting it to repeated vertical loading. This repeated compressive force to the spine may lead to lower-back injuries over long-term exposure.

5. Comparison of the vertical accelerations between the seat and the operator's lumbar and cervical regions clearly appears that the vertical vibration is significantly damped as it travels along the spine upward. However, the repeated exposure of the operator's lower back and neck may constitute significant hazard to the operator's health and safety.

6. The virtual prototype simulation results showed that the RMS values for the operator's lower back and neck, as well as his seat are in strong agreement with the results from Kumar's study. The difference in these values ranged between 1.3% and 6.7%; with only one exception of 9.2% for the operator's seat in the y-

direction (left-right). The simulation results showed that the operator is subjected to high levels of vibration compared to the ISO 2631 exposure limits. These high acceleration values can cause long-term lower back and neck injuries, musculoskeletal disorder and operator's health problems.

8.3. CONTRIBUTIONS OF PHD RESEARCH

The contributions of this PhD study into the body of knowledge on machinery vibrations under HISLO conditions comprise of the following key contributions.

1. This is the first attempt to study the vibrations propagation through dump trucks and their impact on the operator's health under HISLO conditions by using virtual prototyping and simulation techniques.

2. This work introduces a 3D multi-body dump truck dynamic model as a new way to study the 3D vibrations propagation due to HISLO. This research advances the frontier of 3D multi-body dynamic modeling by providing a complete truck model in MSC.ADAMS environment.

3. This research introduces the use of the MSC.ADAMS software environment in the mining industry that provides appropriate standardization allowing easy modification, transformation and advancement because of the wide use of this software by several industries.

4. This research is a pioneering effort towards developing comprehensive vibration theory, dynamic models and practical solutions for solving HISLO problems. It advances the heavy mining machinery vibrations frontier and contributes immensely to its body of knowledge under HISLO conditions.

5. This work provides a potential basis for developing technologies to improve workplace safety and operators' health and safety in surface mining operations. The results could maximize machine availability, minimize maintenance costs, and maximize production economics.

8.4. RECOMMENDATIONS

This research has produced significant evidence that the CAT 793 truck operator is exposed to high levels of vibrations under HISLO conditions within the studied environmental conditions. Further studies are required to enhance work carried out in this study, as discussed below.

1. As indicated in the course of this work, the suspension characteristics used in the 3D simulation model were approximated based on the maximum cylinder stroke. Further work is, thus, necessary in finding the exact truck suspension characteristics to ensure that the simulation model will mimic the actual physical truck even though the results showed agreement with the experimental data available for validation.

2. The operator exposure under HISLO conditions demonstrates a need to reduce the vibration levels for a safer work environment. Design changes for the truck structure and suspension mechanism may be undertaken to isolate the driver from the truck vibration. Moreover, the truck bed design may be modified in such a way that it absorbs part of the shockwaves produced by the HISLO by using an inside layer of flexible material. Additionally, the operator's seat may be modified to include higher cushioning characteristics that minimize the vibrations transmitted to the operator lower-back.

3. On the other hand, the loading configuration may be investigated to lower the impact force generated by the material free fall from the shovel bucket into the truck body. Techniques for gradually releasing the loads from the shovel buckets can be a potential factor in lowering the vibration levels through the truck.

4. Future work can focus on building the truck components to account for deformation using MSC.ADAMS/Flex and the truck model developed in this study as a basis. This will introduce structural deformation and dynamic stress analysis and their effect on the vibration propagation under the HISLO conditions into the complete truck simulation model. The shovel loading process can be optimized based on the findings of this study. Therefore, the focus on the optimization process of shovel loading operation can lower the risk of vibration exposure.

5. Another potential area for future work is modeling the human operator flexibility. The human model can include the different body parts that retain the flexible behavior and damping characteristics of the human body. This human model can be further extended to investigate the severity of the vibrations on the human organs.

APPENDIX A.

MATHEMATICAL MODELING OF

THE 9-DOF SYSTEM

The determinant in equation (4.7) is input into MAPLE as shown in equation A.1. Then the determinant is found by executing expression (A.2).

```
> KK:=linalg [matrix](9,9,[k1/m1-lambda,-k1/m1,0,0,0,0,0,
0,a*k1/m1,-k1/m1,m2,(k1+k2r+k2f+k4)/m2-lambda,-k2r/m2,
-k2f/m2,-k4/m2,0,0,0,(-a*k1-d*k2r+e*k2f+f*k4)/m2,0,-
k2r/(2*m4),((k2r+k3r)/(2*m4))-lambda,0,0,0,-k3r/(2*m4),
0,d*k2r/(2*m4),0,-k2f/m4,0,((k2f+k3f)/m4)-lambda,0,0,0,
-k3f/m4,-e*k2f/m4,0,-k4/m5,0,0,((k4+k5)/m5)-lambda,
-k5/m5,0,0,-f*k4/m5,0,0,0,0,-k5/m6,(k5/m6)-lambda,0,0,0,
0,0,-k3r/m0,0,0,0,(k0+k3r)/m0-lambda,0,0,0,0,0,-k3f/m0,0,
0,0,(k0+k3f)/m0-lambda,0,a*k1/I2,(-a*k1-d*k2r+e*k2f+f*k4)/I2,
d*k2r/I2,-e*k2f/I2,-f*k4/I2,0,0,0,
(a^2*k1+d^2*k2r+e^2*k2f+f^2*k4)/I2-lambda]);
```

(A.1)

```
> DET:=(linalg[det](KK));
```

(A.2)

The results from equation (A.2) represent the characteristic polynomial of the system to the ninth order in terms of λ. Setting this characteristic polynomial to zero and then solving for λ, yields nine different natural frequencies, $\omega_{n,i}$, of the system that describe the different modes of truck vibration.

The results of the 9-DOF undamped free vibration system are completely symbolic, thus, a simple numerical example is performed to check for the stability of the mathematical model. Therefore, the numerical values defined in Tables 6.4 and 6.5 are replaced in equation (A.1) resulting in equation (A.3).

```
> KK:=linalg [matrix](9,9,[18.4-lambda,-18.4,0,0,0,0,0
,0,-.541,-39.5,638-lambda,-354,-244,-.505,0,0,0,-150,0,
-556.81,559.4-lambda,0,0,0,-2.58,0,1480,0,-766.88,0,
772.05-lambda,0,0,0,-5.169,-2489.32,0,-9.918,0,0,
10.32-lambda,-.409,0,0,-32.19,0,0,0,0,-9.86,9.86-lambda,
0,0,0,0,0,-.11181,0,0,0,3.11-lambda,0,0,0,0,0,-.22,0,0,0,
6.22-lambda,0,.234,-30.23,190,-159.6,-.322,0,0,0,1024-lambda]);
```

(A.3)

```
> DET:=(linalg[det](KK));

DET:=1.7049713λ^9 + 2928.7522 λ^8 - 2.3723486510^6 λ^7
+ 1.61696681^8 λ^6 - 3.74676231^9 λ^5 + 3.98891471^10 λ^4
- 2.12683931^11 λ^3 + 5.618717011^11 λ^2 - 6.70732491^11 λ
+ 2.71041641^11
```

(A.4)

Setting equation (A.4) equal to zero and solving for $\lambda = \omega_{n,i}$, yields nine different natural frequencies, $\omega_{n,i}$, as in equations (A.5) and (A.6).

$$1.7049713\lambda^9 + 2928.7522\,\lambda^8 - 2.37234865\text{x}10^6\,\lambda^7 + 1.6169668\text{x}10^8\,\lambda^6 - 3.7467623\text{x}10^9\,\lambda^5 + 3.9889147\text{x}10^{10}\,\lambda^4 - 2.1268393\text{x}10^{11}\,\lambda^3 + 5.61871701\text{x}10^{11}\,\lambda^2 - 6.7073249\text{x}10^{11}\,\lambda + 2.7104164\text{x}10^{11} = 0 \tag{A.5}$$

$$\begin{aligned}
&\omega_{n,1} = 0.89608 \text{ rad/sec} \Rightarrow f_1 = 0.14 \text{ Hz} \\
&\omega_{n,2} = 1.37140 \text{ rad/sec} \Rightarrow f_2 = 0.22 \text{ Hz} \\
&\omega_{n,3} = 1.78896 \text{ rad/sec} \Rightarrow f_3 = 0.28 \text{ Hz} \\
&\omega_{n,4} = 2.50771 \text{ rad/sec} \Rightarrow f_4 = 0.40 \text{ Hz} \\
&\omega_{n,5} = 2.90139 \text{ rad/sec} \Rightarrow f_5 = 0.46 \text{ Hz} \\
&\omega_{n,6} = 3.52073 \text{ rad/sec} \Rightarrow f_6 = 0.56 \text{ Hz} \\
&\omega_{n,7} = 6.29975 \text{ rad/sec} \Rightarrow f_7 = 1.00 \text{ Hz} \\
&\omega_{n,8} = 23.27224 \text{ rad/sec} \Rightarrow f_8 = 3.70 \text{ Hz} \\
&\omega_{n,9} = 48.29122 \text{ rad/sec} \Rightarrow f_9 = 7.69 \text{ Hz}
\end{aligned} \tag{A.6}$$

The same 9-DOF truck model is built and simulated in ADAMS for the frequency response purposes. The frequencies of the virtual model are tabulated in Table A.1.

Table A.1. Natural Frequencies of the Virtual Model versus the Mathematical Model

	Virtual Model in ADAMS	Mathematical Model in MAPLE	Absolute Difference (Hz)
f_1	0.14 Hz	0.14 Hz	~0
f_2	0.25 Hz	0.22 Hz	0.03
f_3	0.31 Hz	0.28 Hz	0.03
f_4	0.38 Hz	0.40 Hz	0.02
f_5	0.47 Hz	0.46 Hz	0.01
f_6	0.63 Hz	0.56 Hz	0.07

f_7	1.09 Hz	1.00 Hz	0.09
f_8	3.87 Hz	3.70 Hz	0.17
f_9	7.92 Hz	7.69 Hz	0.46

The MAPLE results are comparable to the ADAMS results, which mean that the mathematical model developed in Chapter 3.0 is a stable model.

The natural frequencies of the mathematical model are then compared with their counterparts within the 38-DOF virtual model.

Table A.2. Natural Frequencies of the Mathematical Model versus the 38-DOF Virtual Model

	Virtual Model in ADAMS (38-DOF)	Mathematical Model in MAPLE	Absolute Difference (Hz)
f_1	0.04 Hz	0.14 Hz	0.10
f_2	0.11 Hz	0.22 Hz	0.11
f_3	0.19 Hz	0.28 Hz	0.09
f_4	0.26 Hz	0.40 Hz	0.15
f_5	0.32 Hz	0.46 Hz	0.14
f_6	0.41 Hz	0.56 Hz	0.15
f_7	0.65 Hz	1.00 Hz	0.35
f_8	2.90 Hz	3.70 Hz	0.80
f_9	6.71 Hz	7.69 Hz	0.98

The difference between the two natural frequencies is expected showing that the values uniformly lower than those from the 9-DOF model.

APPENDIX B.

VIRTUAL PROTOTYPE SIMULATION RESULTS OF THE 38-DOF SYSTEM

Appendix B summarizes the virtual prototype model simulation results that were not included in Chapter 7.0 of this research.

Figures B.1 and B.2 illustrate the displacement and velocity in the z-direction at the cervical region, respectively.

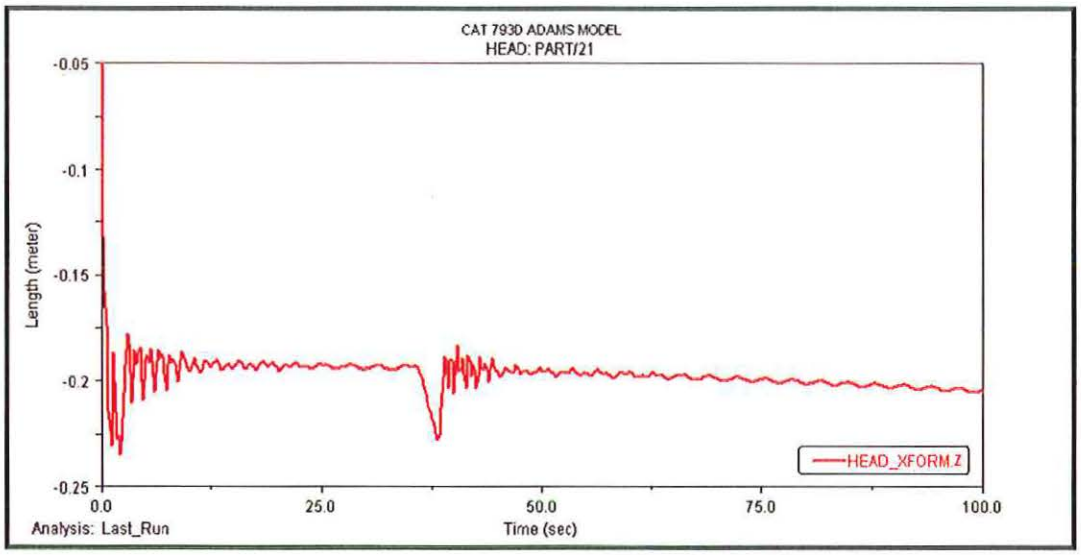

Figure B.1. Cervical Region Vertical Displacement

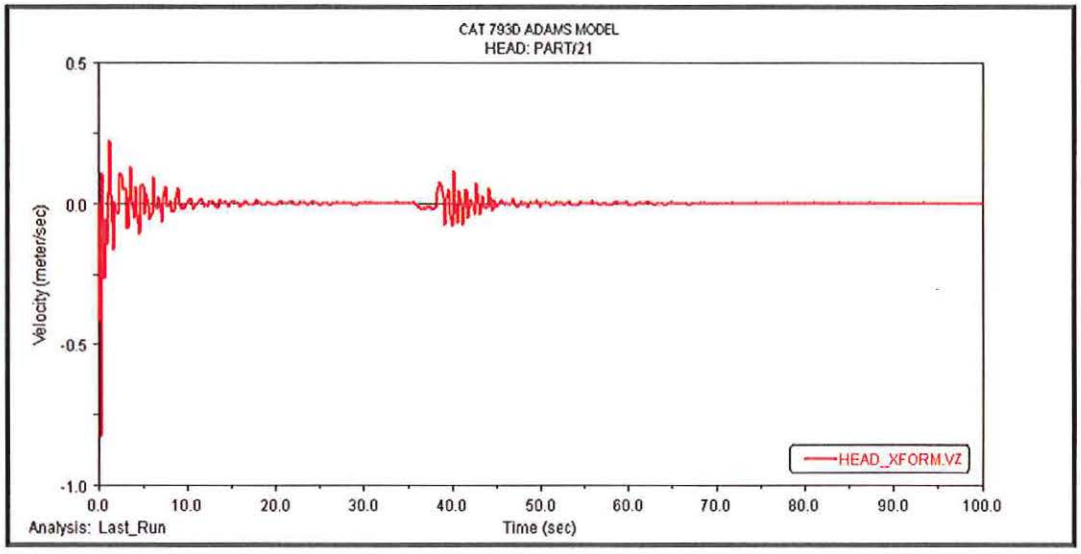

Figure B.2. Cervical Region Vertical Velocity

Figures B.3 and B.4 illustrate the displacement and velocity in the z-direction at the lumbar region, respectively.

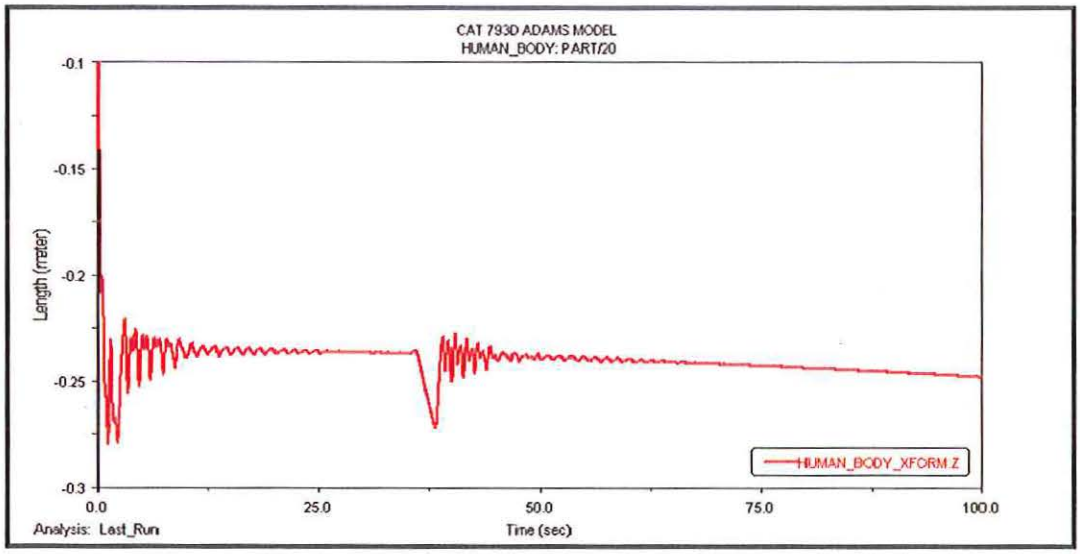

Figure B.3. Lumbar Region Vertical Displacement

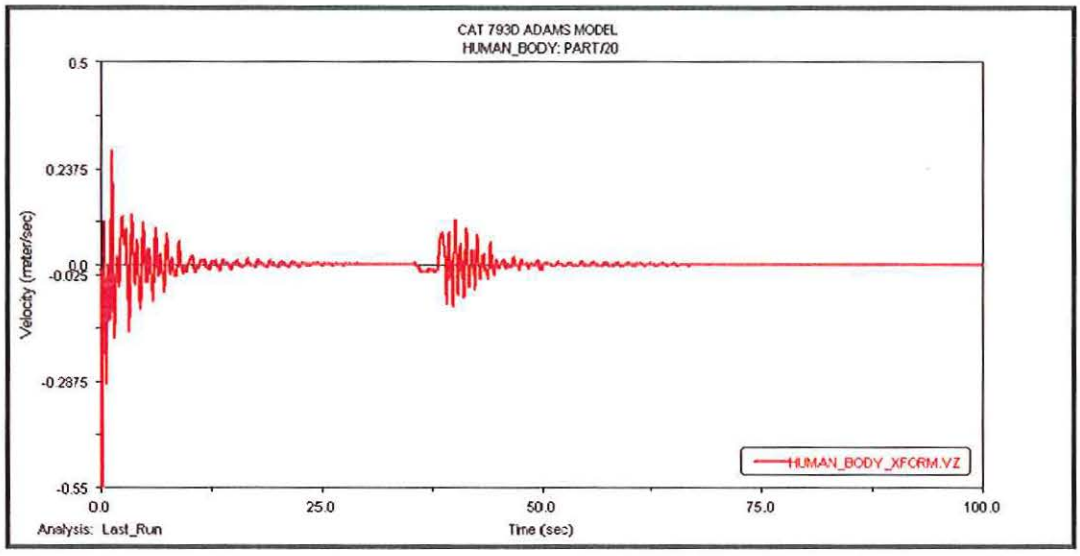

Figure B.4. Lumbar Region Vertical Velocity

Figures B.5 and B.6 illustrate the displacement and velocity in the z-direction at the operator's seat, respectively.

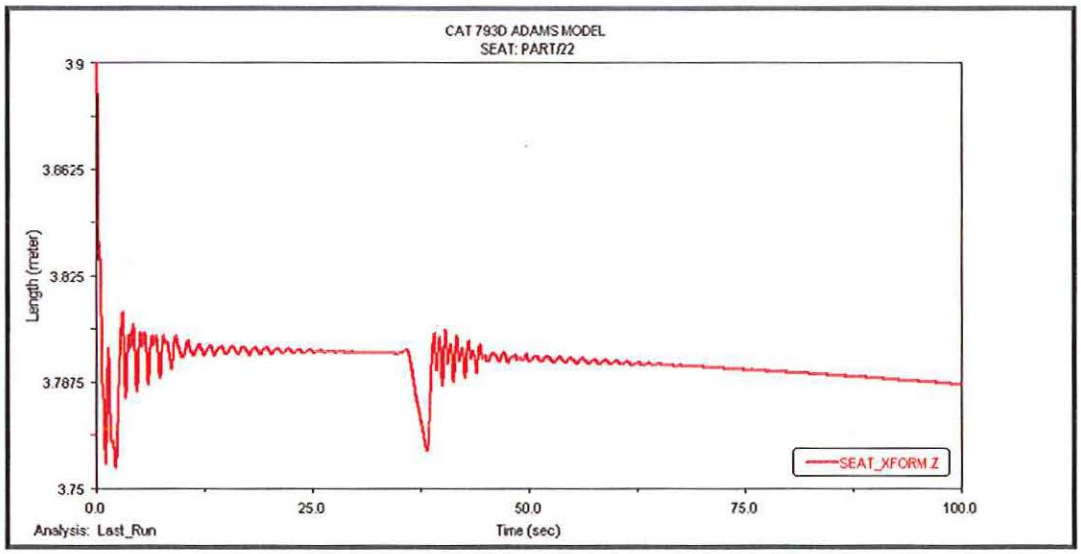

Figure B.5. Operator's Seat Vertical Displacement

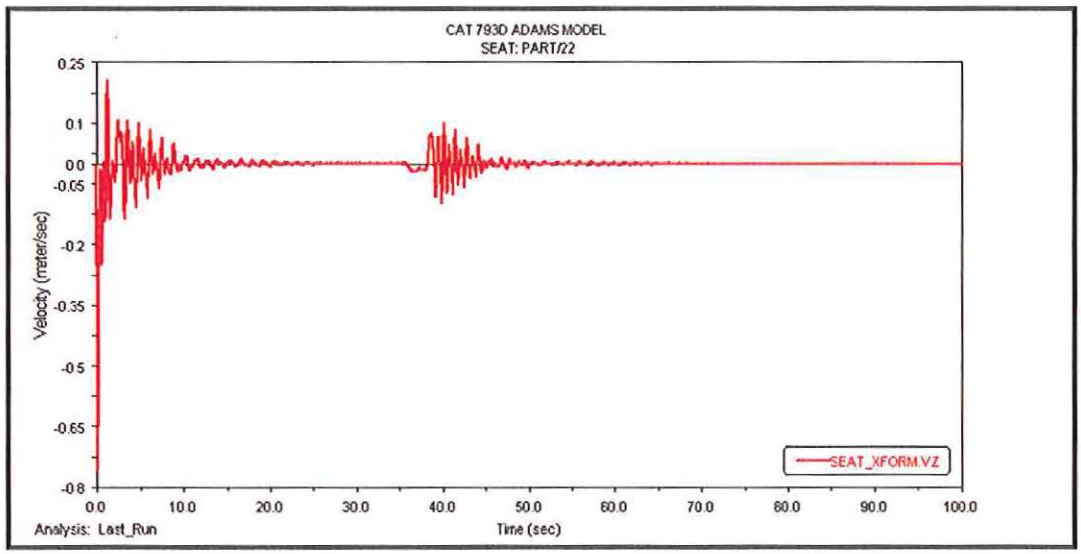

Figure B.6. Operator's Seat Vertical Velocity

Figures B.7 and B.8 illustrate the displacement and velocity in the z-direction of the truck cabin, respectively.

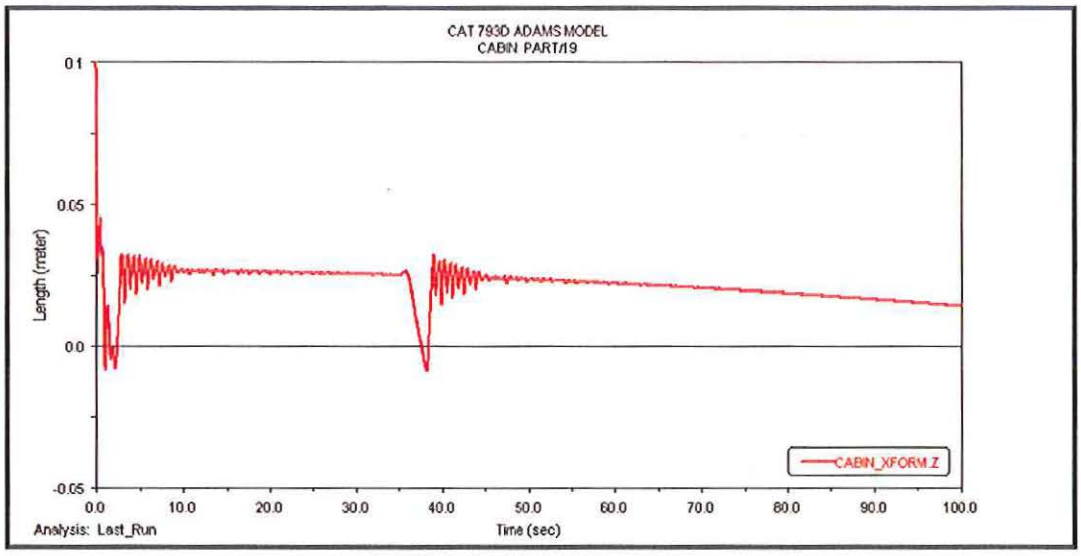

Figure B.7. Cabin Vertical Displacement

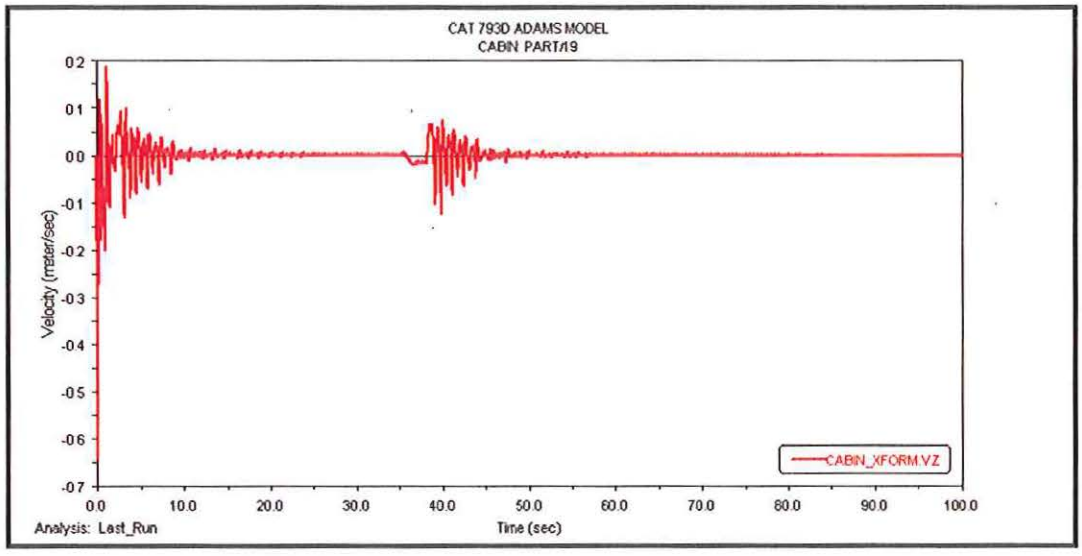

Figure B.8. Cabin Vertical Velocity

Figures B.9 and B.10 illustrate the displacement and velocity in the z-direction of the truck chassis, respectively. Figure B.9 shows that the chassis, and hence, the truck sinks under the applied load due to the medium-hard ground conditions encountered in the oil sands in Canada.

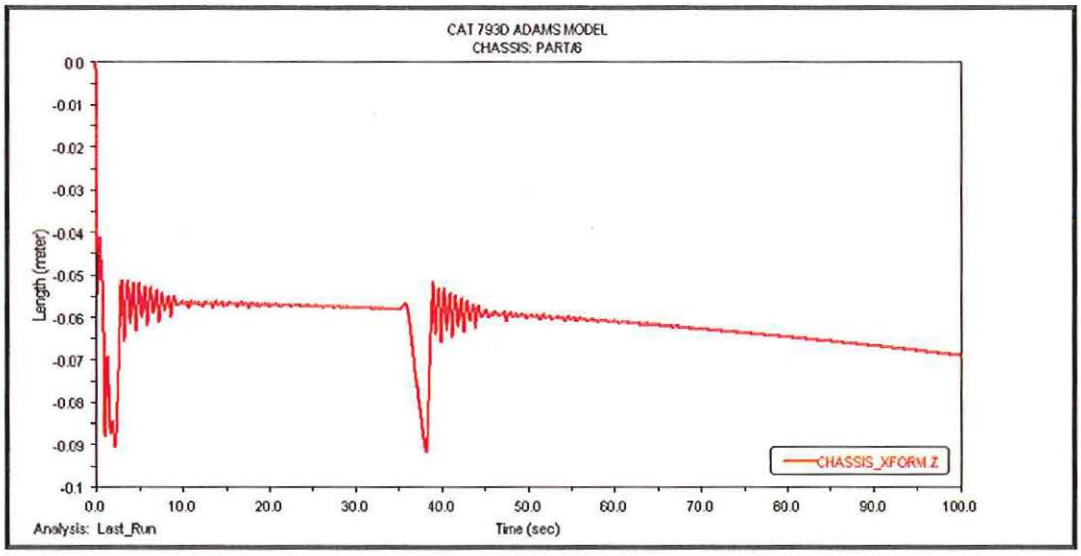

Figure B.9. Chassis Vertical Displacement

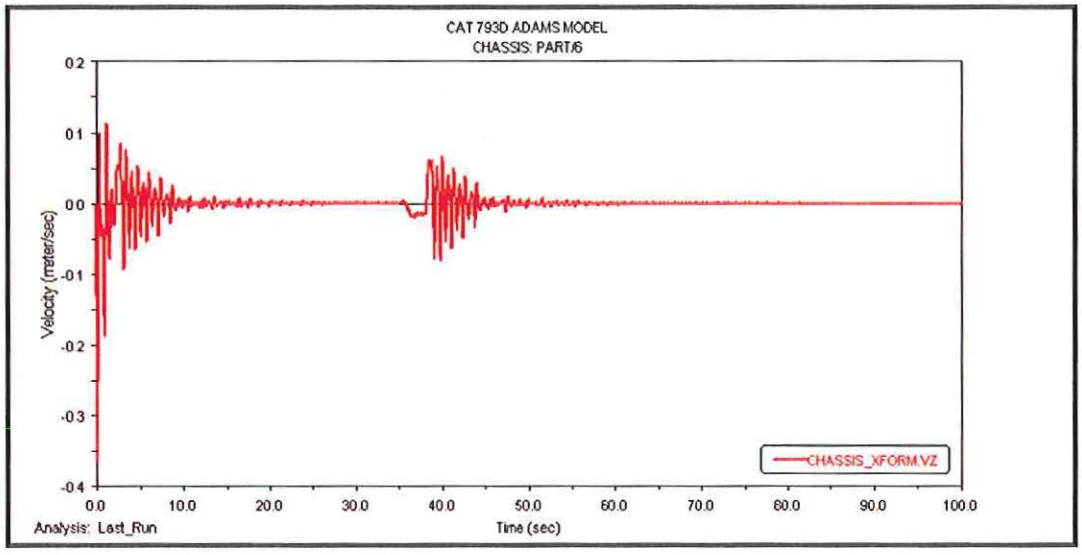

Figure B.10. Chassis Vertical Velocity

Figures B.11 and B.12 illustrate the displacement and velocity in the z-direction of the truck body, respectively.

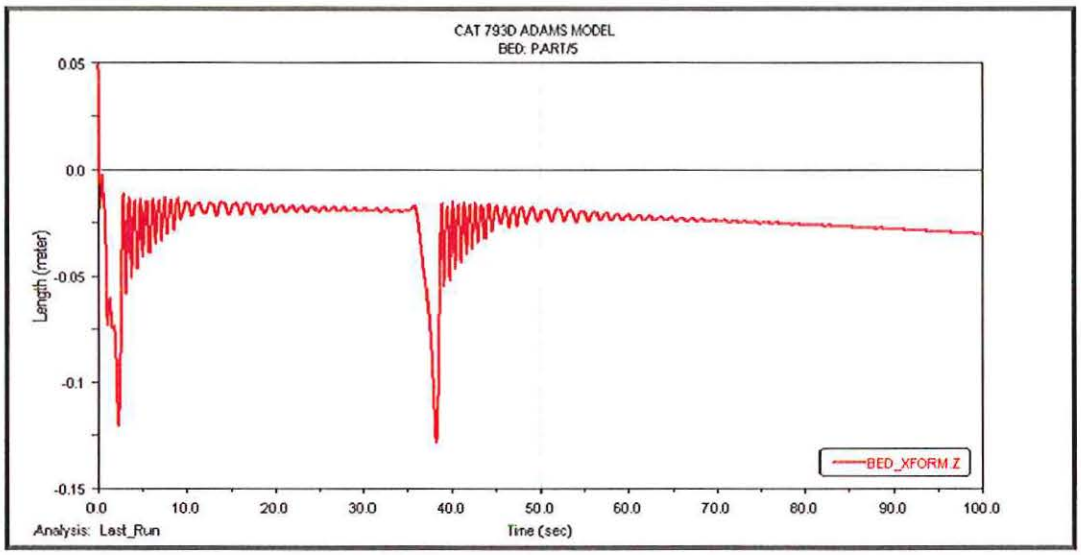

Figure B.11. Truck Body Vertical Displacement

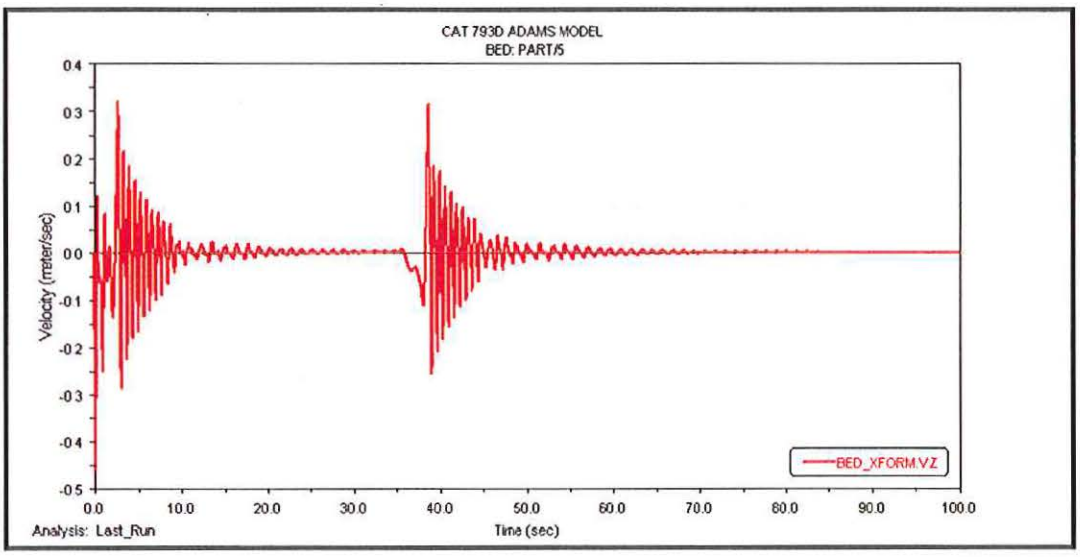

Figure B.12. Truck Body Vertical Velocity

Figure B.13 shows the input force modeling the first and second shovel passes at *t=0.1 sec.* and *t=38 sec.*, respectively.

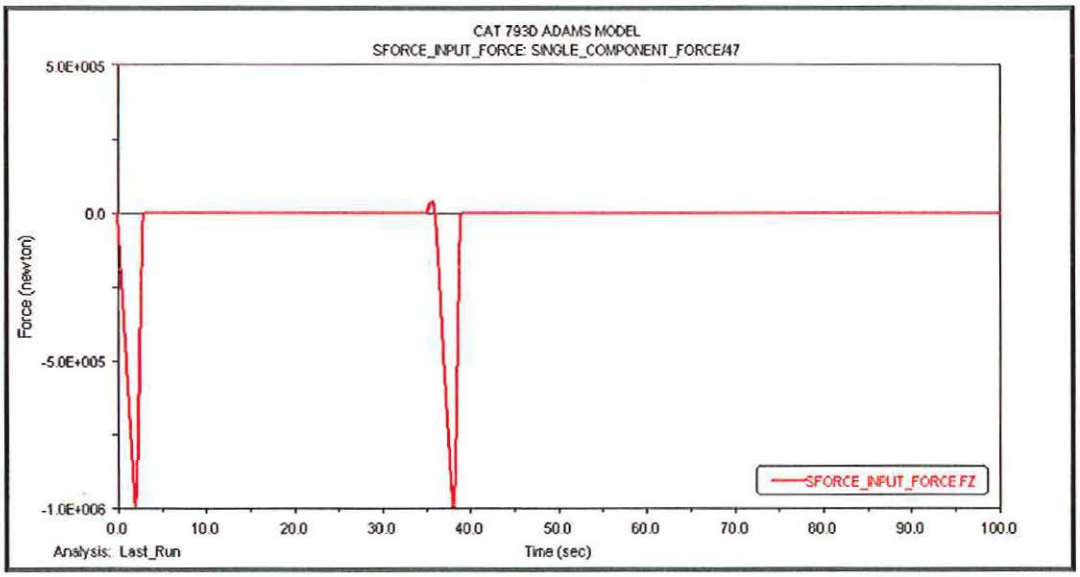

Figure B.13. Input Force on the Truck Body

APPENDIX C.

HISTORICAL BACKGROUND OF

JOSEPH-LOUIS LAGRANGE

Joseph-Louis Lagrange: Comte de l'Empire (Jan. 25, 1736-April 10, 1813 in Turin, baptized in the name of *Giuseppe Lodovico Lagrangia*). He was an Italian-French mathematician and astronomer who made important contributions to all fields of analysis and number theory and to classical and celestial mechanics as arguably the greatest mathematician of the 18th century. It is said that he was able to write out his papers complete without a single correction required. Before the age of 20 he was a professor of geometry at the royal artillery school at Turin. By his mid-twenties he was recognized as one of the greatest living mathematicians because of his papers on wave propagation and the maxima and minima of curves. His greatest work, *Mécanique Analytique* (Analytical Mechanics) (4. ed., 2 vols. Paris: Gauthier-Villars & fils, 1888-89. First Edition: 1788), was a mathematical masterpiece and the basis for all later work in this field. On the recommendation of Euler and D'Alembert, Lagrange succeeded the former as the director of mathematics at the Berlin Academy. Under the First French Empire, Lagrange was made both a senator and a count; he is buried in the Panthéon.

It was Lagrange who created the calculus of variations, which was later expanded by Weierstrass, solved the isoperimetrical problem on which the variational calculus is based in part, and made some important discoveries on the tautochrone which would contribute substantially to the then newly formed subject. Lagrange also established the theory of differential equations, and provided many new solutions and theorems in number theory, including Wilson's theorem. Lagrange's classic *Theorie des fonctions analytiques* laid some of the foundations of group theory, anticipating Galois. Lagrange developed the mean value theorem which led to a proof of the fundamental theorem of calculus, and a proof of Taylor's theorem. Lagrange also invented the method of solving differential equations known as variation of parameters, applied differential calculus to the theory of probabilities and attained notable work on the solution of equations. He studied the three-body problem for the Earth, Sun, and Moon (1764) and the movement of Jupiter's satellites (1766), and in 1772 found the special-case solutions to this problem that are now known as Lagrangian points. Above all, he reformulated Newtonian mechanics creating what is today known as Lagrangian mechanics from his results on applying the calculus of variations to mechanics (Wikipedia, 2007).

BIBLIOGRAPHY

Aldinger, J. A., Kenney, J. M. and Keran, C. M. (1995), "Mobile Equipment Accidents in Surface Coal Mines," U.S. Bureau of Mines, Information Circular 9428, 51pp.

Aantaa, E., Virolainen, E. and Karskela, V. (1977), "Permanent Effects of Low Frequency Vibration on the Vestibular System," *Acta Oto-Laryngolocica, Vol. 83*, pp. 470-474.

Anderson, D. and Schade, G. (2001), "Tractor/Semi Trailer Ride Quality Prediction Using a Template Based Approach," *Proc. of the 2001 North American Users Conference*, Novi, Michigan, USA, 19-20 June, 2001.

Arn, K. E. (2004), "Design of a Non-Contact Vibration Measurement and Analysis System for Electronic Board Testing," MSc. Thesis, Massachusetts Institute of Technology, Cambridge, MA, USA 137pp.

Awuah-Offei, K. (2005), "Dynamic Modeling of Cable Shovel-Formation Interactions for Efficient Oil Sands Excavation," PhD. Dissertation, University of Missouri-Rolla, Rolla, MO, USA 147pp.

Barber, A. J. (1999), "Accurate Models for Bushings and Dampers using the Empirical Dynamics Method," *Proc. of the 14th European ADAMS Users Conference,* Berlin, Germany, 17-18 Nov, 1999.

Beevis, D. and Forshaw, S. E. (1985), "Back Pain and Discomfort Resulting from Exposure to Vibration in Tracked Armoured Vehicles," *Proc. of the 378th Advisory Group for Aerospace Research and Development Conference: Backache and Back Discomfort (AGARD-CP-378)* (Paper No. 4), Neuilly Sur Seine, France.

Benaroya, H. (2004), "Mechanical vibration Analysis, Uncertainties, and Control," Second Edition, Published by Marcel Dekker Inc., New York, USA 712pp.

Bohn, C., Cortabarria, A., Härtel V. and Kowalczyk, K. (2004), "Active Control of Engine-Induced Vibrations in Automotive Vehicles using Disturbance Observer Gain Scheduling," *Control Engineering Practice, Vol. 12*, pp. 1029-1039.

Bovenzi, M. and Hulshof, C. T. J. (1999), "An Updated Review of Epidemiologic Studies on the Relationship between Exposure to Whole-Body Vibration and Low Back Pain (1986-1997)," *International Archives of Occupational and Environmental Health, Vol. 72,* pp. 351-365.

Campbell-Kyureghyan, N., Vikas Yalla, S. and Burnett, D. (2007), "Effect of Orientation on Failure Criteria for Lumbar Spine Segments," *American Society of Biomechanics 2007 Annual Conference,* Stanford University, CA, August 22-25, 2007.

Cartwright, J. H. E. and Piro, O. (1992), "The dynamics of Runge-Kutta methods," *International Journal of Bifurcation and Chaos,* Vol. 2(3), pp. 427-449.

CAT Performance Handbook Edition 37 (2007), Published by Caterpillar Inc., Peoria, Illinois, USA.

Choi, Y. T. and Wereley, N. M. (2003), "Vibration Control of a Landing Gear System Featuring Electrorheological/Magnetorheological Fluids," Journal of Aircraft, Vol. 40(3), pp. 432-439.

Dittmann, K. J., Albright, F. J. and Leser, C. (2002), "Validation of Virtual Prototypes via a Virtual Test Laboratory," *Proc. of the 1st European MSC.ADAMS Users' Conference,* London, United Kingdom, 13-14 Nov, 2002.

Dhingra, H., Tewari, V., and Singh, S. (2003), "Discomfort, Pressure Distribution and Safety in Operator's Seat – *A Critical Review,*" *Agricultural Engineering International: The CIGR Journal of Scientific Research and Development, Invited Overview Paper, Vol. V.*

Duhamel, J. M. (1797-1872), "Eléments de calcul infinitésimnal," http://www-history.mcs.st-andrews.ac.uk/Biographies/Duhamel.html (Accessed on May 9, 2006).

Eger, T., Smets, M., Grenier, S., and Vibration Research Group (2005), "Whole-Body-Vibration Exposure Experienced During the Operation of Small and Large Load-Haul-Dump Vehicles," *Proc. of 5th Canadian Rural Health Research Society Conference and the Fourth International Rural Nurses Congress*, Sudbury, ON.

Fairely, T. E. and Griffin, M. J. (1989), "The Apparent Mass of the Seated Human Body: Vertical Vibration," *Journal of Biomechanics, Vol. 22(2),* pp. 81–94.

Fairley, T. E. and Griffin, M. J., (1990), "The Apparent Mass of the Seated Human Body in the For-and-aft and Lateral Directions," *Proc. of the Journal of Sound and Vibration, Vol.139 (2)*, pp. 299–306.

Freeport-McMoRan Copper & Gold Inc. (2007), http://www.fcx.com (Accessed on September 3, 2007).

Friedmann, P. P. (1997), "A Fundamental Study of Active Vibration Control in Rotorcraft using the ACSR Approach," *US Army Research Office, Engineering and Environmental Science Division,* Research Triangle Park, NC 27709-2211.

Fries, R. H., Cooperrider, N. K. and Larson, R. E. (1993), "Locomotive and Road Vehicle Ride Quality Assessments," *ASME Rail Transportation, RTD Vol. 6*, pp. 219-227.

Frimpong, S. (2005), "Biomechanics of Operator Vibration Control and Safety in High-Impact Shovel Loading Operations," Unfunded NIOSH Grant Proposal, 2005, 20pp.

Frimpong, S. (2006), Course Notes on MI ENG 326, "Surface Mining Methods and Equipment," ©, Missouri University of Science and Technology, Rolla, MO, USA.

Frimpong, S., Li, Y. and Aouad, N. (2007), "Intelligent Machine Monitoring and Sensing for Safe Surface Mining Operations," *Proc. Of the 1st International Conference on Environmental Research, Technology and Policy,* Accra, Ghana, 17-19 July, 2007, pp. 30-37.

Frimpong, S. and Li, Y. (2006), "Real-Time Monitoring of Cable Shovel Stress for Improved Machine Health," *SME National Conference Meeting*, Saint Louis, Missouri, 26-29 March, 2006.

Froom, P., Hanegbi, R., Ribak, J. and Gross, M. (1987),"Low Back Pain in a AH-1 Cobra Helicopter," *Aviation Space Environmental Medicine Vol. (58),* pp. 315-322.

Gibson, R. G. and Gibbons, J. D. (2006), "A Case Study of Whole-Body Vibration Exposures Associated with Ordinary Passenger and Recreational Vehicles," *Proc. of the 1st American Conference on Human Vibration,* Morgantown, West Virginia, USA, 5-7 June, 2006, pp. 48-49.

Gillespie, T. D. (1999), "Fundamentals of Vehicle Dynamics," Published by Society of Automotive Engineers, Inc., Warrendale, PA, USA, 495pp.

Griffin, M. J. (1990), *Handbook of Human Vibration,* London: Academic Press.

Griffin, M. J. (1998a), "A Comparison of Standardized Methods for Predicting the Hazards of Whole-Body Vibration and Repeated Shocks," *Journal of Sound and Vibration, Vol. 215*, pp. 883-914.

Griffin, M. J. (2004), *Handbook of Human Vibration,* London: Academic Press.

Griffin, M.J. (2004), "Minimum Health and Safety Requirements for Workers Exposed to Hand-Transmitted Vibration and Whole-Body Vibration in the European Union; A Review," *Occupational and Environmental Medicine, Vol. 61*, pp. 387- 397.

Hanagud, S., Roberts, P. (2005), "Analysis and Support Initiative for Structural Technology (ASIST). Delivery Order 0018: Active Vibration Control of Buffet-Induced Vibrations in the Vertical Tail of F/A-18," Public release by the Air Force Research Laboratory Wright Site (AFRL/WS) Public Affairs Office (PAO), PAO Case Number: AFRL/WS-06-1414, June 2nd, 2006.

Harrer, K., Yniguez, D., Majar, M., Ellenbecker, D., Estrada, N., and Geiger, M., (2005), "Whole Body Vibration Exposure for MH-60S Pilots," *Naval Medical Center San Diego, CA, Published in the Proceedings of the 43rd Annual SAFE Association Symposium,* Salt Lake City, Utah, 24-26 Oct, 2005, pp. 303-314.

Hedge, A. (2007), Course Notes on DEA350, "Whole-Body Vibration," ©, Cornell University, http://ergo.human.cornell.edu/studentdowloads/DEA 350pdfs/Whole-body%20Vibration.pdf (Accessed on September 24, 2007).

Hong, H-J and Moshchuk, N. (2001), "Automotive Truck Haulaway and Railcar Shipping Simulation," *Proc. of the 2001 North American MDI User Conference,* Novi, Michigan, USA, 19-20 June, 2001.

Hopcroft, R. and Skinner, M. (2005), "C-130J Human Vibration," *Published by Air Operations Division, DSTO Defence Science and Technology Organisation*, Victoria, Australia, August 2005.

Hoy, J., Mubarak, N., Nelson, S., Sweerts de Landas, M., Magnusson, M., Okunribido, O. and Pope, M. (2005), "Whole body vibration and posture as risk factors for low back pain among forklift truck drivers," *Journal of Sound and Vibration Vol. 284,* pp. 933-946.

Hustrulid, W. and Kuchta, M. (1995), "Open Pit Mine Planning and Design, Vol. 1," A. A. Balkema, Rotterdam, Netherlands, p. 95.

Inman, D. J. (2001), "Engineering Vibration," Second Edition, Published by Prentice Hall, USA 621pp.

ISO 2631 – 1 (1997), "Mechanical Vibration and Shock -- Evaluation of Human Exposure to Whole-Body Vibration -- Part 1: General requirements," *International Organization for Standardization*, Switzerland.

ISO 2631 – 2 (2003) is titled as "Mechanical vibration and shock -- Evaluation of human exposure to whole-body vibration -- Part 2: Vibration in buildings (1 Hz to 80 Hz)," *International Organization for Standardization*, Switzerland.

ISO 2631 – 4 (2001), "Mechanical vibration and shock -- Evaluation of human exposure to whole-body vibration -- Part 4: Guidelines for the evaluation of the effects of vibration and rotational motion on passenger and crew comfort in fixed-guideway transport systems," *International Organization for Standardization*, Switzerland.

ISO 2631 – 5 (2004), "Mechanical vibration and shock -- Evaluation of human exposure to whole-body vibration -- Part 5: Method for evaluation of vibration containing multiple shocks," *International Organization for Standardization*, Switzerland.

Joubert, D. M. (2002), "Whole-body vibration exposures in a developing country: a pilot study in South Africa amongst forklift drivers at the port of Durban," Central Queensland University, School of Health and Human Performance Australia.

Joubert, D. M. and London, L. (2007), "A cross-sectional study of back belt use and low back pain amongst forklift drivers," *International Journal of Industrial Ergonomics, Vol. 37,* pp. 505-513.

Johanning, E., Fischer, S., Christ, E., Göres, B., and Landsbergis, P., (2002), "Whole-Body Vibration Exposure Study in U.S. Railroad Locomotives – An Ergonomic Risk Assessment," *AIHA Journal, Vol. 63,* pp. 439-446.

Kim, W., Lee, J-W., Kim, H-K. and Doo, M-S., (2001), "Handling Analysis of Active Height Control System Using ADAMS," *Proc. of the North American MDI Users' Conference,* Novi, Michigan, USA, 18-20 June, 2001.

Kitazaki, S. and Griffin, M. (1998), "Resonance Behavior of the Seated Human Body and Effects of Posture," *Journal of Biomechanics, Vol. 31*, pp. 143-149.

Kittusamy, N. K. (2002), "Ergonomic Risk Factors – A study of Heavy Earthmoving Machinery Operators," *ASSE Foundation Research,* Oct. 2002, pp. 38-45.

Kittusamy, N. K. (2003), "A Checklist for Evaluating Cab Design of Construction Equipment," *Applied Occupational and environmental Hygiene, Vol.18*, pp. 721-723.

Kittusamy, N. K. (2003), "Self-Reported Musculoskeletal Symptoms Among Operators of Heavy Construction Equipment," *XVth Triennial Congress, International Ergonomics Association,* Seoul, Korea, August 24-29, 2003.

Kittusamy, N. K. and Miller, R. E. (2003) "Comparison of Jolting and Jarring in a Newer and Older Dozer at a Highway Construction Site," *XVth Triennial Congress, International Ergonomics Association.*

Kittusamy N. K., Mayton A. G., Jobes, C. C. and Ambrose, D. H. (2003), "N361 A Systematic Comparison of Different Seats on Shuttle Cars Used in Underground Coal Mines," *The 32nd International Congress and Exposition on Noise Control Engineering*, Seogwipo, Korea, August 25-28, 2003.

Kittusamy, N. K. and Buchholz, B. (2004), "Whole Body Vibration and Postural Stress among Operators of Construction Equipment: A Literature Review," *Journal of Safety Research, Vol. 35(3)*, pp. 255-261.

Kittusamy, N. K., Viswanathan, M. and Jorgensen, M. J. (2005), "Field Study to Evaluate the Effectiveness of a Continuous Passive Lumber Motion System," *XIX Annual International Occupational Ergonomics and Safety Conference,* Las Vegas, Nevada, USA.

Kjellberg, A. (1990), "Psychological Aspects of Occupational Vibration," *Scandinavian Journal of Work and Environmental Health, Vol.16 (1),* pp. 39-43.

Kowalczyk, K., Svaricek, F., Bohn, C., Karkosch, H. J. (2004), "An Overview of Recent Automotive Applications of Active Vibration Control," *Paper presented at the RTO AVT Symposium on "Habitability of Combat and Transport Vehicles: Noise, Vibration and Motion,"* Prague, Czech Republic, 4-7 Oct, 2004, Published in RTO-MP-AVT-110.

Krüger, W. R., Vaculín, O. and Spieck, M. (2004), "Evaluation of Active Damping for Reduction of Noise, Vibration and Motion of Ground Vehicles by Multibody Simulation," *Paper presented at the RTO AVT Symposium on "Habitability of Combat and Transport Vehicles: Noise, Vibration and Motion,"* Prague, Czech Republic, 4-7 Oct, 2004, Published in RTO-MP-AVT-110.

Kumar, S. (1999), "A Study of: Effect of Vibration and Impact on Drivers of Heavy Haulers in Winter Conditions at Syncrude," Department of Physical Therapy, Faculty of Rehabilitation Medicine, University of Alberta, Edmonton, Alberta, Canada.

Lagrange, J. L. (1788), "Mécanique Analytique (Analytical Mechanics)," Fourth Edition, 1888-89, Published by Gauthier-Villars & fils, Paris, First Edition in 1788.

Lagrange, J. L., (2007), http://en.wikipedia.org/wiki/Joseph_Louis_Lagrange (Accessed on August 24, 2007)

Law, S. S., Wu, Z. M. and Chan, S. L. (2004), "Vibration Control Study of a Suspension Footbridge Using Hybrid Slotted Bolted Connection Elements," *Engineering Structures, Vol. 26*, pp. 107-116.

MAPLE CLASSIC Version 10.00 (2006), © Maplesoft, a division of Waterloo Maple Inc.

Mayton A., Ambrose, D., Jobes C. and Kittusamy N. K. (2003), "Ergonomic and Existing Seat Designs Compared on Underground Mine Haulage Vehicles," *Proc. of the 47th Human Factors and Ergonomics Society annual meeting*, 2003.

Mayton, A., Jobes, C., Kittusamy, N. K. and Amirouche, F. (2006), "Comfort Evaluation for Mine Shuttle Car Seat Designs," *Proc. of the 1st American Conference on Human Vibration,* Morgantown, West Virginia, USA, 5-7 June, 2006, pp. 29-30.

McDowell, T. W., Wiker, S. F., Dong, R. G. and Welcome, D. E. (2006), "The Effects of Vibration on Psychophysical Grip and Push Force-Recall Accuracy," *Proc. of the 1st American Conference on Human Vibration,* Morgantown, West Virginia, USA, 5-7 June, 2006, pp. 27-28.

McManus, S. J., St. Clair, K. A., Boileau, P. É., Boutin, J. and Rakheja, S. (2002), "Evaluation of Vibration and Shock Attenuation Performance of a Suspension Seat with a Semi-Active Magnetorheological Fluid Damper," *Journal of Sound and Vibration, Vol. 253(1)*, pp. 313-327.

Miller, R. E., Boman, P., Walden, J., Rhoades, S. and Gibbs R. (2000), "Acceleration and GPS Data Monitor Truck-Haulage Jolts," *Mining Engineering 2000, Vol. 58(2)*, pp. 20-22.

Miller, R. E., Lowe, N. T. and Thompson R. (2004), "A GPS Based System for Minimizing Jolts to Heavy Equipment Operators," *SAE Commercial Vehicle Engineering Congress and Exhibition, 26-28 Oct, 2004,* Chicago, IL. Warrendale, PA: Society of Automotive Engineers International, pp. 1-4.

Moses, R.W. (1997), "Vertical-tail-buffeting alleviation using piezoelectric actuators: some results of the actively controlled response of buffet-affected tails (ACROBAT) program," *Proc. SPIE, Vol. 3044*, pp. 87-98.

MSC.ADAMS (2007), "MSC Software Corporation," © MSC.ADAMS Santa Ana, CA, USA.

Nakashima, Y., Maeda, S. (2006), "A Method of Evaluating Vehicle Seat Vibration with Consideration of Subjective Judgment," *Proc. of the 1st American Conference on Human Vibration,* Morgantown, West Virginia, USA, 5-7 June, 2006, pp. 31-32.

Negrut, D. and Ortiz, J.L. (2005), "An Approach for the Linearization of the Differential Algebraic Equations of Multi-Body Dynamics," *ASME/IEEE International Conference on Mechatronic and Embedded Systems and Applications.*

Pope, M. H., Wilder, D. G. and Donnermeyer, D. D. (1985), "Muscle Fatigue in Static and Vibration Seating Environments," *Proc. of the 378th Advisory Group for Aerospace Research and Development Conference: Backache and Back Discomfort (AGARD-CP-378)* (Paper No. 25), Neuilly Sur Seine, France.

Prakash, J., Nandi, S. K. and Sivakumar, J. (2006), "Dynamic Stress and Durability Analyses: Time Vs Frequency Domain Approaches," *MSC Software Corporation's 2006 Americas Virtual Product Development Conference,* Huntington Beach, CA, USA, 17-19 July, 2006.

Press, W. H., Flannery, B. P., Teukolsky, S. A., and Vetterling, W. T. (1992) "Numerical Recipes in FORTRAN: The Art of Scientific Computing," Second Edition, Published by Cambridge, England, Cambridge University Press, pp. 91-95.

Ramazzini, B. (1713) "De Morbis Artificum (Diseases of workers)," Translation by WC Wright, 1964, New York, Hafner Publishing Co.

Randolph, R. F. and Boldt, C. M. (1996) "Safety Analysis of Surface Haulage Accidents," *Proc. of the 27th Annual Institute on Mining Health, Safety and Research,* Blacksburg, VA, Virginia Polytechnic Institute and State University, Jan. 1996, pp. 29-38.

Rao, S. S., (1995), "Mechanical Vibrations," Third Edition, Published by Addison – Wesley Publishing Company, World Student Series, 912pp.

Rasmussen, G. (2006), "Human Body Vibration Exposure and its Measurement," http://www.zainea.com/body.htm (Accessed in November 8, 2007).

Riepl, A., Schmid, M. and Reinalter, W. (2000), "Application of ADAMS/Car in Vehicle Development," *Proc. of the 2000 North American ADAMS User Conference,* Orlando, FL, USA, 19-21 June, 2000, 9pp.

Rosen, J. and Arcan, M., (2003), "Modeling the Human Body/Seat System in a Vibration Environment," *Journal of Biomechanical Engineering, Vol. 125(2)*, pp. 223-231.

Seidel, H. (1993), "Selected Health Risks Caused by Long-term Whole-Body Vibration," *American Journal of Industrial Medicine, Vol. 23(4),* pp. 589-604.

Schwarze, S., Notbohm, G., Dupuis, H. and Hartung, E. (1998), "Dose-Response Relationships between Whole-Body Vibration and Lumbar Disk Disease – A Field Study on 388 Drivers of Different Vehicles," *Journal of Sound and Vibration, Vol. 215,* pp. 613-628.

Singh, K. V. and Ram, Y. M. (2000), "Dynamic Absorption by Passive and Active Control," *Journal of Vibration and Acoustics, American Society of Mechanical Engineers, Vol. 122,* pp. 429-433.

Smith, S. D. (1996), "Resonance behavior of females and males exposed to whole-body vibration," *Proc. of the 1996 15th Southern Biomedical Engineering Conference,* 29-31 March 1996, pp. 247-250.

Smith, S. D. (1998) "The Effect of Prototype Helicopter Seat Cushion Concepts on Human Body Vibration Response," *Journal of Low Frequency Noise, Vibration and Active Control, Vol. 17(1),* Multi – Science Publishing Co. Ltd., United Kingdom.

Smith, S. D., Smith J. A. and Newman R. J. (2006), "Vibration Transmissibility Characteristics of Occupied Suspension Seats," Air Force Research Laboratory Wright Site Public Affairs Office, Doc. Number AFRL-WS 06-2711, Nov. 20, 2006.

Soedel, W. (2004), "Vibrations of Shells and Plates," Third Edition, Revised and Expanded, Published by Marcel Dekker Inc., New York, USA 592pp.

Sohoni, V.N. and Whitesell, J. (1986), "Automatic Linearization of Constrained Dynamical Systems," *ASME Journal of Mechanisms, Transmissions and Automation in Design, Vol. 108(3),* pp. 300-304.

Subramanyam, V., Monkaba, V. and Alexander, T. (2000), "Visteon's Approach to All-Wheel Drive Vehicle Dynamics Model Simulation and Correlation," *Proc. of the 15th European ADAMS Users' Conference, Technical Papers,* Rome, Italy, 15-17 Nov, 2000.

Suzuki, H. (1997) "A Study on the Vibrational Factors Determining the Riding Comfort of Railway Vehicle," *The Japanese Journal of Ergonomics, Vol. 33(6),* pp. 349-355.

Syncrude (1996), *At Face Slurrying: Provisional Data*; Syncrude Canada Ltd., Edmonton, Canada.

Thomson, W. T. (1992), "Theory of Vibration with Applications," Fourth Edition, Published by Prentice Hall, October, 1992, 546pp.

Trangsrud, C., Law, E. H., and Janajreh, I. (2004), "Ride Dynamics and Pavement Loading of Tractor Semi-Trailers on Randomly Rough Roads," *SAE International, Vehicle Dynamics & Chassis Development, SP-1904, 2004-01-2622,* pp. 23-46.

Uehara, K., Shinotoh, S., Hattori, K., Cheng, Y., Adachi, Y. and Yamanaka, T. (2000), "A Web Based Vehicle Natural Frequency Map Created by An ADAMS Virtual Prototyping System," *Proc. of the North American MDI Users Conference,* Novi, Michigan, USA, 18-20 June, 2001.

Vaningen-Dunn, C., Richards, M. K., (1992), "Feasibility of Reducing Incidence of Low Back Pain in Helicopter Pilots Using Improved Crewseat Cushions," *AL-SR-1991-0009, Air Force Material Command,* Wright-Patterson AFB, OH, Dec.

Wang, K. W. (2006), "Piezoelectric Tailoring with Enhanced Electromechanical Coupling for Concurrent Vibration Control of Mistuned Periodic Structures," Air Force Office of Scientific Research, Arlington, VA 22203-1768.

Waters, T. R., Li, F., Huston, R. L. and Kittusamy, N. K. (2003), "Biomechanical Modeling of Spinal Loading Due to Jarring and Jolting for Heavy Equipment Operators," *XVth Triennial Congress International Ergonomics Association.*

Watts, H.A. and Shampine, L. F. (1979), "Design of a User Oriented Package of ODE Solvers," Technical Report Sand 79-2374, DEPAC Sandia National Laboratories, Albuquerque, New Mexico, USA.

Wenzhang, Z., Yi, L., Guobiao, S. and Ligong, W. (2000), "Study on Non-Linear Dynamic Characteristic of Vehicle Suspension Rubber Component," *Proc. of the 2000 North American ADAMS User Conference,* Orlando, FL, USA, 19-21 June, 2000.

Wickramasinghe, V., Zimcik, D. and Chen Y. (2004), "A Novel Adaptive Structural Impedance Control Approach to Suppress Aircraft Vibration and Noise," *Paper presented at the RTO AVT Symposium on "Habitability of Combat and Transport Vehicles: Noise, Vibration and Motion,"* Prague, Czech Republic, 4-7 Oct, 2004, Published in RTO-MP-AVT-110.

Winthrop, M. F. (2004), "Engineering Tools for Variable Stiffness Vibration Suppression and Isolation," PhD. Dissertation, Department of the Air Force, Air Force Institute of Technology, Wright Patterson Air Force Base, Ohio, USA 211pp.

Yaguchi, E., Yanagishima, T., Akatsu, Y., Hanai, T. and Kato, K. (1994), "Whole-Body Vibration and Ride Comfort," *Proc. of the International Congress on Noise Control, Inter-noise 94*, pp. 905-910.

Yamakawa, H., Sakai, Y., Yamamoto, Y., Barber, A. J. and Wakabayashi, Y. (2002), "An Application of Full Vehicle ADAMS Modeling with Detailed Force Elements: Collaborative activity among Design, Experiment & CAE in the field of vehicle dynamics," *Proc. of the International Symposium on Advanced Vehicle Control (AVEC-02), Society of Automotive Engineers of Japan (JSAE),* Hiroshima, Japan, September 2002.

Young, H. D. and Freedman, R. A. (1999), "Sears and Zemansky's University Physics," Tenth Edition, Published by Addison-Wesley, 1999, 45pp.

Yoshimura T., Nakai, K. and Tamaoki G. (2005), "Multi-Body Dynamics Modelling of Seated Human Body under Exposure to Whole-Body Vibration," *Industrial Health 2005, Vol. 43(3),* pp. 441-447.

VITA

Nassib Aouad was born on July 10, 1978. He obtained his Bachelor of Engineering in Mechanical Engineering from Notre Dame University (NDU), Lebanon from 1997 to 2002. Then he worked as a resident engineer at a waste treatment plant for six month before he enrolled in the masters program. He holds a Masters of Science in Mechanical Engineering from Youngstown State University (YSU), Youngstown, OH (2003 to 2004). In August 2005, he joined the PhD program in Mining Engineering at Missouri University of Science & Technology (MS&T) in Rolla, MO, formerly known as University of Missouri Rolla (UMR). During his PhD candidacy, he worked as a research assistant on dump truck vibration analysis as part of the Heavy Mining Machinery Research Group under the guidance of Dr. Samuel Frimpong. He is expected to receive his PhD in Mining Engineering in August 2008.